MICROWAVE AND MILLIMETER-WAVE RECTIFYING CIRCUIT ARRAYS AND ULTRA-WIDEBAND ANTENNAS FOR WIRELESS POWER TRANSMISSION AND COMMUNICATIONS

A Dissertation

by

YU-JIUN REN

Submitted to the Office of Graduate Studies of
Texas A&M University
in partial fulfillment of the requirements for the degree of

DOCTOR OF PHILOSOPHY

May 2007

Major Subject: Electrical Engineering

MICROWAVE AND MILLIMETER-WAVE RECTIFYING CIRCUIT ARRAYS AND ULTRA-WIDEBAND ANTENNAS FOR WIRELESS POWER TRANSMISSION AND COMMUNICATIONS

A Dissertation

by

YU-JIUN REN

Submitted to the Office of Graduate Studies of
Texas A&M University
in partial fulfillment of the requirements for the degree of

DOCTOR OF PHILOSOPHY

Approved by:

Chair of Committee,	Kai Chang
Committee Members,	Robert D. Nevels
	Ohannes Eknoyan
	Je-Chin Han
Head of Department,	Costas N. Georghiades

May 2007

Major Subject: Electrical Engineering

ABSTRACT

Microwave and Millimeter-wave Rectifying Circuit Arrays and Ultra-wideband Antennas for Wireless Power Transmission and Communications. (May 2007)

Yu-Jiun Ren, B.S., National Chung-Hsing University;

M.S., National Chiao-Tung University

Chair of Advisory Committee: Dr. Kai Chang

In the future, space solar power transmission and wireless power transmission will play an important role in gathering clean and infinite energy from space. The rectenna, i.e., a rectifying circuit combined with an antenna, is one of the most important components in the wireless power transmission system. To obtain high power and high output voltage, the use of a large rectenna array is necessary.

Many novel rectennas and rectenna arrays for microwave and millimeter-wave wireless power transmission have been developed. Unlike the traditional rectifying circuit using a single diode, dual diodes are used to double the DC output voltage with the same circuit layout dimensions. The rectenna components are then combined to form rectenna arrays using different interconnections. The rectennas and the arrays are analyzed by using a linear circuit model. Furthermore, to precisely align the mainbeams of the transmitter and the receiver, a retrodirective array is developed to maintain high efficiency. The retrodirective array is able to track the incident wave and resend the signal to where it came from without any prior known information of the source location.

The ultra-wideband radio has become one of the most important communication systems because of demand for high data-rate transmission. Hence, ultra-wideband antennas have received much attention in mobile wireless communications. Planar monopole ultra-wideband antennas for UHF, microwave, and millimeter-wave bands are developed, with many advantages such as simple structure, low cost, light weight, and ease of fabrication. Due to the planar structures, the ultra-wideband antennas can be easily integrated with other circuits. On the other hand, with an ultra-wide bandwidth, source power can be transmitted at different frequencies dependent on power availability. Furthermore, the ultra-wideband antenna can potentially handle wireless power transmission and data communications simultaneously. The technologies developed can also be applied to dual-frequency or the multi-frequency antennas.

In this dissertation, many new rectenna arrays, retrodirective rectenna arrays, and ultra-wideband antennas are presented for microwave and millimeter-wave applications. The technologies are not only very useful for wireless power transmission and communication systems, but also they could have many applications in future radar, surveillance, and remote sensing systems.

DEDICATION

To my parents,
and my wife, Yu-Chieh

ACKNOWLEDGMENTS

I would like to express my sincere gratitude to Dr. Kai Chang for his guidance and support with regards to my graduate studies and research at Texas A&M University. I also appreciate Dr. Robert D. Nevels, Dr. Ohannes Eknoyan, Dr. Je-Chin Han, and Dr. Krzysztof A. Michalski for serving as my committee members and for their helpful comments. I would also like to thank Dr. James McSpadden at Raytheon, Dr. Berndie Strassner and Dr. Christopher Rodenbeck at Sandia National Laboratories, and Mr. Chieh-Ping Lai at Pennsylvania State University for their helpful suggestions in the development of the technologies described in this dissertation. My appreciation is also extended to Mr. Ming-Yi Li, Dr. Wen-Hua Tu, Dr. Seung-Pyo Hong, Mr. Shih-Hsun Hsu, Dr. Lung-Hwa Hsieh, Dr. Chulmin Han, Dr. Sang-Gyu Kim, Mr. Samuel Kokel, and other members of the Electromagnetics and Microwaves Laboratory at Texas A&M University for their technical assistance and invaluable discussions. Lastly, I would like to express my deep appreciation to my parents, whose love, encouragement, and financial contributions have made all of this possible.

TABLE OF CONTENTS

Page

CHAPTER Page

CHAPTER Page

LIST OF FIGURES

FIGURE Page

FIGURE Page

FIGURE Page

FIGURE Page

FIGURE Page

FIGURE Page

LIST OF TABLES

CHAPTER I

INTRODUCTION

1. Introduction and research background

In the past few decades, space solar power transmission (SPT) and microwave wireless power transmission (WPT) have become an interesting topic as one of the technologies for solving the world energy problems in the future. WPT can be considered as a three-dimensional means of transferring electrical power from one location to another. WPT using a microwave beam presents many advantages compared to other methods of transporting electricity. Microwave power transfer and DC conversion fulfills the necessity of integration to the environment at a relatively low implementation cost. One of the most important and the main requirement of a WPT system is the efficient transfer of electric power. The overall DC (or RF) to DC efficiency of the WPT system characterizes this performance criterion. The rectenna, the rectifying circuit integrated with an antenna, is the key component in determining the efficiency in WPT, whose development has been reviewed in [1-4].

Recently, a new dual frequency rectenna was reported in [5] where a circularly polarized ring-slot antenna was used. The rectenna has been shown to have a useful application for portable wireless devices. A rectenna with a harmonic-rejecting circular-sector antenna was presented in [6] and the rectenna can avoid the use of the lowpass

---

The journal model for this dissertation is *IEEE Transactions on Microwave Theory and Techniques*.

filter connecting the antenna and the rectifying diode. A new patch antenna with a high gain of 9 dBi was designed for the finite-ground coplanar waveguide (CPW) rectenna [7]. The patch antenna has characteristics comparable to those of a two-element antenna array and hence it can allow the rectenna not only to receive more power but also be more compact. Furthermore, a new two-slot patch antenna was proposed to build the rectenna [8]; one of these slots generates a right-hand circular polarization and the other generates a left-hand circular polarization.

It seems that circular polarization (CP) has become one of the important characteristics in designing rectennas [5][8-11]. Circular polarization avoids the variation of the output voltage due to the rotation of the transmitter or receiver. Traditionally, dipoles or patch antennas are used in rectenna design. The coplanar stripline (CPS) is normally used to feed the dipole or dipole-like antennas. It can be used to combine several antenna elements for higher gain and also to form an antenna array more easily. Many CPS-fed rectennas have been recently studied in [11-14]. Using a high gain antenna reduces the number of rectenna elements needed. In most cases, an antenna with a higher gain will cover a larger effective area. So there is a trade off between the antenna gain and the antenna area.

However, even with circular polarization, the efficient power transmission still requires a precise mainbeam alignment between the transmit antenna and the receive rectenna array. The transmit antenna usually has a quite narrow beam-width at the broadside. Despite the fact that a circularly polarized antenna can maintain a constant output voltage when the transmitter or the receiver rotates, it cannot prevent the output

voltage variations due to improper mainbeam alignment. In [15], it was proposed that using a non-uniform antenna array replaces the traditional uniform antenna array in the microwave power transmission applications. The array aperture of the non-uniform array can be designed to form a uniform amplitude antenna pattern on both the E-plane and H-plane and also widen the main-lobe beam-width. The rectenna with a broadened mainbeam can keep the output voltage invariant even if the rectenna has an improper beam alignment. Although this method indeed makes the mainbeam broadened, numerous antenna elements with various sizes are needed and the non-uniform array gain may be lower than that of the uniform array. The process is complicated and difficult to implement.

The second method to solve this problem is to use a retrodirective antenna array [16-18]. A retrodirective array does not require accurate information of the source location but is able to resend the incident wave in the direction it came from. This automatic beam steering feature has been widely used in many wireless communication systems [19-22], including multi-path fading reduction [23] and spatial power combining [24]. The retrodirective antenna has two basic array architectures: the phase-conjugated array and the Van Atta array. The phase-conjugated array needs a mixer circuit that requires a large frequency difference between RF and LO signals and the RF leakage has to be suppressed for good performance. It has many circuit components and is difficult to integrate with the rectenna. The Van Atta array is simpler. It consists of array elements connected by transmission lines. The Van Atta array can be either passive active, unlike the phase-conjugated array that always requires active devices [25]. The

advantages of the Van Atta array make it easy to combine with the rectennas.

The Van Atta array can scan the signals in both E-plane and H-plane simultaneously by suitably interconnecting the array elements using transmission line networks. Although array elements and the transmission line networks can be placed on the same plane, the array size will be limited due to complicated networks for a large array. Separating them on different layers can simplify the design and an array with a large size can be built. The multiple-layer structure may result in a thick substrate. However, one advantage of using a thick substrate is that it could be used to design a wideband antenna.

To supply high DC output, the rectenna array has to be able to rectify a large amount of incoming power. The rectenna array can be built by using different interconnections of rectenna elements [10][26-27]. Each connection has its own output feature. In order to obtain the optimum output voltage, identical rectenna elements and optimum load resistance should be used. Otherwise, careful combination of rectenna elements has to be considered [28]. On the other hand, the harmonic signals radiated by the rectifying circuits are a potential problem in rectenna design. The power level of the third-order harmonic may have the same order as that of the second-order harmonic [29-30]. Therefore it is better to use a high-order harmonic-rejecting device to simultaneously suppress the higher order harmonic signals. Alternatively, a frequency selective surface can be used to diminish the reradiated harmonics.

With the demand for the high-speed data rates and high capacity, broadband and ultra-wideband (UWB) antennas have already received much attention in wireless

communications. With an ultra-wide bandwidth, the signals can be transmitted by high-speed impulses or using multi-band groups. To increase the bandwidth of traditional microstrip antennas, various technologies have been applied including embedding slots/slits with various shapes, using stacked structures, using air layers or foam substrates, increasing electrical thickness, adding capacitive loading, and using impedance matching technique, etc.

Many broadband/UWB antennas have been reported for applications in the UHF band (0.3-3 GHz) [31-35]. However, these reported antennas have a maximum bandwidth below 85%. For microwave applications, broadband ring antennas have been reported in [36-44]. However, it is difficult to find wideband ring antenna designed for millimeter-wave applications. Compared with the common shape of microstrip antennas such as rectangular, circular, and the triangular, relatively few broadband antennas adopt the elliptic shape [45-49], especially in millimeter-wave frequencies, in which the elliptical patch configuration is used instead of the ring configuration. Thus ultra-wideband planar antennas adopting circular ring and elliptic ring need to be explored and developed for microwave and millimeter-wave bands, which can be used in mobile communications and wireless power transmission. Due to the difficulty to enhance the effective bandwidth of the UHF wideband antenna, ultra-wideband UHF antennas need to be further studied.

To develop the ultra-wideband antenna, a simple and efficient design is preferred. The monopole antenna has many advantages such as wide operation bandwidth, simple structure, good radiation patterns, lightweight, and ease of fabrication. With a planar

structure, the antenna can be easily integrated with the circuits. Hence the monopole planar antenna is a good candidate to be designed as an UWB antenna.

From the above discussions for microwave and millimeter-wave wireless power transmissions, it is concluded that (1) circular polarized antenna element is preferred to avoid voltage variation due to the rotation of the transmitter or receiver, (2) the function of the bandpass filter should be integrated with that of the antenna to form a harmonic-rejecting antenna that can make the circuit more compact, (3) the rectenna arrays have to be built to obtain higher output power/voltage, (4) the rectenna alignment problem needs to be considered and using the retrodirective array is one solution, and (5) ultra-wideband antennas are necessary for the future wireless applications. To efficiently transmit the energy, these concepts should be considered while designing future wireless power transmission systems.

2. Dissertation organization

This dissertation presents a variety of topics, including rectennas and rectenna arrays, retrodirective arrays and retrodirective rectennas, and ultra-wideband antennas designed for UHF, microwave, and millimeter-wave frequencies covering from 600 MHz to 48 GHz. The rectenna, rectenna array, and retrodirective array with high-orders of harmonic rejection avoid the performance reduction due to the harmonics resulting from the rectifying circuit. Many new antenna elements and filters are developed for these arrays.

The dissertation consists of eight chapters. Chapter II reviews the WPT system and

the operation theory of the rectenna. Then a 5.8 GHz circularly polarized dual-diode rectenna is presented. The coplanar stripline structure is used to design the antenna and the bandpass filter for the rectenna. The CPS antenna can be easily extended to from a traveling-wave array with a higher gain. For the purpose of high output power, the rectennas can be interconnected series, parallel, or cascaded to form the rectenna arrays. A simple linear circuit model is used to analyze the rectenna element and the rectenna arrays. The term "voltage ratio" is proposed to evaluate the linearity of the rectenna array.

Chapter III introduces the idea to combine the retrodirective array with the rectenna. At first, a rectenna with a non-uniform antenna array having a broadened beam-width is designed to reduce the output variation while the mainbeam scans, which is compared to the rectenna with a uniform antenna array. Then, a retrodirective array is designed and assembled with the rectifying circuits to form a retrodirective rectenna array. A 2x2 array and a 4x4 array are demonstrated. A circularly polarized antenna element is designed with the ability to reject the harmonics from the rectifying circuits, which avoids the use of the filter and hence saves the space for building a large array. Finally, a 5.8 GHz active wireless power transmission system is proposed.

Chapter IV describes rectenna arrays and retrodirective arrays for millimeter-wave communications and power transmission. An ultra-wideband harmonic-rejecting antenna is designed as the receiving element of the arrays, which can be tuned to cover from Ka-band to W-band. The rectenna with the ultra-wideband antenna can be assembled to form a large rectenna array with a predictable output performance. The antenna is then

used to build a Van Atta retrodirective array with 8x16 elements, which is assembled using planar 4x4 sub-arrays.

Chapter V discusses a compact dual-frequency rectenna designed for the ISM (industry, science, and medical) band. The proposed dual-frequency rectenna is the smallest dual-frequency rectenna ever reported. A circular slot antenna for 2.45 GHz and a square slot antenna for 5.8 GHz are integrated. The rectenna with a compact hairpin bandpass filter can reject the harmonic signals up to the sixth order.

Chapter VI introduces four newly developed ultra-wideband monopole antennas, including annual ring, elliptical ring, and patch antennas. All of them adopt a planar structure to be easily integrated with the print circuit board. They can cover 0.6-2.1 GHz and 2.8-12.3 GHz.

Chapter VII proposes a new class of millimeter-wave harmonic components using the high-order modes of the resonators. These harmonic components include commonly used antenna, bandpass filter, antenna array, and the rectenna. Their performances are demonstrated and compared with the traditional components using the fundamental mode.

Chapter VIII summarizes the research accomplishments in this dissertation and presents recommendations for further studies.

CHAPTER II

CIRCULARLY POLARIZED DUAL-DIODE RECTENNA AND RECTENNA ARRAY FOR MICROWAVE WIRELESS POWER TRANSMISSION*

1. Introduction

In the past rectenna developments, the single diode configuration is adopted in most rectifying circuits, which is acted as a half-wave rectifier. The half-wave voltage doubler structure is rarely used, which can be found in [5] and [9]. To obtain double or even higher output, the full-wave rectifier can be applied. However, compared with the half-wave rectifier, the full-wave rectifier may need more rectifying diodes and require more components, which result in a more complicated circuit and larger circuit size.

Several circuit analysis models have been proposed to analyze the rectenna [50-52]. Since the diode is not a linear device, which may produce harmonic signals, it is not easy to formulate a perfectly correct model. Although both a linear circuit model and a non-linear circuit model can be used to predict the rectenna behavior, the non-linear model has better accuracy, especially when each rectenna element has relatively different input power [27].

In this chapter, the WPT system and the operation theory of the rectenna are reviewed at fist. Then a low cost, compact, and high output voltage rectenna is proposed. A circular polarized CPS-fed truncated patch rectenna is designed that looks like a two-element patch antenna array and hence has a higher gain than a single patch antenna. A high-order harmonic-rejecting CPS bandpass filter is designed to suppress the harmonic signals from the rectifying circuit. The rectenna includes two diodes in the rectifying circuit. By using the dual-diode configuration, the rectenna can produce at least twice higher DC output voltage than the single diode rectenna, while the size of the rectenna is unchanged.

These novel rectennas, called dual-diode rectennas, can be easily combined by interconnections to provide even higher DC output voltage or power. Three types of interconnections are demonstrated, including series, parallel, and cascaded connections. A simple linear model is used to predict the output characteristics of the interconnected rectenna arrays. When the power density is lower, the CPS-fed antenna and rectenna circuit can be easily extended to become a traveling wave antenna array with higher gain to collect more RF power. A six-patch and a sixteen-patch antenna array are demonstrated for the dual-diode rectenna applications.

2. System review and rectanna operation theory

A. Wireless power transmission system

A WPT system consists of three main functional blocks. The first block is to convert the electricity (DC or AC) into microwaves. After radiated through the antenna

of microwave radiators, the RF power is carried within a focused microwave beam that travels across free space towards a receiver. This receiving block will convert the RF energy back to DC electricity. Figure 1 shows the basic components of a WPT system with associated efficiencies, which will be explained as the followings.

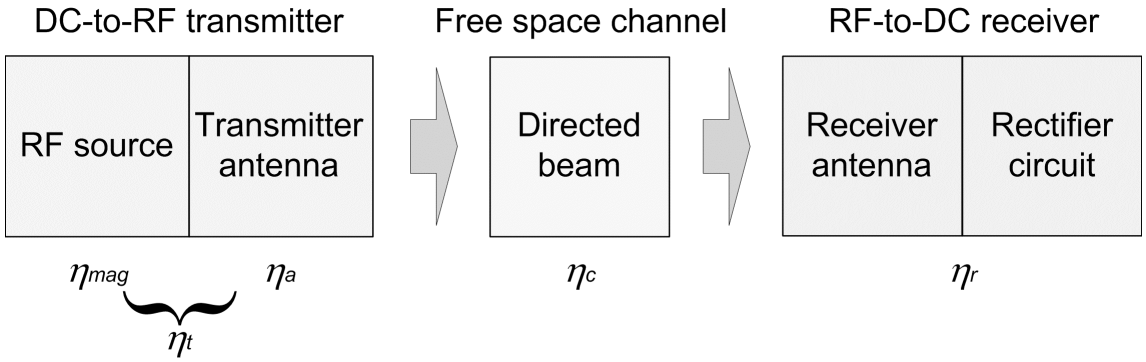

Fig. 1. Wireless power transmission system schematic.

The efficiency of a system is basically equivalent to its transfer function. The general definition of any efficiency (η) used hereafter is the ratio of output power P_{out} over input power P_{in} , i.e., $\eta = P_{out} / P_{in}$. The overall efficiency (η_{all}) of a WPT system is the ratio of the DC output power at the receiver end over the DC (or AC) input power at the transmitter end, which is given by

$$\eta_{all} = \eta_t \cdot \eta_c \cdot \eta_r \tag{1}$$

As shown in Figure 1, this end-to-end efficiency includes all the sub-efficiencies starting from the DC supply feeding the RF source in the transmitter to the DC power interface at the receiver output. It is comprised of three distinct sub-efficiencies: the electric to microwave conversion efficiency η_t (or transmitter efficiency), the collection efficiency

η_c, and the microwave to electric conversion efficiency η_r (or rectenna efficiency).

The first term (η_t) is equal to the product of the magnetron efficiency (η_{mag}) and the transmitter antenna efficiency (η_a). The magnetron efficiency is used to express how efficient the RF source works. The antenna efficiency at the transmitter represents the ability of the antenna to radiate the distributed RF power fed from the RF source and launched into free-space. It is assumed that both the magnetron efficiency and the antenna efficiency are equal to 100%, which means the projector is an ideal device that can provide wanted transmitting power.

The collection efficiency (η_c) is the ratio of the received power over the transmitted power. For maximum collection efficiency, an optimum power density distribution must be selected for the transmitting antenna aperture. A non-uniformly illuminated aperture increases the collection efficiency and it has been seen that the optimal taper is of Gaussian type. The collection efficiency should be very high, when the impedance looking into the receiver is matched to the free space impedance. The collection efficiency is proportional to a design parameter τ, which is expressed as Goubau's relation [1][30]

$$\tau = \frac{\sqrt{A_r A_t}}{\lambda_0 D} \tag{2}$$

where A_r and A_t are the aperture areas of the receiver and the transmitter antennas. As can be seen from this equation, Goubau's relation can be used to determine the size of the apertures involved. The collection efficiency is given by

$$\eta_c = (1 - \mathrm{e}^{-\tau^2}) \times 100\% \tag{3}$$

which is proportional to the power density and the incremental area of the antenna. For example, as A_t becomes larger, the incident power density also increases leading to a higher collection efficiency as seen through τ. This translates into a tradeoff between the efficiency and the size.

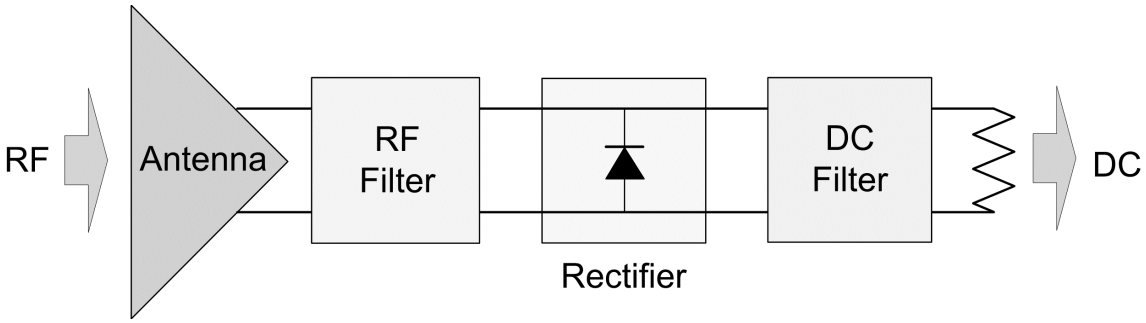

Fig. 2. Rectenna block diagram.

The receiver function is to collect the incoming RF power and convert it back to DC electricity. An appropriate choice of device to accomplish these tasks is the diode type rectenna, which as the name indicates that the electromagnetic waves are collected by antennas and rectified by diodes. Figure 2 shows the basic components of the rectenna element. An antenna element attaches to a RF filter (bandpass or lowpass filter) that transforms the impedance of the antenna to the rectifier impedance and prevents the high-order harmonics resulted from the rectifier reradiating. The rectifying diode is the core element of the rectifier. The output DC filter of a large capacitor effectively shorts the RF energy and passes the DC power. A load resistor is placed at the output terminal to measure the DC output voltage.

An important feature of the rectenna is the capacity to efficiently convert the

incident RF power density into DC power. This conversion efficiency is strongly dependent on the power density (P_d) distribution across the receiver aperture. The maximum incident power density can be derived as follows. Assuming a uniform taper at the transmitter, an optimal directivity of

$$D_0 = \frac{4\pi A_{te}}{\lambda_0^2} \tag{4}$$

is obtained, which means the power of the mainbeam is magnified by D_0 in a certain direction. For a 100% efficiency antenna, $A_{te} = A_t$. This magnification is reduced by the decay of the field strength with distance as expressed by the factor $1/(4\pi D^2)$. The distance D needs to be relatively large for the system to operate in the far field. Combining these two opposing effects into one expression, the peak power density at the center of an aperture is obtained

$$P_{d,peak} = \frac{P_t A_{te}}{\lambda_0^2 D^2} \tag{5}$$

From this equation, a higher P_d requires a larger A_{te}. Also, the power handling capacity of the receiver depends on the area A_r and the power density ratings of the rectifying elements.

To align the mainbeam of the transmitter or the receiver, retrodirective technique can be used. Although the mainbeam alignment is not necessary for the proposed demonstration, a retrodirective technique can be used to stabilize system if the mainbeam is drifted away from the transmitter or receiver due to malfunction. A simple retrodirective method is to have a low power pilot beam from the transmitter to the

center of the rectenna array. This pilot beam can operate at a different frequency. The research discussing about the rectenna and the retrodirective array will be conducted in Chapter III.

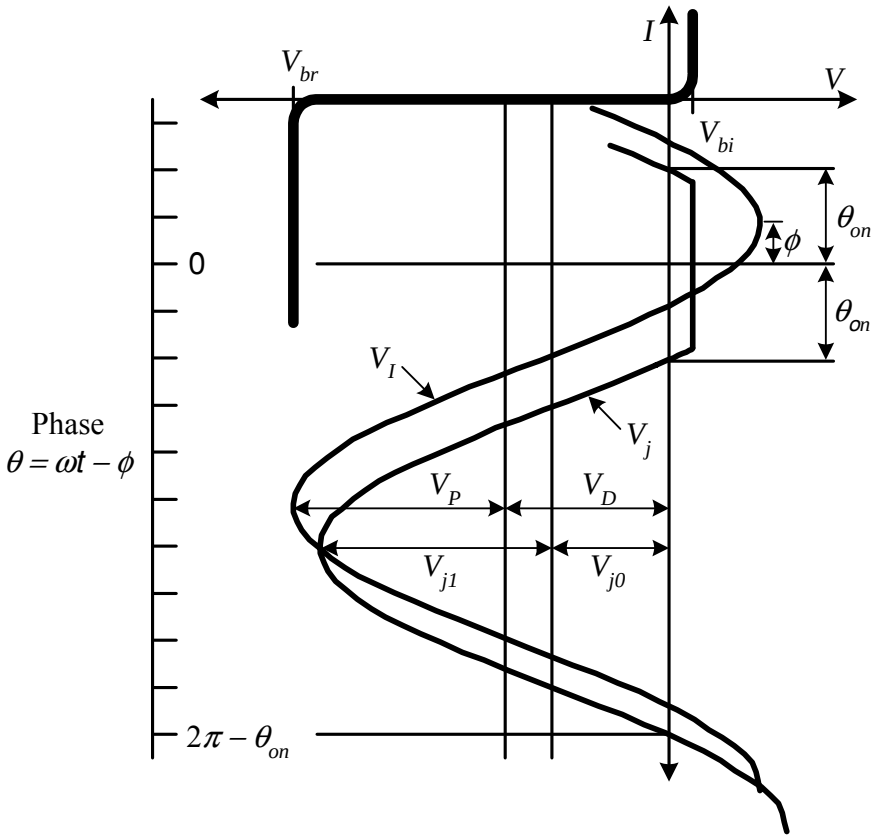

Fig. 3. Diode current-voltage characteristic curves with the incident fundamental and diode junction voltage waveforms.

B. Rectenna operation theory

The basic operation theory of the half-wave rectifier can be found in [53]. The rectenna operation theory has been studied in [11], [12], and [50], and parts of important concepts are reviewed here. Figure 3 shows a RF voltage waveform operating across the

diode and the diode junction voltage. This model assumes the harmonic impedances seen by the diode are either zero of infinite that avoids the power loss by the harmonics. The fundamental voltage wave will not be corrupted by the higher order harmonic components. Then the rectenna conversion efficiency only depends on the diode electrical parameters and the circuit losses at DC and the fundamental frequency.

The voltage waveform can be expressed as

$$V_I = -V_D + V_P \cos(\omega t) \tag{6}$$

where V_D is the self-bias DC output voltage across the resistive load R_L, and V_P is the peak voltage amplitude of the incident RF power. The rectifying diode acts as a mixer that produces a self-bias voltage. As the incident power is increased, the rectified self-biasing will become more reversed biased. The diode junction voltage is

$$V_j = \begin{cases} -V_{j0} + V_{j1} \cos(\omega t - \phi), & V_j < V_{bi} \\ V_{bi}, & V_j \geq V_{bi} \end{cases} \tag{7}$$

where V_{j0} and V_{j1} are the DC and fundamental frequency components of the diode junction voltage, respectively; V_{bi} is the diode's built-in turn-on voltage; θ_{on} is the forward bias turn-on angle. When the junction voltage exceeds V_{bi}, the diode will operate in forward conduction. Figure 3 also shows that the diode's junction waveform slightly lags the incident power by a phase difference ϕ.

The equivalent circuit used to determine the diode's efficiency is shown in Figure 4. The diode parasitic reactive elements are excluded from the circuit. The diode model consists of a series resistance R_S, a nonlinear junction resistance R_j, a non-linear junction

capacitance C_j, and a load resistor R_L. The junction rsistance R_j is assumed to be zero for forward bias and infinite for reverse bias. Applying Kirchoff's voltage law in the equivalent circuit, we have

$$V_D + I_D R_S + V_{j,dc} = 0 \tag{8}$$

With $V_D = I_D R_L$, the DC output voltage is given by

$$V_D = -V_{j,dc} \frac{R_L}{R_S + R_L} \tag{9}$$

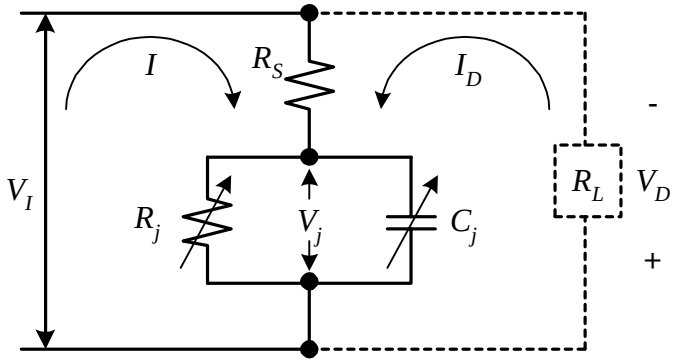

Fig. 4. Equivalent circuit model of the half-wave rectifier.

The DC output voltage is determined from the rectified voltage across the diode junction V_j. In each cycle, the average value of V_j is

$$V_{j,dc} = \frac{1}{2\pi} \int_{-\theta_{on}}^{\theta_{on}} V_{bi}\, \mathrm{d}\theta + \frac{1}{2\pi} \int_{\theta_{on}}^{2\pi-\theta_{on}} \left(-V_{j0} + V_{j1} \cos\theta\right) \mathrm{d}\theta \tag{10}$$

The first term and the second term represent the forward-biased and the reverse-biased cases. Integrate the equation gives

$$V_{j,dc} = \frac{\theta_{on}}{\pi} V_{bi} - V_{j0}\left(1 - \frac{\theta_{on}}{\pi}\right) - \frac{V_{j1}}{\pi}\sin\theta_{on} \tag{11}$$

When the diode switches from off to on, $V_j = V_{bi}$. Then we have

$$-V_{j0} + V_{j1}\cos\theta_{on} = V_{bi} \tag{12}$$

When the diode is off, R_j is infinite. Applying Kirchoff's voltage to the other loop gives

$$-V_I + IR_S + V_j = 0 \tag{13}$$

with

$$I = \frac{dC_j V_j}{dt} \tag{14}$$

These two equations can be rewritten by

$$\frac{d\left(C_j V_j\right)}{dt} = \frac{(V_I - V_j)}{R_S} \tag{15}$$

where C_j can be expressed as a harmonic function of V_D

$$C_j = C_0 + C_1\cos\left(\omega t - \phi\right) + C_2\cos\left(2\omega t - 2\phi\right) + \ldots \tag{16}$$

Using above two equations yields

$$\omega R_S\left(C_1 V_{j0} - C_0 V_{j1}\right)\sin\theta = V_{j0} - V_D + \left(V_P\cos\phi - V_{j1}\right)\cos\theta - V_P\sin\phi\sin\theta \tag{17}$$

where $\theta = \omega t - \phi$. Because this equation also holds for the off period, each sinusoidal term can be collected as

$$V_{j0} = V_D \tag{18}$$

$$V_{j1} = V_P\cos\phi \tag{19}$$

$$V_P \sin\phi = \omega R_S \left(C_1 V_{j0} - C_0 V_{j1} \right) \tag{20}$$

Substitute (18) to (11) and insert (9) into (11) give

$$\frac{R_S}{R_L} = \frac{V_{j1}}{V_D} \frac{1}{\pi} \sin\theta_{on} - \frac{\theta_{on}}{\pi} \left(1 + \frac{V_{bi}}{V_D} \right) \tag{21}$$

It can be shown that the phase difference ϕ can be approximated to be zero, which results in $V_P = V_{j1}$. Inserting this and (18) into (12) and (21) to obtain

$$\tan\theta_{on} - \theta_{on} = \frac{\pi R_S}{R_L \left(1 + \frac{V_{bi}}{V_D} \right)} \tag{22}$$

This transcendental expression allows obtaining θ_{on} iteratively, which is dependent on the diode input power that determines both V_{bi} and V_D.

The diode efficiency can be expressed as

$$\eta_D = \frac{P_{dc}}{P_L + P_{dc}} \tag{23}$$

where P_L is the power dissipated by the diode and P_{dc} is the DC output power across R_L. They are given by

$$P_L = L_{on,R_S} + L_{off,R_S} + L_{on,diode} \tag{24}$$

$$P_{dc} = \frac{V_o^2}{R_L} \tag{25}$$

The three terms of the diode loss P_L can be expressed by

$$L_{on,R_S} = \frac{1}{2\pi}\int_{-\theta_{on}}^{\theta_{on}} \frac{\left(V_I - V_{bi}\right)^2}{R_S} d\theta \tag{26}$$

$$L_{off,R_S} = \frac{1}{2\pi}\int_{\theta_{on}}^{2\pi-\theta_{on}} \frac{\left(V_I - V_d\right)^2}{R_S} d\theta \tag{27}$$

$$L_{on,diode} = \frac{1}{2\pi}\int_{-\theta_{on}}^{\theta_{on}} \frac{\left(V_I - V_{bi}\right)V_{bi}}{R_S} d\theta \tag{28}$$

Since it is assumed the junction resistance is infinite during the off cycle, the loss through the diode junction has been neglected. These power losses are the time-average products of the current flowing through an element and the voltage across the element. The total power dissipated on the series resistance can be solve by integrating

$$L_{R_S} = \frac{1}{2\pi R_S}\left[\int_{-\theta_{on}}^{\theta_{on}} \left(-V_D - V_{bi} + V_P\cos\theta\right)^2 d\theta + \left(\omega R_S C_j V_P\right)^2 \int_{\theta_{on}}^{2\pi-\theta_{on}} \sin^2\theta d\theta\right] \tag{29}$$

Using the RF current instead of voltage in the second integral, (27) can be rewritten as

$$L_{off,R_S} = \frac{1}{2\pi}\int_{\theta_{on}}^{2\pi-\theta_{on}} \frac{\left(V_I - V_j\right)^2}{R_S} d\theta = \frac{1}{2\pi}\int_{\theta_{on}}^{2\pi-\theta_{on}} \frac{\left(IR_S\right)^2}{R_S} d\theta \tag{30}$$

where I is the RF current flowing through the diode in reverse bias. It is assumed that no current flows through R_j in reverse bias and all of the current flowing through R_S flows through C_j. Then (14) can be expressed as

$$I = C_j \frac{dV_j}{dt} \tag{31}$$

The voltage drop across R_S is so small in the off cycle that the phase difference ϕ is set

zero. Apply this in (21) to obtain $V_{j1} = V_P$. Then

$$I = C_j \frac{d}{dt}\left[-V_{j0} + V_P \cos(\omega t)\right] = -\omega C_j V_P \sin\theta \tag{32}$$

The power dissipated by the diode junction is rewritten as

$$L_{diode} = \frac{1}{2\pi R_S} \int_{-\theta_{on}}^{\theta_{on}} V_{bi}\left(-V_D - V_{bi} + V_P \cos\theta\right) d\theta \tag{33}$$

where V_P is determined, while the diode is off, by

$$V_P = \frac{V_D + V_{bi}}{\cos\theta_{on}} \tag{34}$$

Use the results from (29) and (33) and insert them into (23), we have

$$\eta_D = \frac{1}{1 + A + B + C} \tag{35}$$

where

$$A = \frac{R_L}{\pi R_S}\left(1 + \frac{V_{bi}}{V_D}\right)^2 \left[\theta_{on}\left(1 + \frac{1}{2\cos^2\theta_{on}}\right) - \frac{3}{2}\tan\theta_{on}\right] \tag{36}$$

$$B = \frac{R_S R_L C_j{}^2 \omega^2}{2\pi}\left(1 + \frac{V_{bi}}{V_D}\right)\left(\frac{\pi - \theta_{on}}{\cos^2\theta_{on}} + \tan\theta_{on}\right) \tag{37}$$

$$C = \frac{R_L}{\pi R_S}\left(1 + \frac{V_{bi}}{V_D}\right)\frac{V_{bi}}{V_D}\left(\tan\theta_{on} - \theta_{on}\right) \tag{38}$$

with $\omega = 2\pi f$. The diode junction capacitance is given by

$$C_j = C_{j0}\sqrt{\frac{V_{bi}}{V_{bi} + |V_D|}} \tag{39}$$

where C_{jo} is the zero bias junction capacitance of the diode

The input impedance of the diode can be decided from the current I flowing through R_S in one cycle, that is

$$I = I_0 + I_{1r}\cos(\omega t) + I_{1i}\sin(\omega t) \tag{40}$$

where I_0 is the DC component; I_{1r} and I_{1i} are the real and imaginary parts of the fundamental frequency component, respectively. These current components are

$$I_0 = \frac{1}{2\pi R_S}\left\{\int_{-\theta_{on}}^{\theta_{on}}\left(V_I - V_{bi}\right)d\theta + \int_{\theta_{on}}^{2\pi-\theta_{on}}\left(V_I - V_j\right)d\theta\right\} \tag{41}$$

$$I_{1r} = \frac{1}{\pi R_S}\left\{\int_{-\theta_{on}}^{\theta_{on}}\left(V_I - V_{bi}\right)\cos(\theta+\phi)\,d\theta + \int_{\theta_{on}}^{2\pi-\theta_{on}}\left(V_I - V_j\right)\cos(\theta+\phi)\,d\theta\right\} \tag{42}$$

$$I_{1i} = -\frac{1}{\pi R_S}\left\{\int_{-\theta_{on}}^{\theta_{on}}\left(V_I - V_{bi}\right)\sin(\theta+\phi)\,d\theta + \int_{\theta_{on}}^{2\pi-\theta_{on}}\left(V_I - V_j\right)\sin(\theta+\phi)\,d\theta\right\} \tag{43}$$

The diode input impedance at the fundamental frequency is

$$Z_D = \frac{V_P}{I_{1r} - jI_{1i}} \tag{44}$$

Assume that there is no current flow through C_j during forward bias and that all current flow through during reverse bias, the diode current in one cycle can be found by integrating

$$I_{1r} - jI_{1i} = \frac{1}{\pi R_S}\int_{-\theta_{on}}^{\theta_{on}}\left(-V_D - V_{bi} + V_P\cos\theta\right)\cos\theta\,d\theta + j\frac{\omega C_j V_P}{\pi}\int_{\theta_{on}}^{2\pi-\theta_{on}}\sin^2\theta\,d\theta \tag{45}$$

The second integral is solved similar to that in (29). Then the diode input impedance can

be written as

$$Z_D = \frac{\pi R_S}{\cos\theta_{on}\left(\frac{\theta_{on}}{\cos\theta_{on}} - \sin\theta_{on}\right) + j\omega R_S C_j \left(\frac{\pi - \theta_{on}}{\cos\theta_{on}} + \sin\theta_{on}\right)} \tag{46}$$

If the reactance of the diode impedance is tuned out by using the impedance matching, the diode input impedance can be rewritten as

$$R_D = \frac{\pi R_S}{\cos\theta_{on}\left(\frac{\theta_{on}}{\cos\theta_{on}} - \sin\theta_{on}\right)} \tag{47}$$

The input resistance is a dynamic variable dependent on the input power, as the same as the diode efficiency.

3. Single rectenna element design

A. Rectenna components

The newly developed dual-diode rectenna is shown in Figure 5. It consists of a pair of circular polarized truncated patch antennas, a harmonic-rejecting bandpass filter (BPF) to suppress harmonic signals, two detector diodes for RF-to-DC conversion, and a DC pass filter (the capacitor). The load resistance will affect the output voltage and the rectenna efficiency. The CP truncated patch antenna fed by the coplanar stripline has a high gain and high radiation efficiency. The circuit and antenna can be duplicated and extended to form a traveling-wave antenna array. The BPF passes the generated 5.8 GHz signal and blocks high-order harmonic signals, up to the third-order, from the rectifying diodes. After passing through the diodes, RF power is rectified to become DC power.

The conversion efficiency of the diode is a key factor in determining the rectenna performance. The DC pass filter can not only tune out the reactance of the diode but also block unwanted RF signals from reaching the resistive load. The circuit is printed on the RT/Duroid 5880 substrate. There is no need for any via holes. A full-wave 3-D electromagnetic simulator IE3D [54] is used to design the coplanar stripline, CPS patch antenna, and CPS bandpass filter.

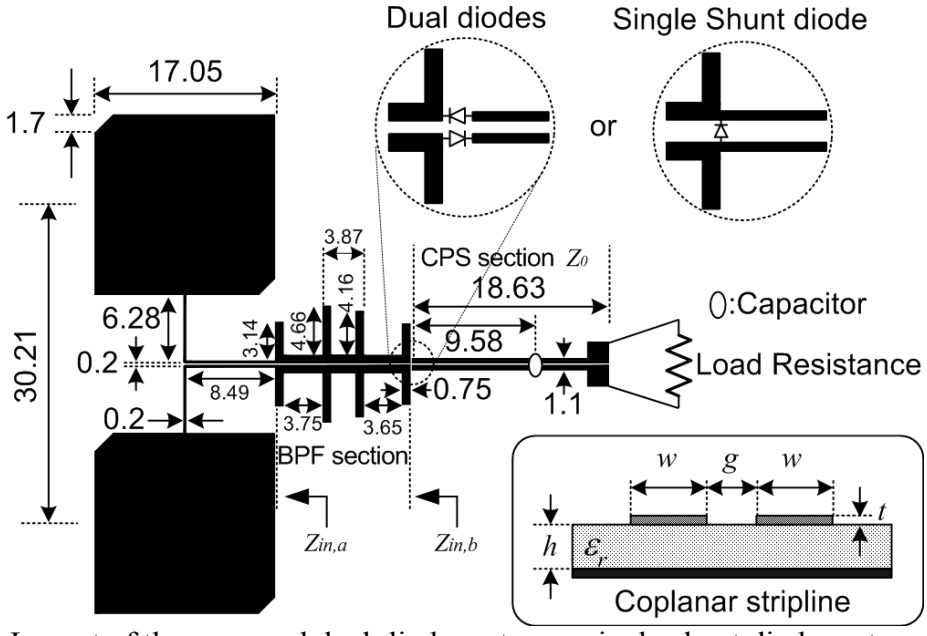

Fig. 5. Layout of the proposed dual-diode rectenna, single-shunt diode rectenna, and the CPS. All dimensions are in millimeter.

B. Coplanar stripline parameters

The coplanar stripline is shown in the inset of Figure 5. The CPS gap (g) is 0.2 mm and width (w) is varied on each section including the antenna feed line, the BPF, and the transmission line for the purpose of impedance matching. The substrate thickness (h) is

0.508 mm (= 20 mil) and the dielectric constant (ε_r) is 2.2. The conductor thickness (t) is 1 oz copper whose metal thickness is 0.036 mm (= 1.4 mil). At 5.8 GHz, the effective dielectric constant ($\varepsilon_{r,eff}$) of the transmission line section (the coplanar stripline from the diode to the load resistance) is 1.84, the guided-wavelength λ_g is 38.06 mm, and its characteristic impedance (Z_0) is 120 Ω. This Z_0 is chosen to match the impedances of the antenna with BPF and the diode [11-14] to reduce the signals reflections between these components.

C. Circularly polarized truncated patch antenna (CP TPA)

The truncated patch antenna has become a popular circular polarized antenna and has been widely used in many systems. The advantage of circular polarization is that the rectenna performance is not significantly affected due to the rotation of the circuit. Usually a single microstrip patch antenna cannot provide high enough gain. Here a novel feeding technique is developed to use a CPS line to feed two CP microstrip patch antennas. The maximum power can be transmitted to the BPF and the losses due to the transition between the patch and the CPS is minimized. Since two patches are used, the antenna gain is increased. The layout of the CPS CP TPA designed for 5.8 GHz is given in Figure 5. The length and width of the patch antenna and its truncated position need to be designed carefully for good antenna performance, especially for low axial ratio (AR). In this case, the truncated position yields a left-hand circular polarization. A right-hand circular polarization can be obtained by truncating the rectangular patch on the other two apexes. To evaluate the rectenna performance, the antenna should be combined together

with the bandpass filter to determine its input impedance and radiation pattern because the bandpass filter will couple to the antenna and hence affect the antenna performance. At this time, the CPS CP TPA has a gain of 6.87 dBi and an AR of 0.14 dB. Its input impedance ($Z_{in,a}$) is 100 Ω.

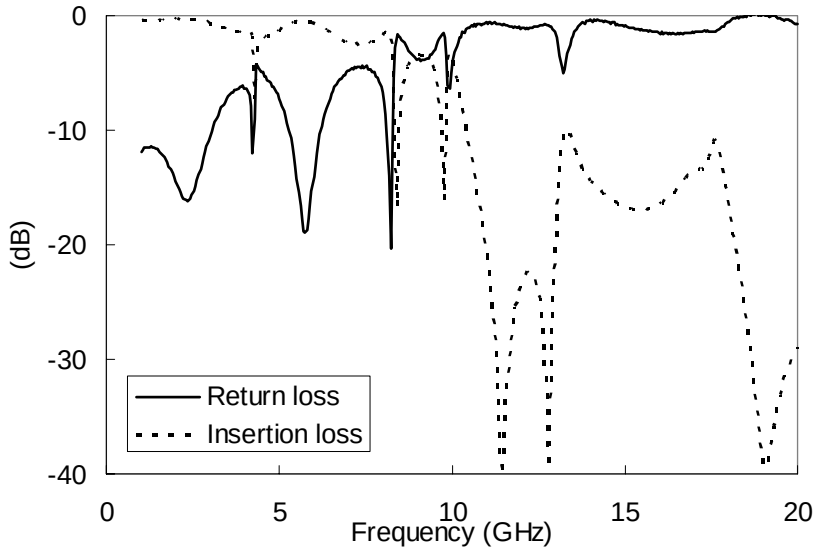

Fig. 6. Measured return loss and insertion loss of the CPS BPF.

TABLE 1. Measured return and insertion losses at fundamental and harmonic frequencies.

Frequency (GHz)	5.8	11.6	17.4
Return Loss (dB)	17.73	0.52	0.81
Insertion Loss (dB)	0.48	32.08	12.02

D. Coplanar stripline bandpass filter (CPS BPF)

A CPS bandpass filter is designed to pass a 5.8 GHz signal from the antenna to

the rectifying circuit. The BPF layout is given in Figure 5. By tuning the size of these stubs, high-order harmonics can be blocked or passed. The BPF was tested by embedding two microstrip baluns to connect the BPF feed lines, i.e., its input and output ports. They have to be used to connect the filter to the coaxial cable connectors of the HP8510C network analyzer. Measured return loss and insertion loss of the CPS BFP are shown in Figure 6. At 5.8 GHz, the return loss and the insertion loss from the antenna to the diode are 17.73 dB and 0.48 dB, respectively. The CPS BPF can effectively block the second and the third harmonics of 11.6 GHz and 17.4 GHz, generated from the rectifying circuit to the patch antenna, as summarized in Table 1. Furthermore, the filter can be used to match the resistance of the antenna to that of the detector diode.

E. CP TPA and CPS BPF

Before integrating the patch antenna and the bandpass filter with the detector diode and the DC pass filter, it is necessary to combine CP TPA and CPS BPF. The feed line of the antenna has been tuned to match the filter. Figure 7 shows the measured return loss for CPS CP TPA and BPF. The bandwidth of 2:1 VSWR at the fundamental frequency of 5.8 GHz is about 4%. The measured CP antenna gain and the AR are shown in Figure 8. At 5.8 GHz, it has a gain of 6.38 dBi and an AR of 0.42 dB. The input impedance ($Z_{in,b}$) is 120 Ω. Due to the coupling between the antenna and the BPF, the antenna performance is slightly changed.

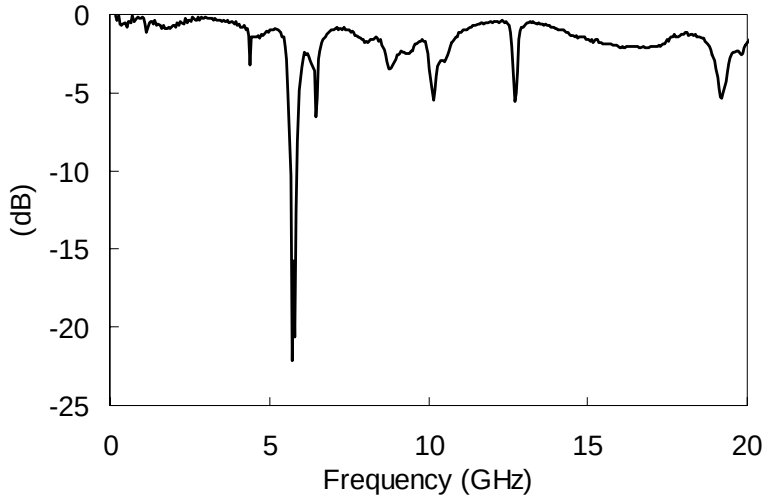

Fig. 7. Measured return loss of the CP antenna with the CPS BPF.

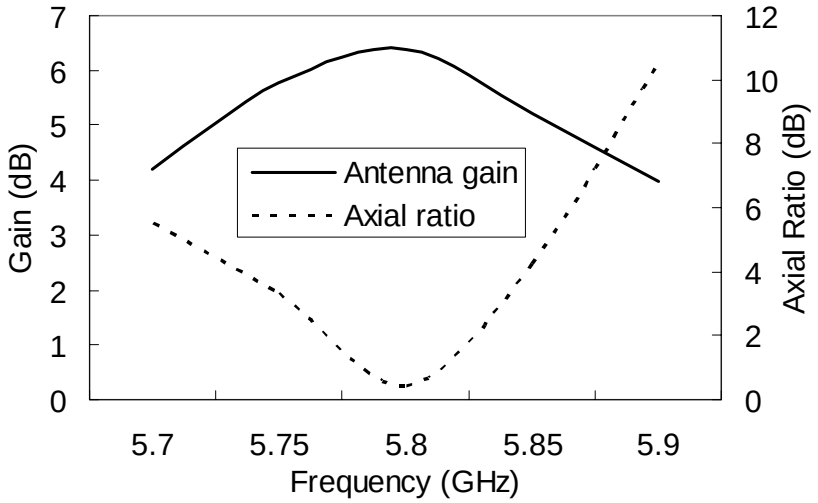

Fig. 8. Measured gain of the CP antenna with the CPS BPF and its axial ratio.

F. Detector diode and DC pass filter

The diodes used in this dissertation are the GaAs flip chip Schottky barrier diodes (Model MA4E1317) from M/A COM. It has a series resistance R_S = 4 Ω, zero-bias junction capacitance C_{j0} = 0.02 pF, forward-bias turn-on voltage V_{bi} = 0.7 V, and

breakdown voltage V_B = 7 V. The junction capacitance (C_j) of the diode, described in (39), significantly affects the diode efficiency, which is a function of the diode output voltage. Equation (39) is rewritten here for convenience

$$C_j = C_{j0}\sqrt{\frac{V_{bi}}{V_{bi}+|V_D|}} \tag{48}$$

V_D is the output self-bias voltage of the diode. Higher V_D results in a smaller junction capacitance, which also gives better conversion efficiency. The maximum efficiency occurs when C_j approaches to zero. Furthermore, the diode should operate as close to its voltage limit as possible to minimize its reactance. This reduces the reflection of the RF power at the diode terminal and hence increases the rectenna efficiency.

In [50], Yoo and Chang proposed a diode model to predict the rectenna performance. The theoretical equation to calculate the RF-to-DC conversion efficiency based on that model has been reviewed in Section 1 of this chapter and it has been shown that the equation can correctly predict the performance of the 2.45 and 5.8 GHz rectennas by using the coplanar stripline structure [12-14]. For the dual-diode circuit, replace R_L in (36)-(38) by (R_L+R_D) and R_S by (R_S+R_L) where R_L is the load resistance and R_D is the resistance of the diode. It is assumed that the diode reactance is tuned out. The input resistance of the diode can be found in (46). It is noted that the diode impedance is dependent on the output voltage, which is affected by the input RF power.

A broadband DC-blocking chip capacitor by Dielectric Laboratories (Model C08BLBB1X5UX) is chosen as the DC pass filter. The DC pass filter not only tunes out the reactance of the diode but also blocks the unwanted RF signals from reaching the

load resistance. The detector diode and the DC-blocking capacitor are mounted across the coplanar stripline by using silver epoxy.

G. Rectenna measurement

The measurement method for the circular polarized rectenna test has been studied in [11]. The equipment setup is shown in Figure 9. The RF-to-DC efficiency of the rectenna (η) can be defined as

$$\eta = \frac{P_{DC}}{P_r} \tag{49}$$

P_{DC} is the DC output power. The Friis transmission equation is used to calculate the power propagating to the CP antenna (P_r). A NARDA standard horn antenna with a 15 dB gain (G_t) is used to transmit the RF power (P_t), and the rectenna gain (G_r) is set equal to 6.38 dB. By changing the distance between the horn antenna and the rectenna, the efficiencies for different power densities are determined. The power density (P_d) is given by

$$P_d = \frac{P_t G_t}{4\pi D^2} \tag{50}$$

where D is the distance between the horn antenna and the center of the rectenna array.

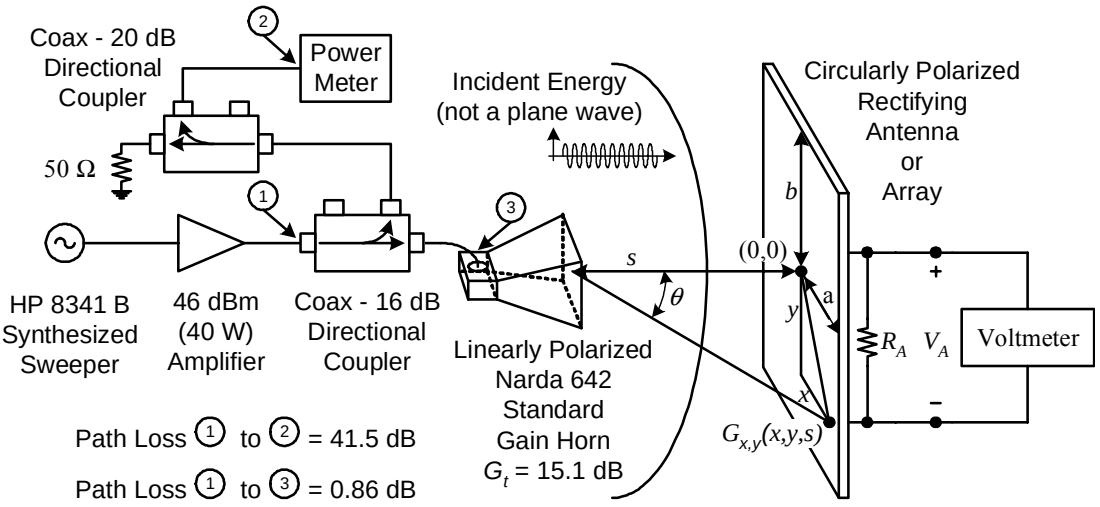

Fig. 9. Free space measurement setup of the rectenna or rectenna array [11].

Figure 10 shows the measured DC output voltage as a function of the power density for various diode configurations and external resistive loads. To compare the rectenna with that of a single shunt diode across the CPS shown in Figure 5, its measured results are also shown in Figure 10. The single shunt diode rectenna can be viewed as a traditional half-wave rectifier antenna. It is obvious that the newly developed rectenna can produce at least twice the DC voltage of a single shunt diode rectenna, despite their same layout dimension. The maximum output voltage ratios of the dual-diode rectenna to the single shunt diode rectenna using 100, 150, 200, and 300 Ω loadings are 2.7, 2.5, 2.6, and 2.5 respectively. There is a similar trend between the rectennas that a higher load resistance will also have a higher output voltage. These results demonstrate that the dual-diode rectenna has a stable performance and can produce higher output comparable to the single shunt rectenna. As the output voltage reaches 11-12 V, the rectenna will be "saturated." After that, the first diode of the

rectifying circuit may break down due to excessive power.

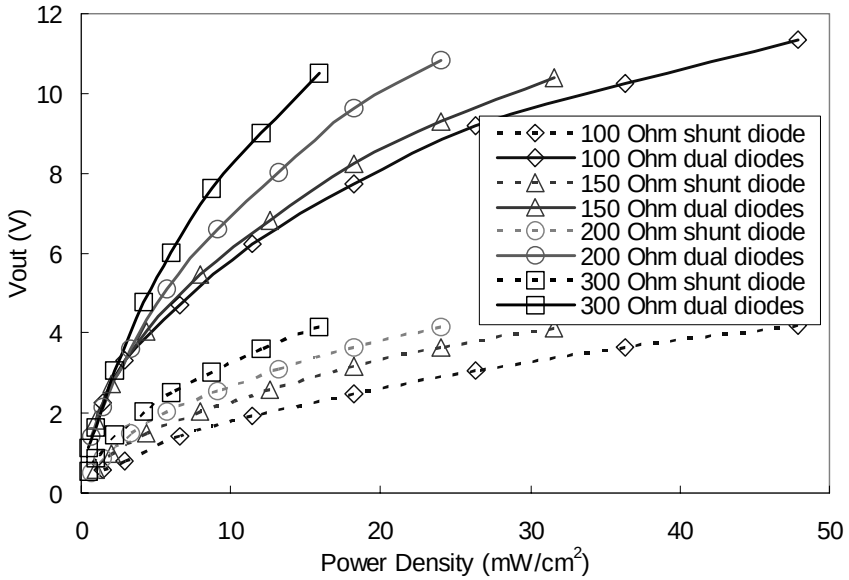

Fig. 10. DC output voltages of the dual-diode and single-shunt diode rectennas.

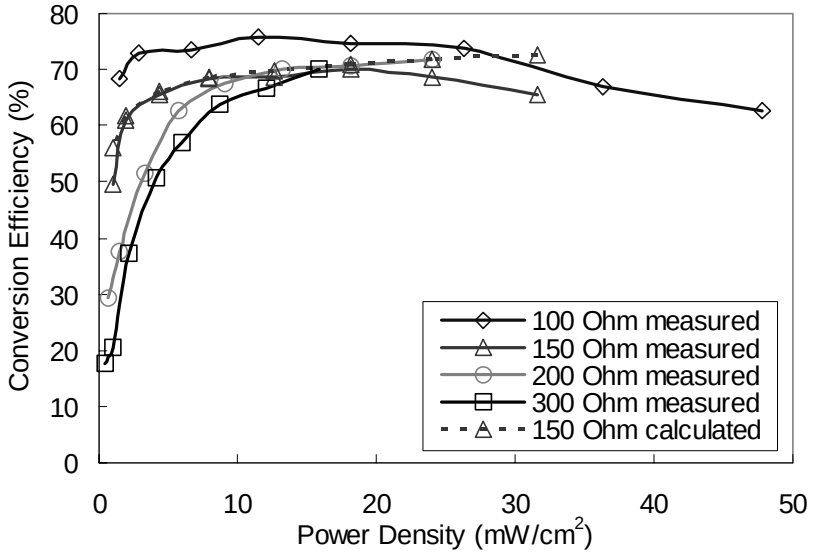

Fig. 11. Measured and calculated conversion efficiencies of the dual-diode rectenna.

Figure 11 shows the RF-to-DC conversion efficiency as a function of the power density for various loadings. Calculated efficiency agrees well with the measured result. The best efficiency, 76%, occurs at a 100 Ω loading while the DC output voltage is 6.22 V. The efficiencies using other loadings are around 70%. It is observed that the efficiency gradually decreases as the load resistance increases, which displays a trend similar to the result reported in [7].

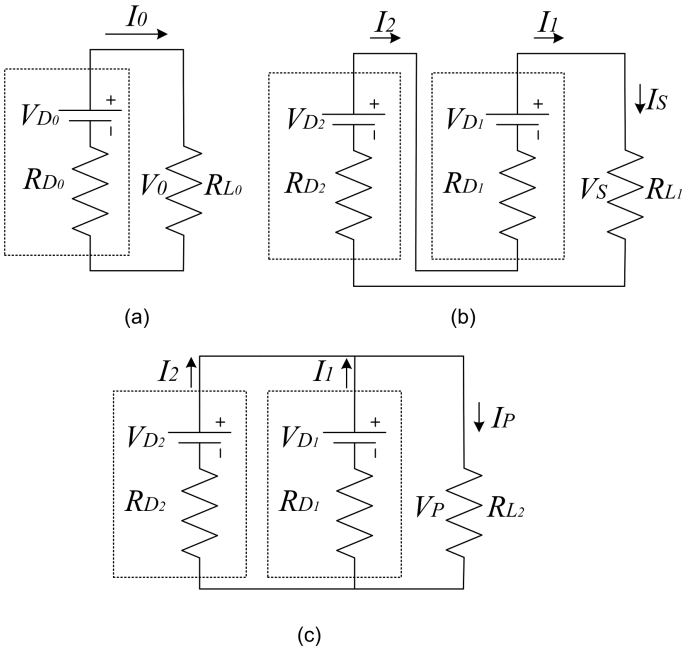

Fig. 12. Linear equivalent circuit model of the rectenna: (a) single element, (b) series connection, and (c) parallel connection. V_{Di} and R_{Di} are equivalent voltage and resistance of the rectifying circuit. I_i and V_i are the current and voltage provided from the rectifying circuit to the output load. R_{Li} is the load resistance.

4. Rectenna array design

In most recent rectenna developments, researchers focus on the study of single rectenna element design. However, it is necessary to develop a rectenna array when a

large DC voltage is desired. Here, rectenna elements are connected to form a rectenna array by different interconnections. Since each interconnection has its own output feature, a simple linear equivalent model is formulated to predict the performance of the rectenna array. The array using the same rectenna elements usually has better performance. However, in practice, careful element position arrangement may be needed when each element receives relatively different power.

A. Linear equivalent model

Each rectifying circuit is a non-linear device so using a non-linear model to analyze the circuit behavior is preferred. Theoretically, the non-linear model should be able to describe the circuit characteristics for the whole range of loadings. In our study, for the purpose of easy analysis, the rectenna is modeled as a linear device. The linear model has been shown to be effective in predicting the output power when the optimum load resistance is used for the rectenna [28]. The equivalent linear model of the single rectenna element is shown in Figure 12(a). Using that equivalent circuit, an analytical model of different rectenna connections can be built. The circuit parameters of the single rectenna element can be expressed by

$$I_0 = \frac{V_{D_0}}{R_{D_0} + R_{L_0}}; V_0 = \frac{V_{D_0} R_{L_0}}{R_{D_0} + R_{L_0}}; P_0 = \frac{V_{D_0}^2 R_{L_0}}{\left(R_{D_0} + R_{L_0}\right)^2} \tag{51}$$

The maximum transferred power, or efficiency, can be obtained by choosing $RD_0 = RL_0$. For the series connection, as shown in Figure 12(b), the circuit parameters are given by

$$I_S = \frac{V_{D_1} + V_{D_2}}{R_{D_1} + R_{D_2} + R_{L_1}} \tag{52}$$

$$V_S = \frac{\left(V_{D_1} + V_{D_2}\right) R_{L_1}}{R_{D_1} + R_{D_2} + R_{L_1}} \tag{53}$$

$$P_S = \frac{\left(V_{D_1} + V_{D_2}\right)^2 R_{L_1}}{\left(R_{D_1} + R_{D_2} + R_{L_1}\right)^2} \tag{54}$$

Assume each rectenna element is the same. Then let $RD_1 = RD_2 = RD_0$ and $RL_1 = RD_1 + RD_2 = 2RL_0$ for the maximum power output, above equations can be rewritten as

$$I_S = \frac{V_{D_1} + V_{D_2}}{2\left(R_{D_0} + R_{L_0}\right)} = \frac{1}{2}\left(I_1 + I_2\right) \tag{55}$$

$$V_S = \frac{\left(V_{D_1} + V_{D_2}\right) R_{L_0}}{\left(R_{D_0} + R_{L_0}\right)} = \left(V_1 + V_2\right) \tag{56}$$

$$P_S = I_S V_S = \frac{\left(I_1 + I_2\right)}{2} \cdot \left(V_1 + V_2\right) \tag{57}$$

In a similar way, the circuit parameters of the parallel connection, as shown in Figure 12(c), are given by

$$I_P = \frac{V_{D_1} + V_{D_2}}{R_{D_0} + R_{L_0}} = \left(I_1 + I_2\right) \tag{58}$$

$$V_P = \frac{\left(V_{D_1} + V_{D_2}\right) R_{L_0}}{2\left(R_{D_0} + R_{L_0}\right)} = \frac{1}{2}\left(V_1 + V_2\right) \tag{59}$$

$$P_P = I_P V_P = \left(I_1 + I_2\right) \cdot \frac{\left(V_1 + V_2\right)}{2} \tag{60}$$

The relation that $RL_2 = (1/RD_1 + 1/RD_2)^{-1} = RL_0/2$ has been used for the maximum efficiency. In theory, series connection should generate twice the output voltage and parallel connection should generate the same output voltage as compared to the single element. Note that both series and parallel interconnections have equal DC output power

if the two rectenna elements are the same. If they are different, the output power may be lower. This can be represented by a difference coefficient k, i.e., let $I_2 = kI_1$ or $V_2 = kV_1$, which will result in $P_2 = k^2P_1$. Then the total output power becomes $(1+k^2)P_1$. If $k < 1$, then the output power decreases. In our experiment, each rectenna element has almost the same performance. This would make the analysis of the rectenna array easy.

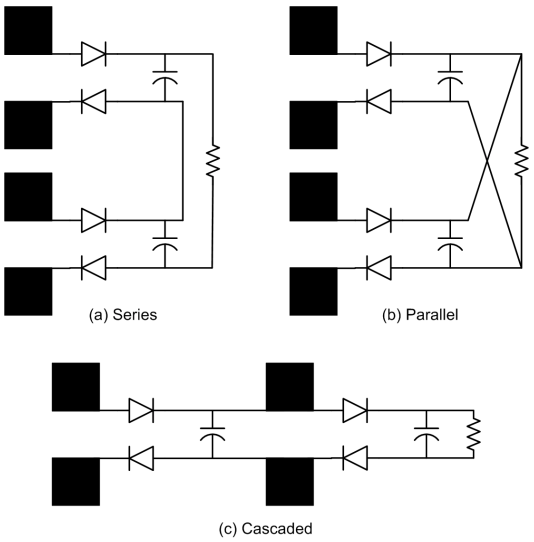

Fig. 13. Layout of the dual-diode rectenna array: (a) series, (b) parallel, and (c) cascaded.

B. Experiments of various rectenna arrays

Three types of rectenna interconnections were tested. They are series, parallel, and cascaded, as shown in Figure 13. The series rectenna array consists of two series-wound rectenna elements. The parallel rectenna array includes two rectenna elements sharing a load resistance together. The cascaded rectenna array can be viewed as a series-parallel circuit.

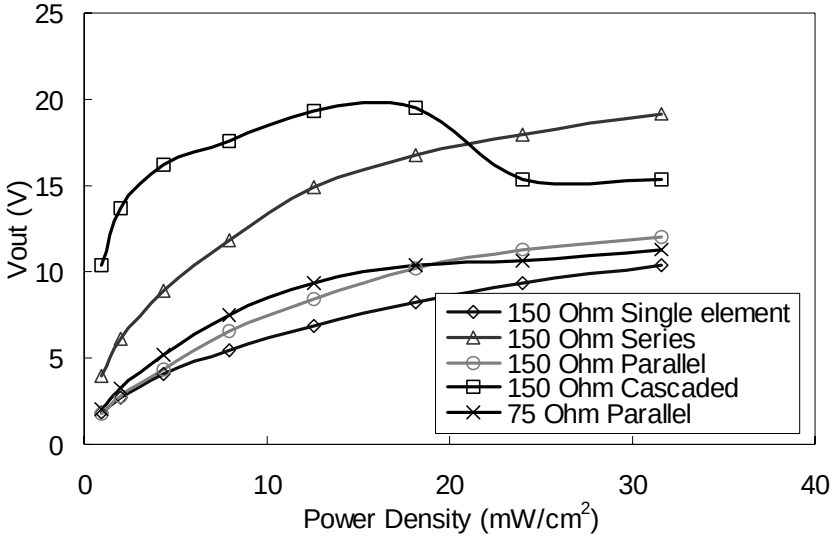

Fig. 14. Measured DC output voltage of the dual-diode rectenna array.

The measured DC output voltages of rectenna arrays are shown in Figure 14. The 150 Ω load resistance is used for the series, the parallel, and the cascaded connections; the 75 Ω load resistance is also used on the parallel connection for the maximum output power test. The measured result of the single rectenna element is also plotted as a comparison. For series and cascaded connections, it is found that the cascade connected rectenna array can provide more output voltage than that of a series connected rectenna array. However, both of them become saturated when the output voltage reaches around 20 V. At that time, each diode approximately rectifies a voltage of 5 V. When the output voltage is greater than 20 V, the detector diode rectifying the most power will break down. If the input power continues to increase, the diode will be burned-out. Then the output voltage and conversion efficiency will be reduced. These conditions also occur when other loadings are used. From measurement results, the first breakdown diode is

that in the upper-left side. Despite its breakdown, other diodes can still work. However, the antenna gain will be decreased resulting in poor rectenna array performance. For the parallel connection, it is found that the rectenna array can provide more voltage than the single rectenna element. Although various load resistances were tested, all of arrays generated output voltages close to one another for the same power density, which means the rectenna array with a smaller load can provide more output power. Similar to the single rectenna element, the rectenna array parallel connected saturates at 12 V.

Figure 15 compares the voltage ratio (VR) of three rectenna arrays to the single rectenna element. The series connected rectenna array provides about 2.1 times output voltage while the rectenna array parallel connected generates about 1.14 times output voltage. These results match the theoretical predictions well. This also implies that the parallel connection can support more output power than the series connection. On the other hand, it is obvious that the cascade connected rectenna array can give the highest output voltage. Its VR is always larger than two until the diodes break down. The measured results are comparable to those found by using a honeycomb lattice array that has nine rectenna elements which includes nine diodes [11]. In most cases, the cascaded rectenna array can provide high DC voltage with only two rectenna elements, which includes four diodes. This improved performance also happens with other loadings such as 100, 200, and 300 Ohms. Therefore, the cascaded rectenna array is very suitable for wireless power transmission of the low-power densities.

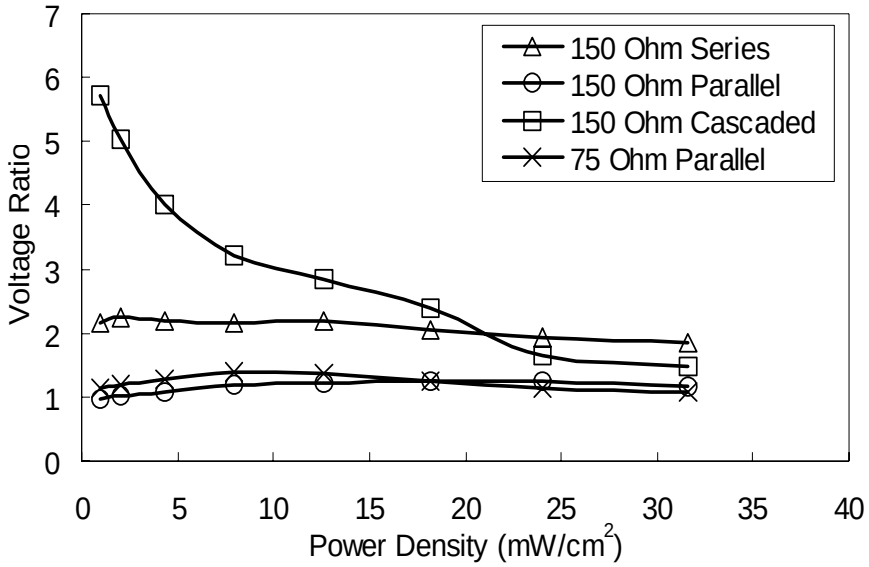

Fig. 15. Measured DC output voltage ratio of the interconnected rectenna array to the single rectenna element.

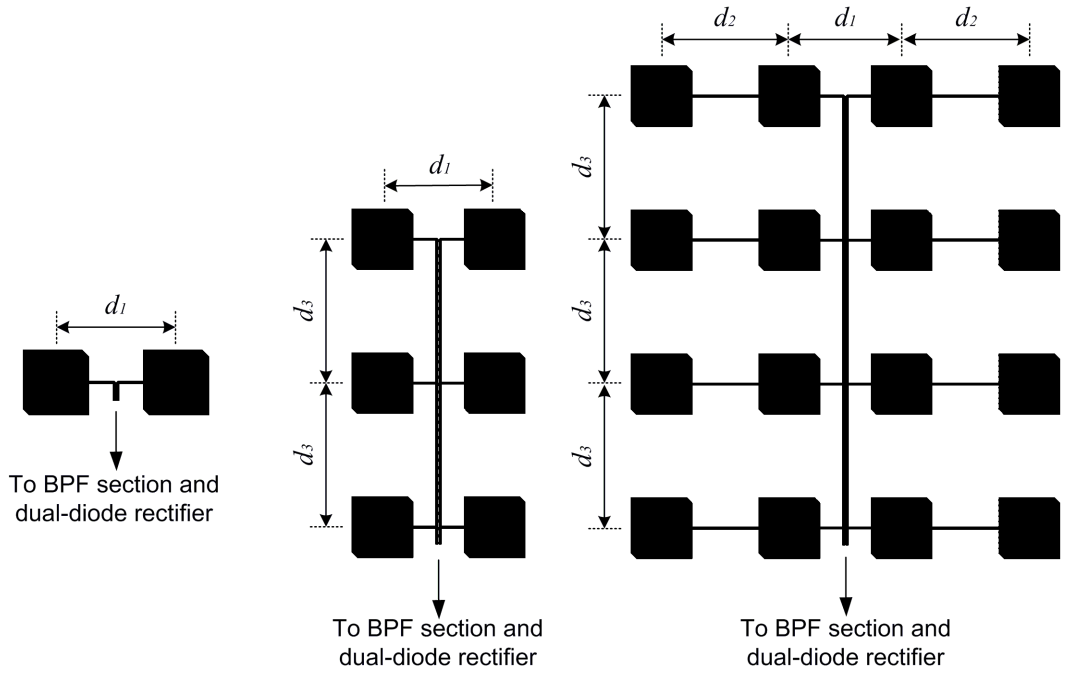

Fig. 16. (a) Dual-patch antenna, (b) 6-patch traveling wave antenna, and (c) 16-patch traveling wave array, where d_1 = 30.2 mm, d_2 = 35.49 mm, and d_3 = 38.06 mm.

C. Arrays for low power density applications

To achieve higher received power, the CPS dual-patch antenna, shown in Figure 16(a), can be extended to become a traveling wave antenna by series-feeding more CPS antenna elements. The wave will propagate from the feed point and travels toward to the end of the antenna. The separation distance of the elements can be designed to steer the antenna mainbeam from broadside.

One traveling wave antenna with three CPS dual-patch antenna elements is shown in Figure 16(b). By carefully designing the feeding system, the traveling wave antenna gain should be double when the patch element number is double. The antenna is still circularly polarized. This 6-patch traveling wave antenna has a gain of 12 dBi and an axial ratio of 0.73 dB. The 16-patch antenna, shown in Figure 16(c), has a gain of 16.5 dBi and an axial ratio of 1.33 dB.

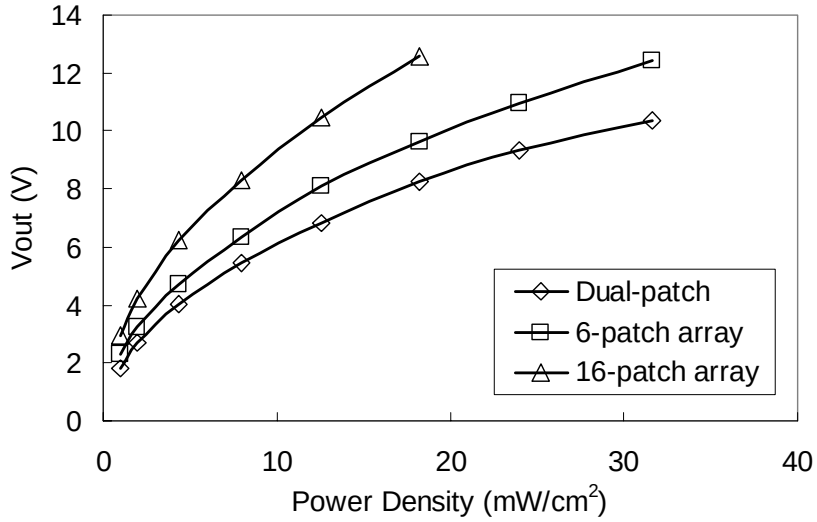

(a)

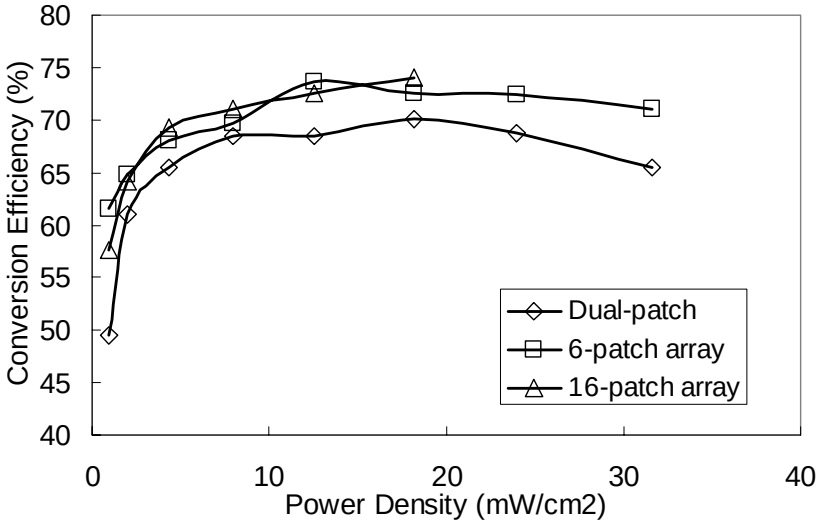

(b)

Fig. 17. Measured performance of the traveling wave rectenna: (a) output voltage and (b) conversion efficiency. The load resistance is 150 Ω.

Measured output voltage and conversion efficiency of the 6-patch traveling wave antenna are shown in Figure 17. The high gain antenna can supply higher DC voltage than that proposed previously with the same power density. However, the output voltage finally saturates at 11-12 volts and cannot exceed 13 V because the diode may be

burned-out. Its conversion efficiency is a slightly higher than that of the dual-patch array. The maximum efficiency is 74% corresponding to 8.12 V output voltage. An example of the array consisting of sixteen patches is shown in Figure 16(c). The 16-patch antenna can get more DC output voltage due to its higher gain. The maximum efficiency is 74% while the output voltage is 12.6 V. By a similar way as previously mentioned, a rectenna using the traveling wave antenna also could be interconnected to form a rectenna array, which is able to reach the requirement of the high output voltage and is suitable for long distance low-power density power transmission. For high output voltage application, a Zener device can be used to protect the rectifying circuit from breakdown.

5. Conclusions

In this chapter, a 5.8 GHz dual-diode rectenna and its arrays have been developed. A truncated dual-patch antenna achieves a circular polarized gain of 6.38 dBi and an axial ratio of 0.42 dB. A CPS bandpass filter is used to suppress the harmonic signals generated from the diodes by over 32 dB, which can block the second-order and the third-order harmonics. The dual-diode rectenna can provide a maximum efficiency of 76% with at least twice as much output voltage as compared to the single shunt diode rectenna, while their circuit layout dimensions are the same.

The rectenna has been interconnected to form different types of rectenna arrays. The cascaded rectenna array can produce the highest output voltage and power, which is very useful for the wireless power transmissions, even with a low power density. The measured results of series and parallel connected rectenna arrays agree very well with

the theoretical predictions. The parallel connected rectenna array can generate higher output power than the series connected rectenna array. It is noted that the diode of the rectenna should be protected from damage when the input power is high. The developed rectenna can be easily extended to form a traveling wave antenna or array, which would be very useful for the applications of long distance power transmission.

CHAPTER III

MICROWAVE CIRCULARLY POLARIZED RETRODIRECTIVE RECTENNA ARRAYS WITH HIGH-ORDER HARMONIC REJECTION*

1. Introduction

To receive high power for the future applications, a rectenna array is required. The rectenna array needs a precise mainbeam alignment for an efficient power transmission because the mainbeam of the rectenna array only has a limitedly narrow beam-width. If mainbeams of the transmitting and the receiving antennas cannot be aligned correctly, the rectenna efficiency would drop significantly. Although many kinds of rectennas have been proposed, most works are focused on the rectenna design using single antenna element without considering the application of the antenna array. Furthermore, despite the fact that circularly polarized antenna can preserve the output voltage constant when the transmitter or the receiver rotates, it cannot prevent the output voltage variation due to the improper mainbeam alignment.

In this chapter, a non-uniform rectenna is designed to overcome the sensitive alignment requirement, while a uniform rectenna is also designed for comparison. The

non-uniform rectenna has a broadened beam-width and the uniform rectenna has a narrower main beam. Both of them can be applied for the low power-density power transmission. However, the non-uniform rectenna with a widened beam-width can keep the output voltage invariant even if the rectenna has an improper beam alignment.

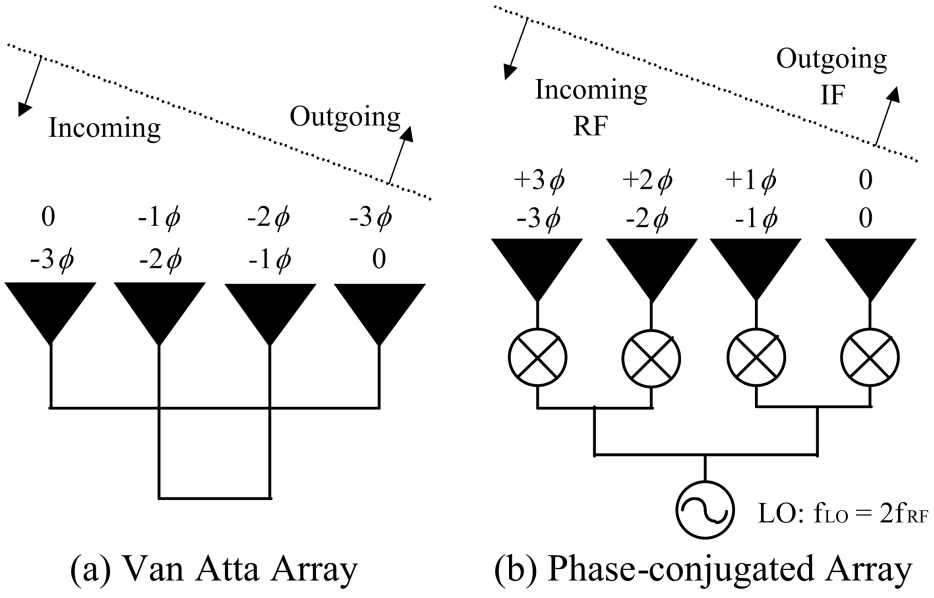

Fig. 18. Two basic architectures of the retrodirective arrays.

Next, two novel retrodirective rectenna arrays are demonstrated, which combine the Van Atta Array, as shown in Figure 18(a), with the rectennas. A circular polarized proximity-coupled microstrip antenna is developed as the array element because this antenna can be designed to block harmonic signals and can be used to easily build the Van Atta array. The antenna array elements are located on one dielectric layer and the circuits of the retrodirective array and the rectenna are located on the other dielectric layer. This two-layer structure provides easy design and fabrication for a large

retrodirective rectenna array. The new retrodirective array can track the power source automatically and hence keep the output voltage nearly constant. The 4x4 retrodirective rectenna arrays can be viewed as a four-series-connected 2x2 array so its output voltage should be four times when an optimum load is used.

Finally, an active retrodirective wireless power transmission system is proposed which uses the phase-conjugated array as shown in Figure 18(b). The system can be used for the long distance power transmission including the satellite communications systems and future space-to-space or ground-to-space power transmission.

2. Broadened beam-width rectenna array

A. Uniform and non-uniform rectenna arrays design

The antenna arrays are shown in Figure 19, which is designed based on the works conducted in Chapter II. The feed-line adopts a CPS structure. The circularly polarized truncated patch antenna is used as the antenna element. For the uniform antenna array, each patch element has a dimension of 17x17 mm^2. Each array has sixteen patches. The patches of the uniform array have the same size while the patches of the non-uniform array have different sizes in order to broaden the beam-width of the main beam. The four largest patch elements have a dimension of 27.8x27.8 mm^2. The area of the non-uniform array is slightly larger due to its irregular dimension change of the patch. However, it is noted that broadened beam-width array has a reduced gain, so there is a trade off between the antenna gain and the beam-width. Each array has a CPS bandpass filter, which has a return loss of 17.7 dB and an insertion loss of 0.48 dB at 5.8 GHz. At 11.6

GHz, it has a return loss of 0.52 dB and an insertion loss of 32.1 dB. The bandpass filter can effectively eliminate the second-order harmonic signals reradiated from the rectifying circuit.

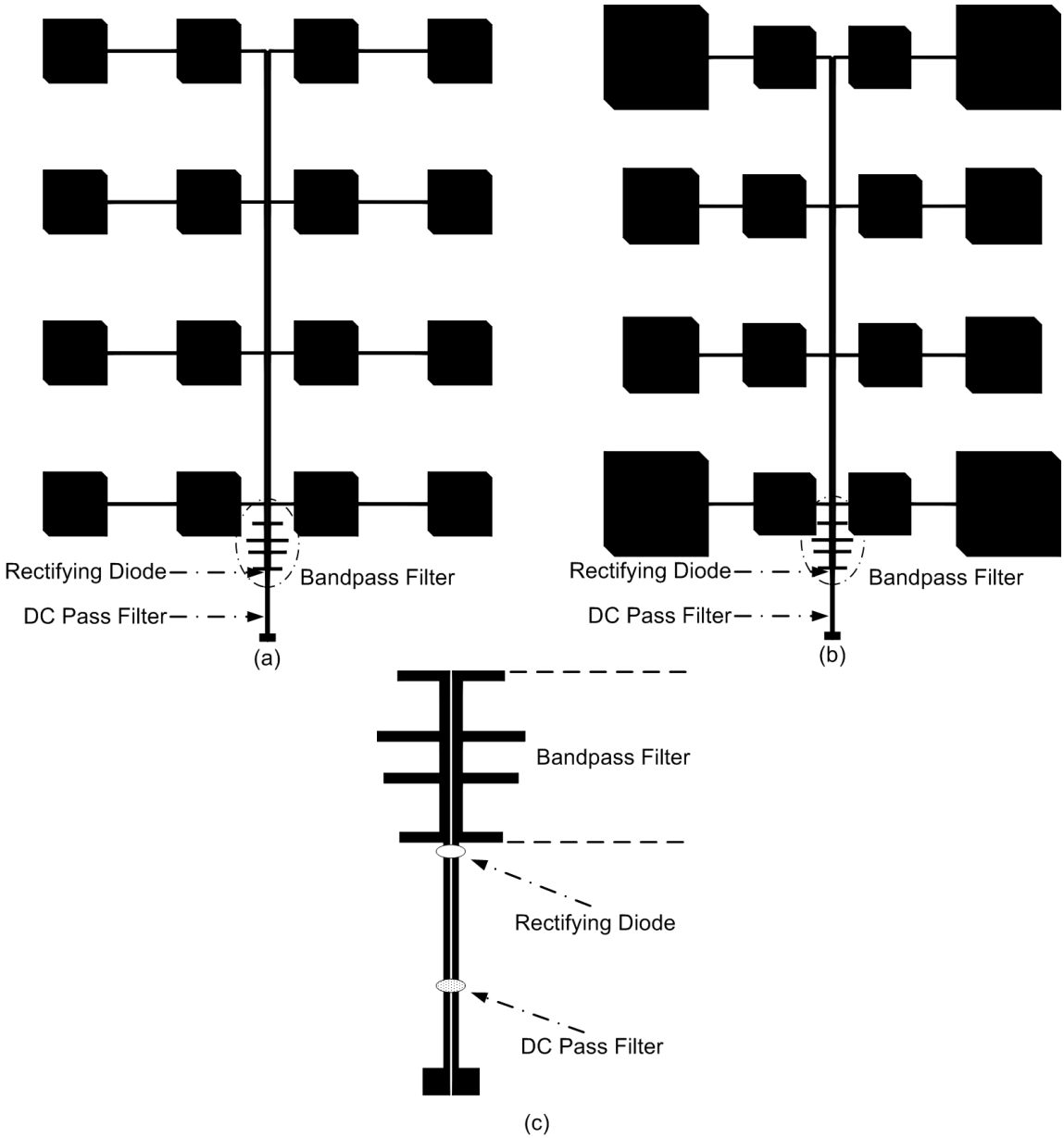

Fig. 19. Configurations of (a) uniform rectenna, (b) non-uniform rectenna, and (c) rectenna circuit and feed lines.

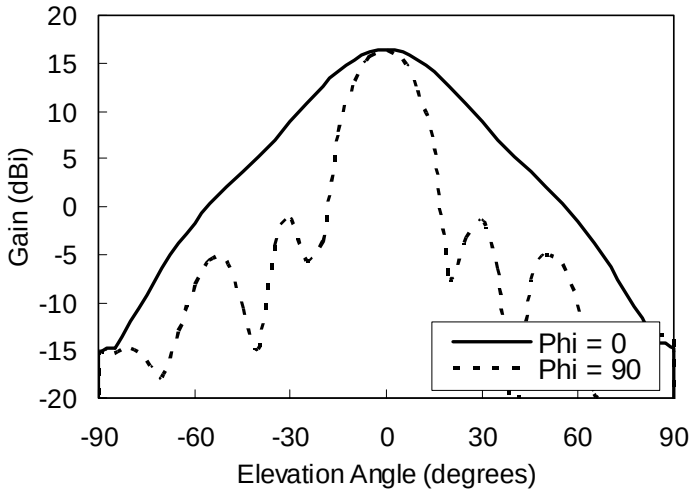

(a)

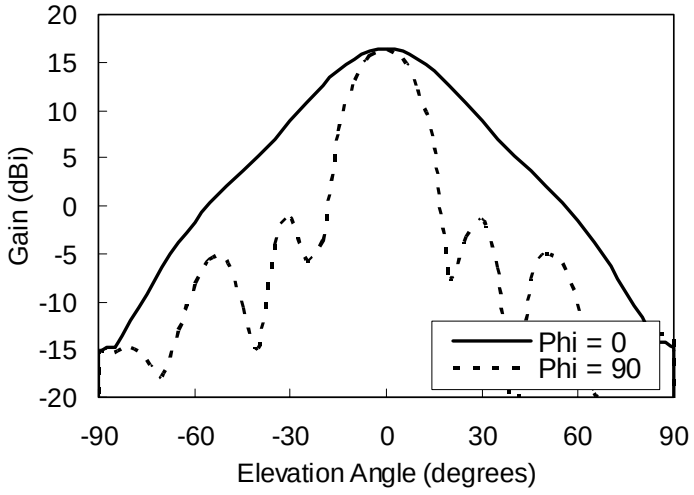

(b)

Fig. 20. Radiation patterns of (a) the uniform array and (b) the non-uniform array.

TABLE 2. Antenna array performance comparison at $\phi = 0^{o}$.

	Return Loss (dB)	Max. Gain (dBi)	Axial Ratio (dB)	HPBW (degrees)	BWFN (degrees)
Uniform array	14	18.8	1.34	19.8	50.4
Non-uniform array	17	16.4	1.81	34.7	180

Theoretically, antenna patterns on both E-plane and H-plane can be widened and they even can have uniform amplitude by a complex antenna element design [15]. To achieve that goal, many patches with various sizes are needed. Here, to simplify the design process, the number of patches is reduced. The antenna patterns in E-plane and H-plane are shown in Figure 20. It is observed that the gain of the non-uniform array at the broadside direction decreases, but its main beam beam-width increases obviously. A comparison between these two arrays is summarized in Table 2, where HPBW and BWFN are half power bandwidth and bandwidth between first nulls, respectively.

B. Rectenna array measurements

The measurement method of the uniform and non-uniform rectenna is the same as that testing the rectenna mentioned in last chapter. Measured DC output voltage and rectenna efficiency of the uniform and the non-uniform rectennas are shown in Figure 21. These results were measured in the broadside direction. At the same power density, the output of the non-uniform rectenna is lower than that of the uniform rectenna because it inherently has a lower gain.

As the power density is 5 mW/cm^2, DC output voltages of the uniform rectenna and the non-uniform rectenna are 4.64 V and 1.96 V, respectively. At that time the efficiencies of the uniform rectenna and the non-uniform rectenna are 75.4 % and 72.1 %. The lower efficiency is due to its lower received RF power.

The DC output voltage versus the elevation angle (θ) is shown in Figure 22(a). When the output voltage of both rectennas is the same, the output of the non-uniform

rectenna does not decay as rapidly as that of the uniform rectenna. This becomes more obvious when the output voltage lowers, which also implies that the superiority of the non-uniform rectenna become apparent being applied in the low-power density power transmission.

The voltage ratio (VR) versus the elevation angle is shown in Figure 22(b). The VR is defined as the ratio of the output voltage at θ to that at $\theta = 0^{o}$. The shape of the VR versus θ is similar to that of the main lobe pattern at $\phi = 0^{o}$. It is found that at $\theta = 15^{o}$, the VR of the non-uniform rectenna is about 0.82 while that of the uniform rectenna decrease to approximately 0.57. At $\theta = 30^{o}$, the VR of the non-uniform rectenna is about 0.52 while that of the uniform rectenna is less than 0.17. Therefore, compared with the uniform rectenna, the non-uniform rectenna performance is obviously improved. The non-uniform rectenna is less sensitive to the elevation angle change, i.e., mainbeam alignment deviation.

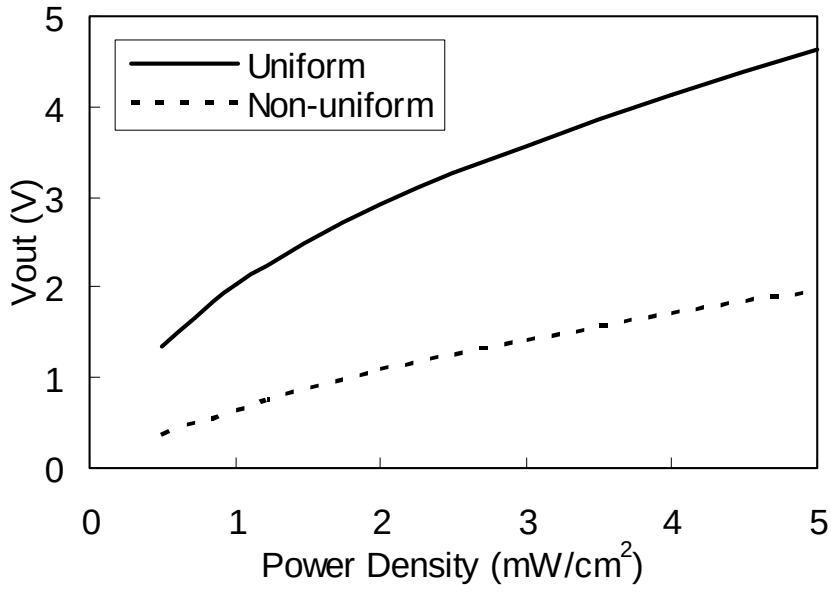

(a)

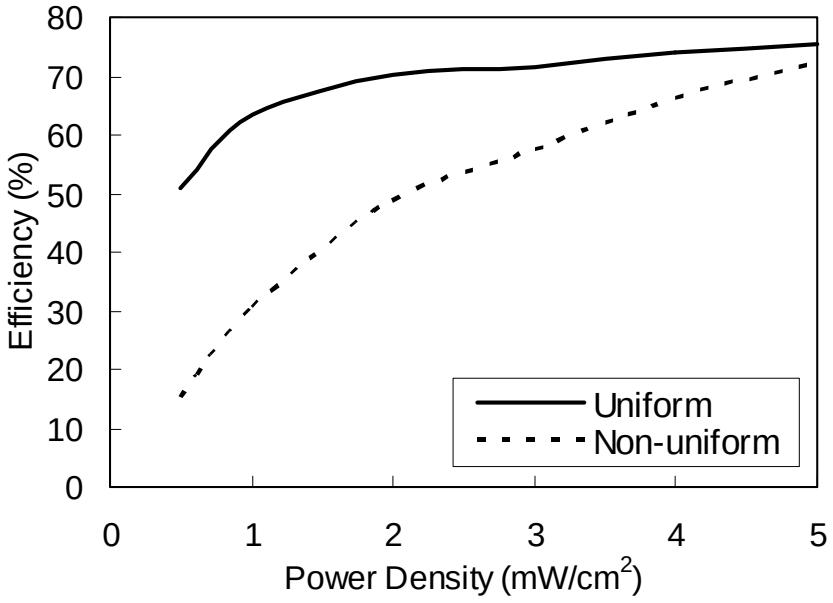

(b)

Fig. 21. (a) DC output voltage of the rectenna and (b) rectenna efficiency.

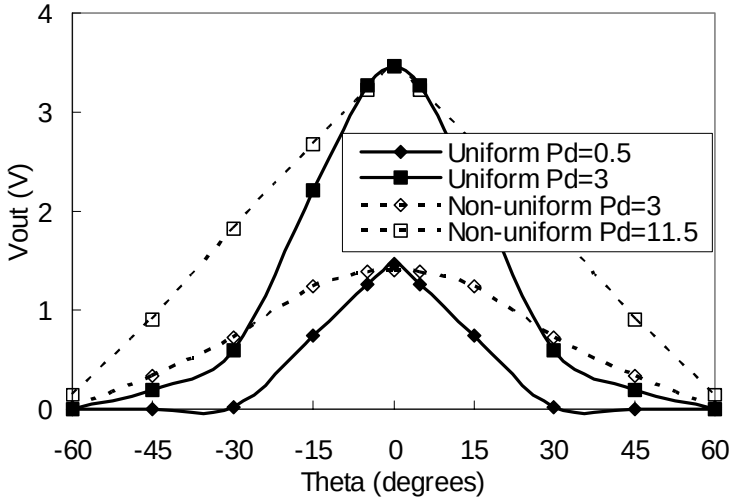

(a)

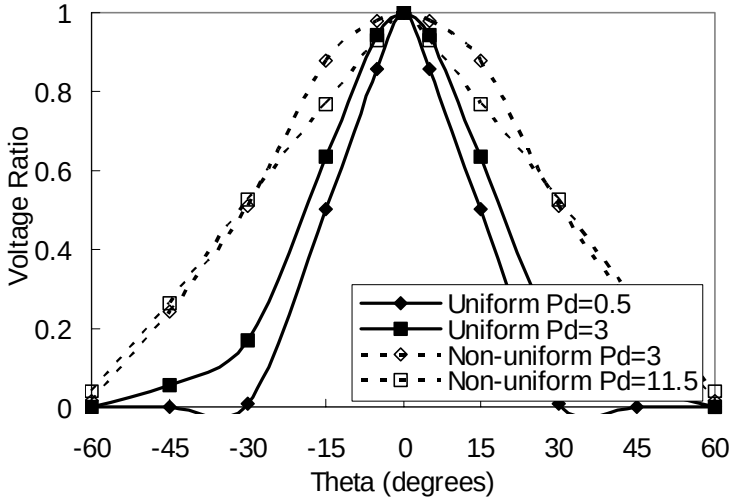

(b)

Fig. 22. (a) Output voltage and (b) voltage ratio versus the elevation angle for various power density (P_d).

3. Retrodirective rectenna arrays

A. Circularly polarized proximity-coupled microstrip antenna

The circular polarized proximity-coupled microstrip ring antenna is chosen as the antenna element of the retrodirective array [55]. Its geometry is shown in Figure 23. The advantages of the proximity-coupled microstrip antenna are its circularly polarized

characteristic and its two-layer structure. When designing the Van Atta array, the transmission line connecting two elements may have a length of multiple wavelengths and its schematic may be complicated. Separating the antenna elements and the transmission line networks on different dielectric layers will reduce the unnecessary coupling between the antenna elements and the transmission lines and provide more space for the retrodirective rectenna array circuits.

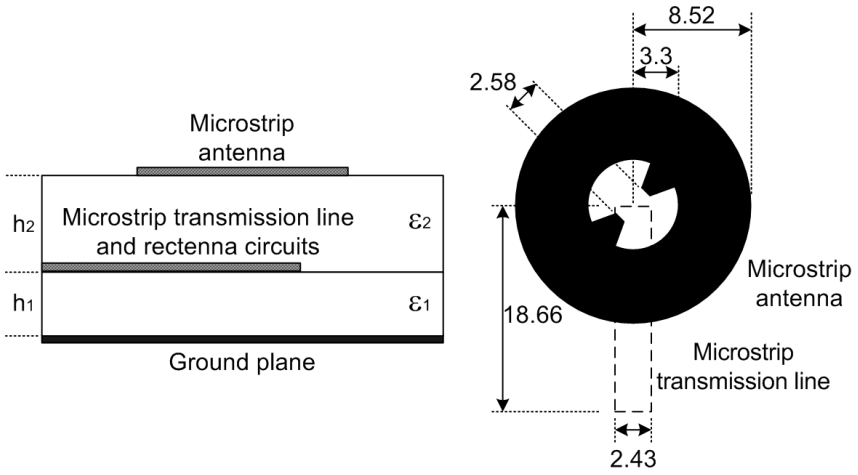

Fig 23. Geometry of the proximity-coupled microstrip ring antenna and the two-layer dielectric structure. All dimensions are in millimeter.

The IE3D is used to design the antenna elements and the retrodirective rectenna array. The proximity-coupled antenna is designed at the center frequency of 5.8 GHz and is printed on RT/Duroid 5880 substrate. The two layers are of the same material, with a thickness $h_1 = h_2 = 0.7874$ mm = 31 mil, a dielectric constant $\varepsilon_1 = \varepsilon_2 = 2.2$, and the conductor thickness of 0.0356 mm (equivalent to 1 oz copper). At 5.8 GHz, the effective dielectric constant ($\varepsilon_{r,eff}$) of the transmission line between the two layers is 1.92 and λ_g is

37.34 mm. The transmission line has a characteristic impedance (Z_0) of 50 Ω, which is chosen to match the impedances of the antenna and the diode to reduce the signal reflections between these components.

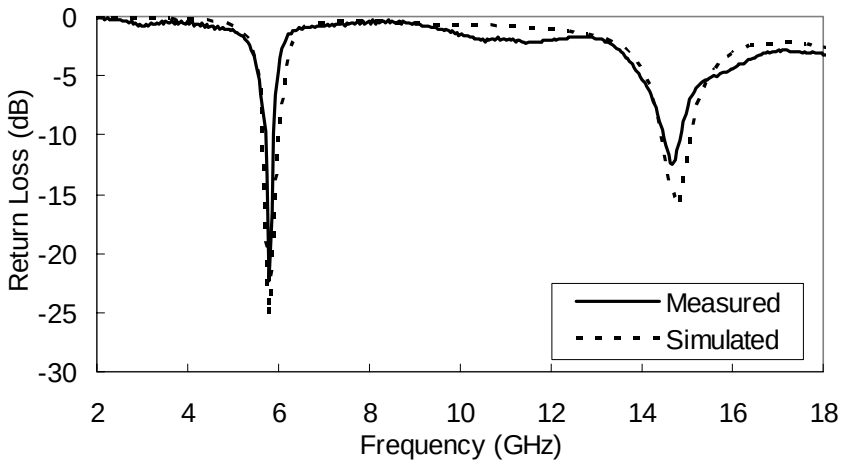

Fig. 24. Measured return loss of the single ring antenna element.

The dumbbell-slot in the antenna center has to be designed carefully for good antenna performance, especially for low axial ratio. The dumbbell-slot yields a left-hand circular polarization. A right-hand circular polarization can be obtained by rotating the dumbbell by 90 degrees. Figure 24 shows the good agreement between the measured return loss and simulated return loss. The bandwidth of 2:1 VSWR at the fundamental frequency of 5.8 GHz is approximately 3.3%. It has a measured gain of 5.89 dBi and an AR of 1.7 dB. The AR can be reduced by tuning the dumbbell-slot. While the antenna in perfect circular polarization (i.e. AR = 0 dB) has its highest CP gain, the corresponding rectenna conversion efficiency is increased until the rectifying diode saturates.

While the proximity-coupled microstrip antenna is used as the antenna element of the retrodirective array, the beam-width of the array mainbeam will not influence the rectenna performance much. This is because the retrodirectivity of the array will require the mainbeam constantly focused on the direction of the incoming waves.

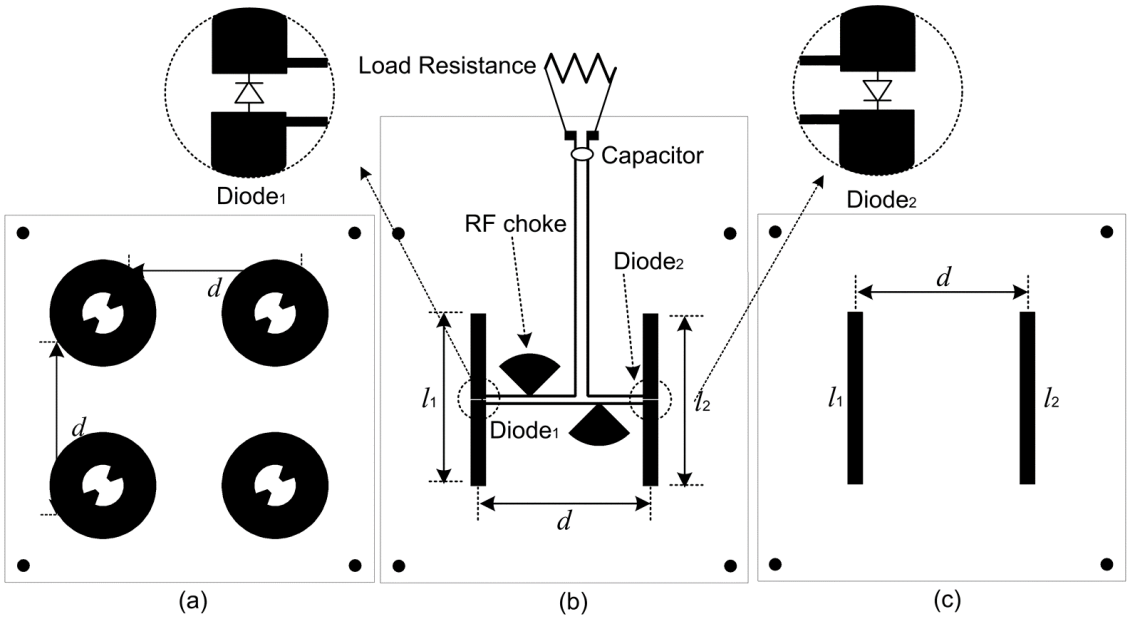

Fig. 25. Geometry of the 2x2 retrodirective rectenna array: (a) antenna array elements, (b) rectenna circuit, and (c) retrodirective array equivalent microstrip line network when the diodes are ON for retrodirective action.

B. 2x2 retrodirective array

The 2x2 retrodirective rectenna array is shown in Figures 25(a) and 25(b). This array consists of two pairs of antenna elements. Each pair of antenna elements is equally spaced from the array center and hence has a transmission line of equal length (l_1 and l_2). The transmission line between the two antennas is used to invert the phase of the incident wave and then steer the mainbeam of the array toward to where the incident

waves come. Each transmission line is connected together through the gap when the diode is turned on by the incident microwave power, as shown in Figure 25(c). At that time, the retrodirectivity activates and the diodes also convert RF power to DC power. Therefore, the diode in the gap acts as a switch for the retrodirective circuit and as a rectifier for the rectenna circuit. The remaining circuits belong to the rectenna rectifying circuit and will be discussed in the next section.

The transmission lines connecting each pair of antenna elements should have the same length or have a length difference equal to a multiple of the microstrip line guided-wavelength (λ_g), i.e., $\Delta l = n\lambda_g$, where n = 0, 1, 2, 3.… To avoid the grating lobes, the spacing between antenna elements has to be considered. The element spacing should satisfy

$$d < \frac{\lambda_0}{\left(1+|\sin\theta_{in}|\right)} \tag{61}$$

where d is the element spacing, λ_0 is the free space wavelength, and θ_{in} is the incident angle of the incoming signals. It assumes the incident angle scans from –90^o to +90^o, so d should be smaller than $0.5\lambda_0$. Here d is chosen as $0.5\lambda_0$ = 25.9 mm at 5.8 GHz. The lengths of the two transmission lines are equal to d, i.e., $l_1 = l_2 = 0.5\lambda_0 = 0.69\lambda_g$, with $\lambda_g = \lambda_0 / \varepsilon_{r,eff}^{1/2}$.

The retrodirectivity of the array can be obtained by measuring the monostatic and bistatic patters [20-21]. In the monostatic measurement, the interrogating and receiving antennas are collocated and moved at the same time to measure the radiation from the retrodirective array. This means $\theta = \theta_0$ and $\phi = \phi_0$, where θ_0 and ϕ_0 are the RF source

angle. Hence the receiving antenna is in the main-lobe direction. The monostatic RCS (radar cross section) is given by [22]

$$\sigma_{mono}(\theta,\phi) = \frac{\lambda_0}{4\pi} G_c D_p^2(\theta,\phi) D_a(\theta,\phi) \tag{62}$$

where G_c is the circuit gain, and D_p and D_a are the directivities of the antenna element and the antenna array, respectively. The array directivity is given by

$$D_a(\theta,\theta_0,\phi,\phi_0) = \frac{\left|AF(\theta,\theta_0,\phi,\phi_0)\right|^2}{U_0(\theta_0,\phi_0)} = \frac{4\pi\left|AF(\theta,\theta_0,\phi,\phi_0)\right|^2}{\int_0^{2\pi}\int_0^{\pi}\left|AF(\theta',\theta_0,\phi',\phi_0)\right|^2 \sin\theta' d\theta' d\phi'} \tag{63}$$

The radiation pattern varies with θ and ϕ, which means the directivity at the peak is dependent on the scanning angle and is not constant. The normalized monostatic pattern can be expressed as

$$\overline{\sigma}_{mono}(\theta,\phi) = \frac{D_p^2(\theta,\phi)/U_0(\theta,\phi)}{\max\left(D_p^2(\theta,\phi)/U_0(\theta,\phi)\right)} \tag{64}$$

where U_0 is the integration of the array factor. The bistatic RCS is given by

$$\sigma_{bi}(\theta,\theta_0,\phi,\phi_0) = \frac{\lambda_0^2}{4\pi} G_c D_p(\theta_0,\phi_0) D_p(\theta,\phi) D_a(\theta,\theta_0,\phi,\phi_0) \tag{65}$$

In the bistatic measurement, the array radiation pattern is fixed because the RF source location is fixed, so the array directivity is dependent on where the receiving antenna is located. This also results in U_0 constant. The normalized bistatic pattern is given as

$$\overline{\sigma}_{bi}(\theta,\phi)\big|_{\theta_0,\phi_0} = \frac{\left|AF(\theta,\phi)\big|_{\theta_0,\phi_0}\right|^2 D_p(\theta,\phi)}{\max\left(\left|AF(\theta,\phi)\big|_{\theta_0,\phi_0}\right|^2 D_p(\theta,\phi)\right)} \tag{66}$$

where AF is the array factor, which is maximum at the angle of the incoming RF signal.

Hence, the main-lobe of the bistatic RCS pattern should point in the direction of the signal source.

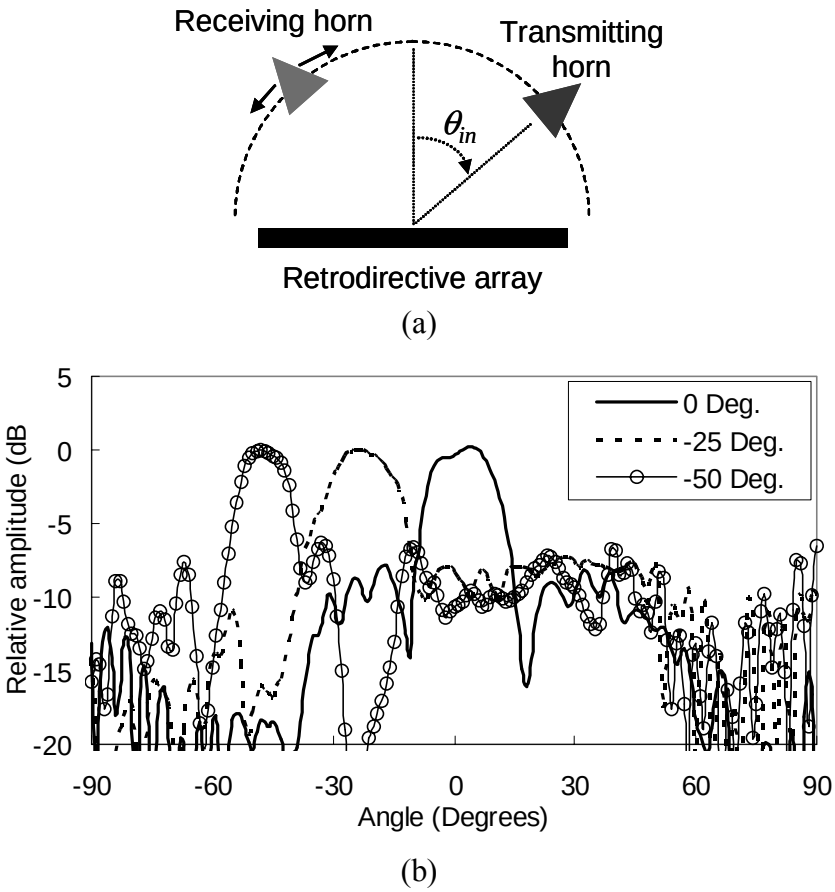

Fig. 26. (a) Measurement setup for the bistatic patterns. (b) Measured bistatic patterns of the 2x2 retrodirective array at different incoming signal directions from 0, -25, and -50 degrees.

The bistatic patterns of the 2x2 retrodirective array are shown in Figure 26, for three different θ_{in} angles. To measure the bistatic patterns, the transmitting horn and the retrodirective array are stationary while the receiving horn scans from -90^{o} to $+90^{o}$, as shown in Figure 26(a). During the scan, both the transmitting power source output and

the distance between the array and the source are kept constant. In Figure 26(b), the incoming waves come from θ_{in} = 0°, -25° and -50° and the patterns are separately normalized to 0 dB, which means their peak gains may be different. The corresponding 3 dB beam-widths of the mainbeam for the array are 18°, 18°, and 13° and the 10 dB beam-widths are 36°, 32°, and 28°. It is observed that the 2x2 retrodirective array can track the incoming signals well.

C. Rectenna circuits of the 2x2 retrodirective array

A rectenna usually consists of a receiving antenna or array, a lowpass or bandpass filter to suppress the second- and/or the third-order harmonic signals, a rectifying diode for RF-to-DC conversion, a DC pass filter, and a resistive load. The diode is the key component in determining the RF-to-DC conversion efficiency. The resistive load also affects the output voltage and the rectenna performance.

The 2x2 retrodirective rectenna circuit is shown in Figure 25(b). In this work, the lowpass or bandpass filter is not needed since a harmonic-rejection antenna is employed. The harmonics of the circular patch antenna is the solution of the Bessel's function. Therefore the harmonic frequencies of the circular patches are different from those of the diodes. The antenna element designed here has such an advantage, which can be observed from Figure 24. The return loss at 5.8 GHz (fundamental frequency) is 22.35 dB and the return losses at 11.6 and 17.4 GHz (harmonic frequencies) are 2.15 and 3.02 dB, respectively. Then the energy re-radiated by the antenna is at 5.8 GHz due to these high harmonic return losses as well as the fact the energy after mixing process is

significantly smaller at the harmonic frequencies comparing to the fundamental frequency. This advantage reduces the space for the rectenna circuit and makes it more compact.

The 2x2 retrodirective rectenna array can be viewed as two series-connected rectenna elements. Each rectenna element includes a pair of antenna elements and a rectifying diode. Each antenna element couples the energy to the connecting transmission line and sends it to the other antenna element for the retrodirective purpose. For power rectification, the diode is mounted across the transmission line at its midpoint by using silver epoxy. Rectenna elements are series-connected by using a thin high-impedance transmission line with RF chokes to reject the unwanted RF signals from each diode and to avoid RF signals leaking. These two series-connected rectenna elements share a resistive load where the DC output voltage is detected. As the diode is ON, signals received by one antenna element can be reradiated by the other antenna element and the beam steering is completed. In other word, the retrodirectivity of the array and the rectifying process will be activated at the same time. It is noted that every rectenna element is behaved as a unilateral device and hence their outputs can be added together.

D. 4x4 retrodirective rectenna

There are two methods to build a 4x4 retrodirective rectenna array. The first one is to arrange four 2x2 retrodirective rectenna arrays described above and connect them by series or parallel arrangement. Both series and parallel connections should collect the

same amount of DC power. This method is easy to implement and can be used to build a large rectenna array. A DC power combiner can be connected to collect higher output power. It is noted the circuit of the multi-way DC power combiner may couple with the transmission line network of the retrodirective rectenna array, which affects the array pattern and reduces the antenna gain.

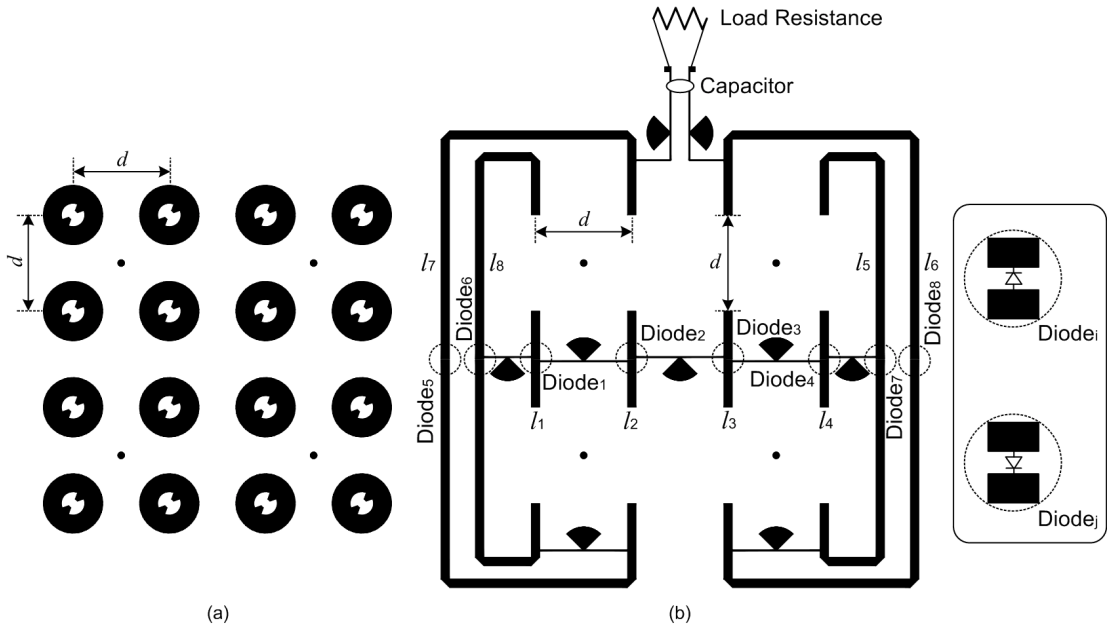

Fig. 27 Geometry of the 4x4 retrodirective rectenna array: (a) antenna array and (b) retrodirective rectenna circuit. The insets show the mounted direction of the $diode_i$ and $diode_j$, where i = 1, 3, 5, 7 and j = 2, 4, 6, 8.

The second method is to build the 4x4 retrodirective rectenna array by designing another distinct transmission line network, as shown in Figure 27. The structure and the operation process of the 4x4 array are similar to the 2x2 array. Eight sections of transmission lines (l_1 to l_8) are used for the retrodirective function. They are also used to link the rectenna elements with other thinner sections to the load resistance. Eight diodes

are used for the rectifying purpose. The lengths of the transmission lines are given by: $l_1 = l_2 = l_3 = l_4 = 0.69\lambda_g$, $l_5 = l_8 = 4.69\lambda_g$, and $l_6 = l_7 = 6.69\lambda_g$. The antenna element spacing is the same as that of the 2x2 array, i.e. $d = 0.5\lambda_0$.

Same as the 2x2 retrodirective rectenna array, the rectifying diode is mounted at the mid-point of each transmission line, as shown in Figure 27(b). The two diodes beside each other ($Diode_i$ and $Diode_j$) are to be mounted in opposite directions, i.e. the anode of one diode links the cathode of the other diode. Intuitionally, this array can be viewed as a series-connected rectenna array because eight rectenna elements are series-connected together via the transmission line network with RF chokes and share the same loading resistance.

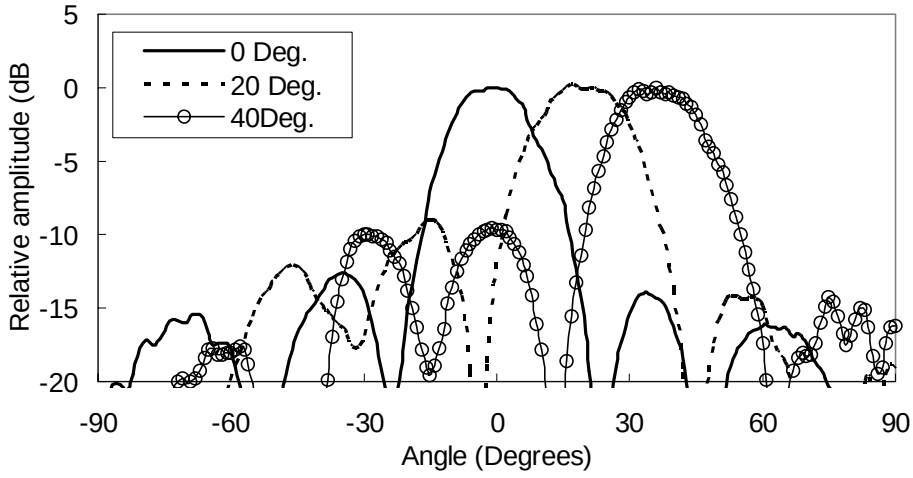

Fig. 28. Measured bistatic patterns of the 4x4 retrodirective rectenna array at different incoming signal directions from 0, 20, and 40 degrees.

Measured bistatic patterns of the 4x4 array are shown in Figure 28. The patterns are separately normalized to 0 dB. The incoming waves come from 0^o, 20^o, and 40^o. The

corresponding 3-dB beam-widths are 19°, 22°, and 19°. The 10 dB beam-widths are 34°, 36°, and 35°. These results demonstrate that the 4x4 retrodirective array can effectively perform the beam steering to align the rectenna array with the power transmitting antenna.

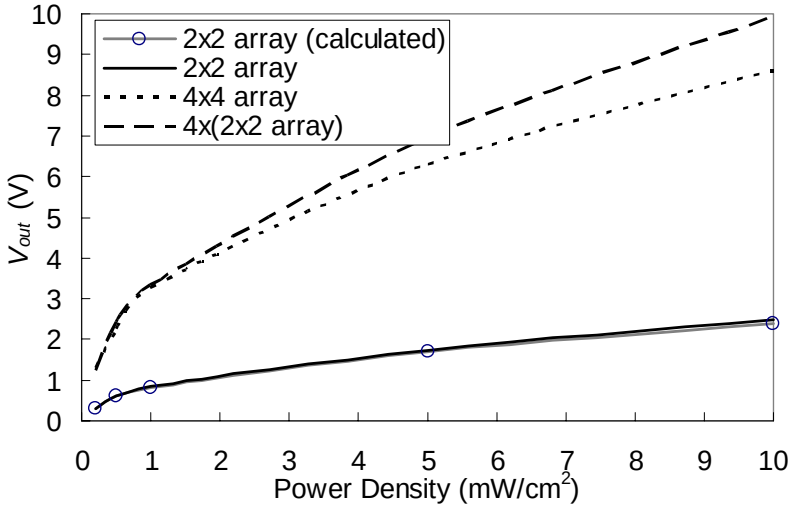

Fig. 29. Measured DC output voltages of the 2x2 array and the 4x4 array at broadside.

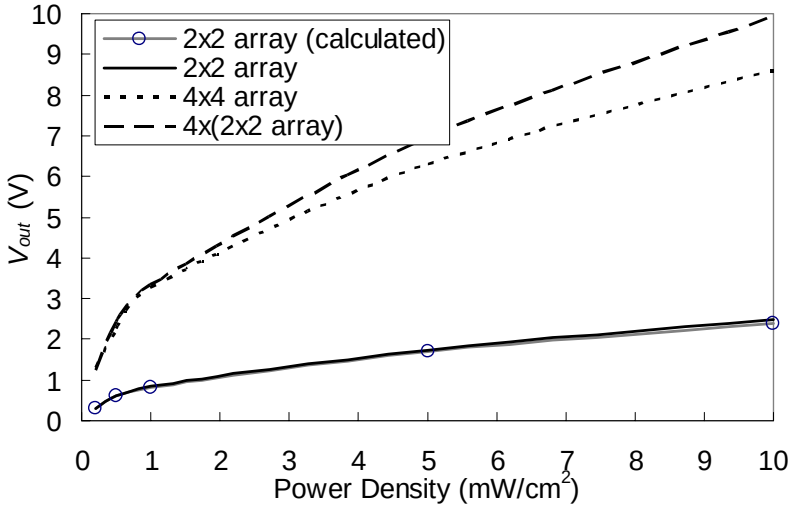

Fig. 30. Measured conversion efficiencies of the 2x2 array and 4x4 array at broadside.

E. Broadside measurement of the retrodirective rectenna arrays

Free space measurements were conducted here. The DC output voltages and the RF-to-DC conversion efficiencies of a 2x2 retrodirective rectenna array are shown in Figures 29 and 30, respectively, as a function of the power densities at the broadside. The external resistive load of the 2x2 array is chosen as 150 Ω for the maximum DC output voltage. The measured results match the calculated results well. When the power density (P_d) is 10 mW/cm^2, the 2x2 array has an output of 2.48 V and a conversion efficiency of 73.3%.

The output voltage of the 4x4 array ($V_{out,4x4}$) is shown in Figure 29 in which four-times 2x2 array output voltage ($4V_{out,2x2}$) is also plotted as a comparison. It is observed that the 4x4 array has a good performance and agree well with $4V_{out,2x2}$ especially at low P_d levels. For example, at P_d = 1 mW/cm^2, $V_{out,4x4}/4V_{out,2x2}$ = 97 %. At P_d = 10 mW/cm^2, $V_{out,4x4}/4V_{out,2x2}$ = 87% while the conversion efficiency is 55% for the 4x4 array, as shown in Figure 30. From these measurement results, when the power density increases, the 4x4 array does not work as well as those at lower power density. One possible reason is that the incident power density is not uniform for a large array. Therefore, not all of the rectenna elements have the same output voltage due to their different positions. When the rectenna elements with different outputs are connected in series or parallel, the rectenna array output will be less than the summation that assumes that same individual rectenna element output. Under this condition, the array output decreases and hence its conversion efficiency is reduced. The other reason affecting the rectenna array

performance is the imperfect circular polarization of the array. Furthermore, the side-lobes of the array patterns also result in the degradation. These characteristics become significant when the incident angle changes, while the power source scans.

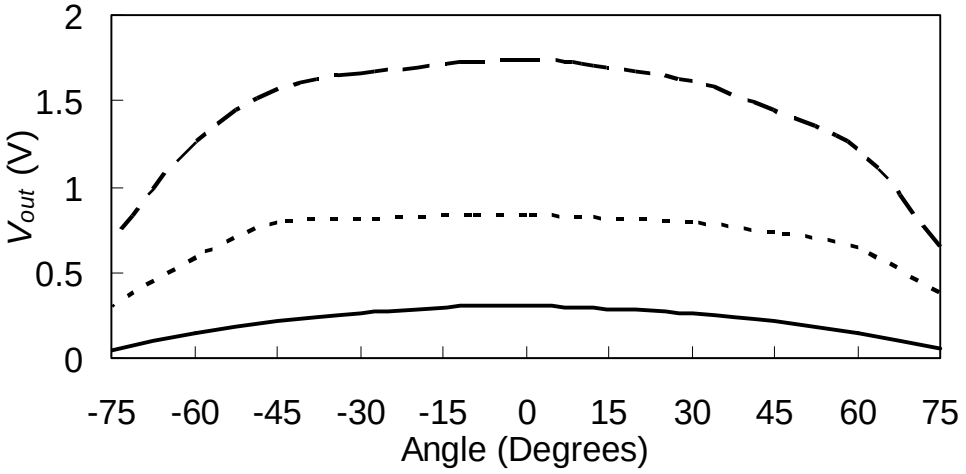

(a)

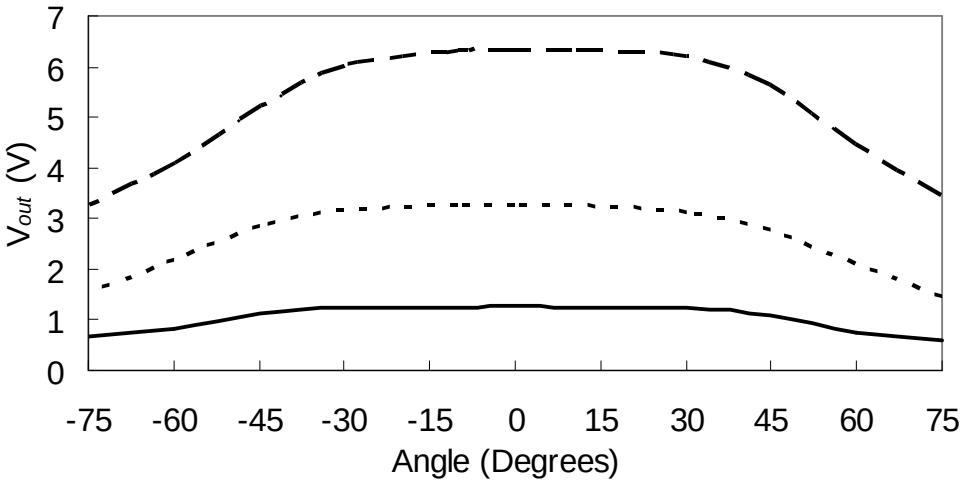

(b)

Fig. 31. Measured DC output voltages as a function of incident angles for the (a) 2x2 array and (b) 4x4 array. Solid line: P_d = 0.2 mW/cm^2; dot line: P_d = 1 mW/cm^2; dash line: P_d = 5 mW/cm^2.

F. Scanning measurement of the retrodirective rectenna arrays

The retrodirectivity of the rectenna arrays was tested by using the same precedure of measuring the bistatic patterns shown in Figure 26(a). During the measurement, the distance between the transmitting horn antenna that provides the microwave power, and the retrodirective rectenna array is constant. Figure 31 shows measured DC output voltages of the retrodirective rectenna arrays as a function of the RF signal incident angles (θ_{in}) for three different power densities. In the past rectenna experiments, the maximum output voltage is confined to be detected at the broadside direction and it drops sharply when the mainbeam does not be aligned with the rectennas. By using the retrodirective arrays, it is obvious that this drawback has been improved significantly. Whether the mainbeam beam-width is narrow or wide, the rectenna array becomes less sensitive to the power incident angle variations, i.e., mainbeam alignment deviation.

The voltage ratios (VR) versus the incident angles are shown in Figure 32. The VR is defined as the ratio of the output voltage at θ_{in} to that at $\theta_{in} = 0^o$. For both 2x2 and 4x4 arrays, the VR within $\pm 10^o$ is larger than 0.98 except the results of 2x2 array with P_d = 0.2 mW/cm^2. This may be due to the low power density resulting in lower output voltage that cannot drive all the rectifying diodes well. In most cases, the VR is very close to 0.9 as $\theta_{in} < 45^o$. When $\theta_{in} > 45^o$, the VR starts to reduce because the gain of the retrodirective rectenna array decreases. The VR becomes smaller than 0.5 when $\theta_{in} > 75^o$. Compared with the traditional rectennas, the retrodirective rectenna arrays indeed can automatically align its mainbeam toward to the power source and achieves good rectenna performance.

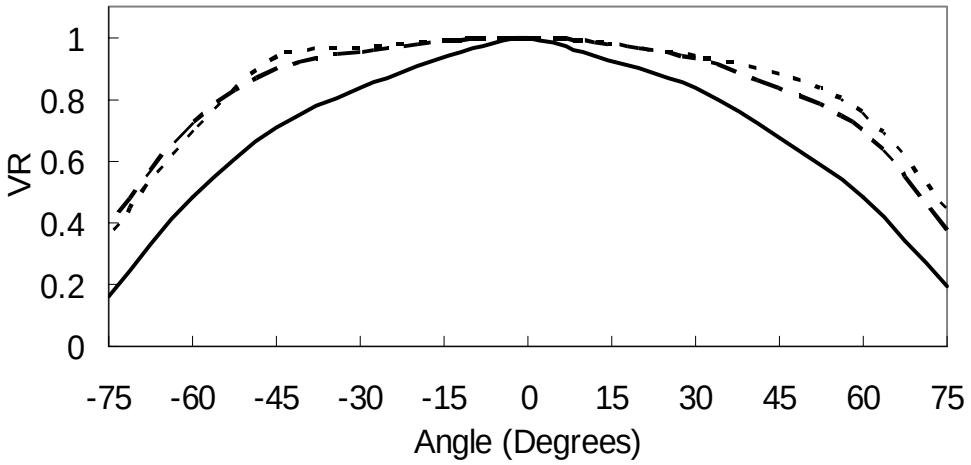

(a)

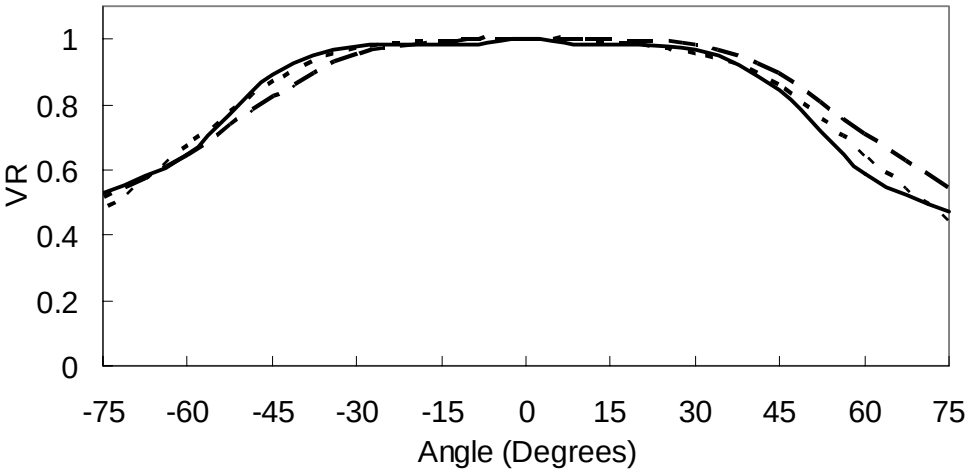

(b)

Fig. 32. The output voltage ratios as a function of incident angles for the (a) 2x2 array and (b) 4x4 array. Solid line: P_d = 0.2 mW/cm^2; dot line: P_d = 1 mW/cm^2; dash line: P_d = 5 mW/cm^2.

4. Retrodirective wireless power transmission system

As mentioned before, to ensure the maximum transmission efficiency and to eliminate healthy and environmental concerns, it is necessary to accurately aim the high

power mainbeam at its target. The Van Atta array is generally simpler to design and of lower cost in comparison with other methods. An alternative method is to use the phase-conjugated retrodirective array. Conjugating the received phases ensures that the mainbeam can focus in the direction of the incoming pilot signals. By modulating to the retransmitted microwave beam or using power amplifiers, its magnitude can be amplified.

As shown in Figure 18(b), the incoming RF signal at each antenna element are mix with the local oscillator (LO) signal, which gives the following mixing products.

$$V_{IF} = V_{RF}\cos(\varpi_{RF}t + \theta_n)\cdot V_{IF}\cos(\varpi_{LO}t) \tag{67}$$

This can be written as

$$V_{IF} = \frac{1}{2}V_{RF}V_{IF}\left(\cos((\varpi_{LO} - \varpi_{RF})t - \theta_n) + \cos((\varpi_{LO} + \varpi_{RF})t + \theta_n)\right) \tag{68}$$

If the LO frequency is twice that of the RF, we have

$$V_{IF} \propto \cos(\varpi_{RF}t - \varphi) + \cos(3\varpi_{RF}t + \varphi) \tag{69}$$

The first term, the lower sideband, is the intermediate frequency (IF) that has the same frequency as the RF but with a conjugated phase. A phase-conjugating array has the same kind of phase reversal as the Van Atta array, which results in the return of the signal towards the source direction.

In this topology, undesired signals should be eliminated so that only the phase-conjugated signal reradiates [22]. The upper sideband product in (64) and the LO leakage can be suppressed using filters. Another one is the RF signal leaking from the input to the output of the phase conjugator, which has the same frequency as the desired

IF signal but not phase-conjugated. This will creates a mirror beam of the desired retrodirective beam. The balanced mixer technique can be used to eliminate the undesired signals.

An active retrodirective rectenna system for 5.8 GHz wireless power transmission using the phase-conjugating technique is shown in Figure 33. The system includes a transmitter and a receiver. The transmitter is in charge of phase-conjugating. The receiver behaves as the rectenna. At first the receiver will send an interrogating signal to the transmitter. After it is received by the transmitter, phased-conjugated and amplified RF signals will be retransmitted back to the receiver and then be converted to DC power. This architecture can be used in the satellite communication systems, and space-to-space or space-to-ground power transmissions. With a broadband antenna or array, the system can transmit the energy and conduct the data communication simultaneously.

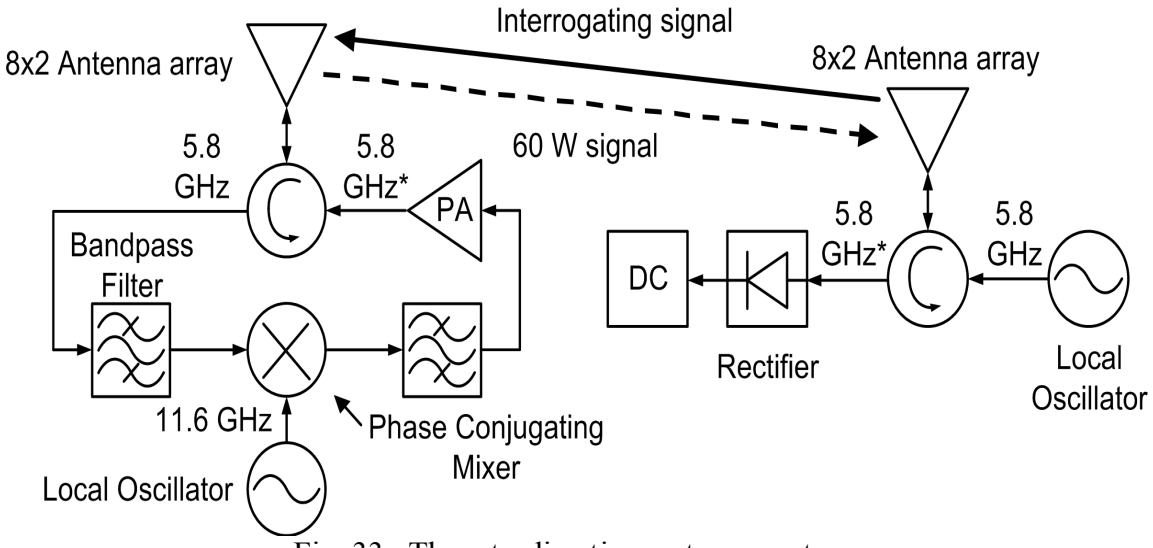

Fig. 33. The retrodirective rectenna system.

5. Conclusions

It is concluded that though the uniform rectenna has larger conversion efficiency, its BWFN is much smaller than that of the non-uniform rectenna. The mainbeam beam-width significantly affects the output voltage at each elevation angle. The non-uniform rectenna has a broadened mainbeam and hence its output voltage changes much less than that of the uniform rectenna. This technique can be applied to the wireless power transmission with huge power, which usually equip with many antenna elements and hence can be designed to have a uniform amplitude pattern.

A 2x2 and a 4x4 C-band circular polarized retrodirective rectenna arrays have been demonstrated. No bandpass filter is needed in the retrodirective rectenna array because the antenna element of the array is inherently able to reject the reradiated harmonic signals. The antenna element is a proximity-coupled microstrip ring antenna that has a circular polarized gain of 5.89 dBi and an axial ratio of 1.7 dB. At the broadside, the conversion efficiencies of the 2x2 and 4x4 retrodirective rectenna arrays are 73.3% and 55%, respectively when the incident power density is 10 mW/cm^2. The DC output voltages are 2.48 V and 8.59 V, respectively. The output voltage and the conversion efficiency can be higher if a larger incident power density is used.

The mainbeam of the retrodirective rectenna array can steer toward to the power source automatically. The output voltage is almost constant within $\pm 10^o$ of the incident angle. For $\theta_{in} < 45^o$, the VR is still as high as 0.9. These results show that the DC output voltage will not change due to the improper mainbeam alignment. This technique is very suitable for the wireless power transmissions with a high gain but narrow beam-width

transmitting antenna array. The array is usually consists of many elements and hence the tracking is very critical.

An active retrodirective rectenna system is proposed for the applications of long distance and high power transmission. The system features a 5.8 GHz retrodirective array transmitter and a rectenna array receiver. The transmitter receives a pilot signal from the rectenna position and generates amplified phase-conjugated signals that can steer the transmitted power beam to the remote rectenna array.

CHAPTER IV

ULTRA-WIDEBAND RECTENNA ARRAY AND RETRODIRECTIVE ARRAY FOR MILLIMETER-WAVE APPLICATIONS*

1. Introduction

Most rectenna elements and rectenna arrays are developed for frequencies below 15 GHz, especially for the ISM (industry-science-medical) bands. Only a few rectennas are reported for the millimeter-wave operation and they are focused on single element performances [30][50][56-57]. Rectennas operating at millimeter-wave frequencies have the advantages of compact sizes and higher overall system efficiency for long distance transmission. On the other hand, despite that the retrodirective arrays have been used in many wireless communication systems, they are used for lower frequency applications but have not been widely reported in the open literatures for millimeter-wave applications.

Ultra-wideband antennas have received much attention in mobile wireless communications lately. With a broadband antenna, source power can be transmitted at different operation frequencies dependent on power availability [10][58]. The broadband antennas also can potentially handle wireless power transmission and data

communications simultaneously. Compared with the common shapes of microstrip antennas such as rectangular, circular, and the triangular, relatively few broadband antennas adopt the ring structure, especially in millimeter-wave frequencies.

In this chapter, a new millimeter-wave rectenna arrays are proposed. An ultra-wideband harmonic rejecting dual-ring antenna is designed as the receiving element of the rectenna. Two dual-ring antennas are used to build a single rectenna element, as well as 2x1 and 2x2 rectenna arrays. The antenna elements and the transmission line networks are separately placed on two different layers to simplify the rectenna array design. These small rectenna arrays can be used as building blocks to construct a large rectenna array for millimeter-wave wireless power transmission. Furthermore, a broadband 8x16 retrodirective array for millimeter-wave applications is presented. A 4x4 array is built as a sub-array and then it is used to construct an 8x16 array. Due to the ultra-wide bandwidth characteristics of the array element, the rectenna array and the retrodirective array are capable of covering most Ka-band applications.

2. Ultra-wideband dual-ring antenna

A. Dual ring antenna

The ultra-wideband proximity-coupled dual-ring antennas are shown in Figure 34. The antenna is printed on RT/Duroid 5880 substrate coated with 1 oz copper. The two layers are of the same material ($\varepsilon_1 = \varepsilon_2 = 2.2$) with the thickness of $h_1 = 0.79$ mm and $h_2 = 0.51$ mm. The dimensions of these rings are optimized by using the 3-D electromagnetic simulator HFSS [59].

Since multiple rings can operate at several frequencies simultaneously, the frequency bands could be overlapped in part when two or more rings are used at the same time [60]. This technique can be applied to enhance the frequency bandwidth by carefully choosing the resonant frequencies. The resonant frequency f_0 of the TM_{n10} mode is given by [61]

$$f_0 = ck/(2\pi\sqrt{\varepsilon_{err}}) \tag{70}$$

with

$$k = 2n/(R+r) \tag{71}$$

where c is the light velocity, ε_{err} (= 1.87) is the effective dielectric constant, and R and r are the outer and the inner radii of the ring, respectively. The center frequency (f_c) of the wideband antenna is defined as

$$f_c = \frac{1}{2}(f_H + f_L) \tag{72}$$

where f_H and f_L are the upper and lower operating frequencies of the wideband antenna. The antenna bandwidth (BW) is the difference between f_H and f_L, which is given by

$$BW = f_H - f_L = \frac{f_H - f_L}{f_c} \text{ in \%} \tag{73}$$

The resonant frequencies of the TM_{110} mode of the outer and inner rings (without the stub) shown in Figures 34(b) and 34(c) are 34.6 and 51.7 GHz. The feed-line length needs to be tuned to obtain the best impedance matching. Two stubs are added to the inner ring in order to enhance the coupling between the outer and the inner rings while combining them to form a dual-ring, as shown in Figure 34(d). Due to the stubs, the

resonant frequency of the inner ring drops to 44 GHz. The simulated return losses of these three ring antennas are shown in Figure 35. The thick two-layer structure increases the bandwidth of the ring resonator. Both the outer ring and the inner ring have a bandwidth of over 23%. The dual-ring covers most operation bands of the two rings, whose bandwidth is more than 40%.

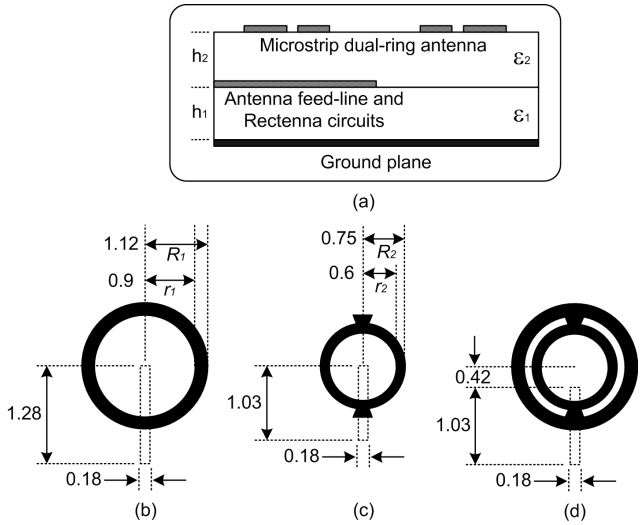

Fig. 34. Geometry of the broadband ring antenna: (a) two-layer structure, (b) outer ring, (c) inner ring, and (d) dual-ring (with outer ring and inner ring). All dimensions are in millimeter.

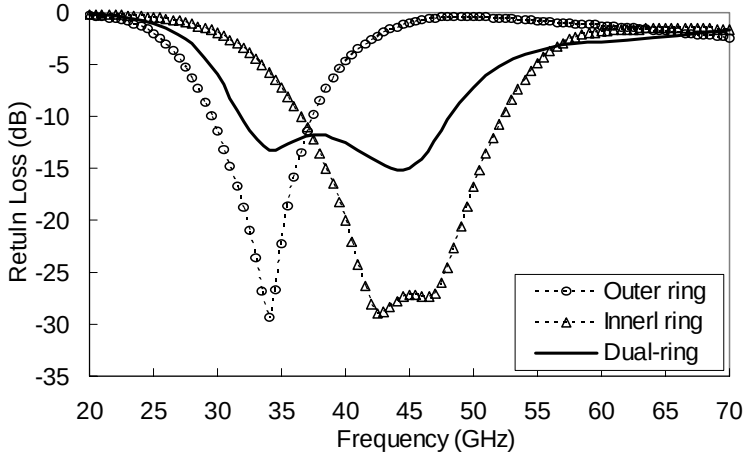

Fig. 35. Return losses of the outer ring, the inner ring, and the dual-ring.

B. Antenna performance

To satisfy the system performance for the antenna and rectenna, the feed-line length of the dual-ring antenna is designed to be 1.28 mm. Figure 36 shows the measured and simulated return losses of the final dual-ring antenna. The measured results follow the simulated results very well. The 10 dB bandwidth is approximately equal to 33.2% (31-42.8 GHz), while the simulation result is 33.8% (30-42 GHz). An antenna with such wide operation bandwidth can cover most Ka-band (26.5-40 GHz) applications and the 35 GHz wireless power transmission. According to the simulation results, the return loss from 50 GHz to 100 GHz is less than 3 dB, as shown in Figure 35. This performance avoids the re-radiation of the second harmonics generated by the rectifying diode. Operation bands and bandwidths of the broadband antennas mentioned above are summarized in Table 3.

The measured and simulated antenna gains from 30 to 40 GHz are between 4 and 5 dBi, with an averaged value of 4.49 dBi, as shown in Figure 37. The radiation patterns at 35 GHz are shown in Figure 38. The measured cross-polarization patterns at broadside are more than 20 dB below the co-polarization patterns.

The two-layer structure gives some advantages to the broadband antenna applications. The first is that one can control the wideband performance by tuning the feed-line easily. Varying the substrate thickness also can tune the effective bandwidth. The second one is that the two-layer structure is helpful to reduce the electromagnetic coupling and simplify the circuit layout since the antenna element and the circuit

components are separated. This is helpful while designing the rectenna and the rectenna array.

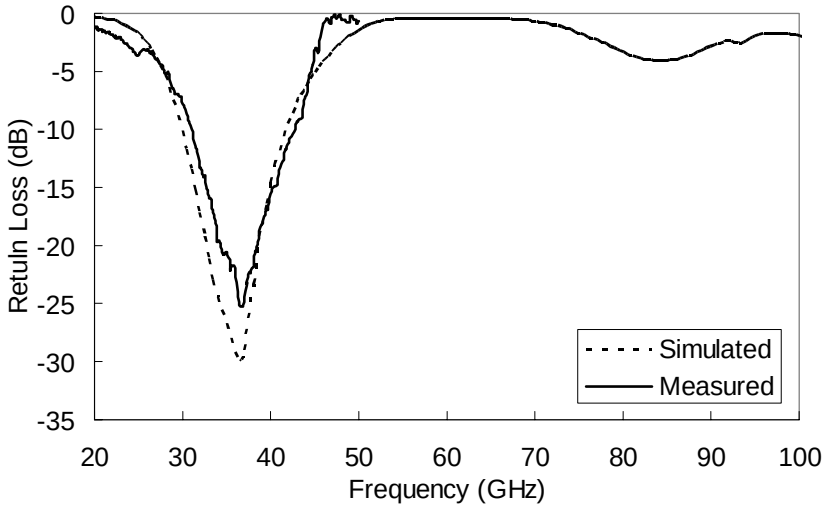

Fig. 36. Measured and simulated return losses of the tested dual-ring antenna.

TABLE 3. Summary of the simulated dual-ring antenna performance.

Antenna item	f_0 (GHz)	Operation band (GHz)	Bandwidth (%)
Big-ring	34.6	29.5-37.5	23.1
Small-ring	44	36.5-52.5	36.4
Dual-ring	39	32-48	41
Final dual-ring	35.5	30-42	33.8
Final dual-ring (measured)	35.5	31-42.8	33.2

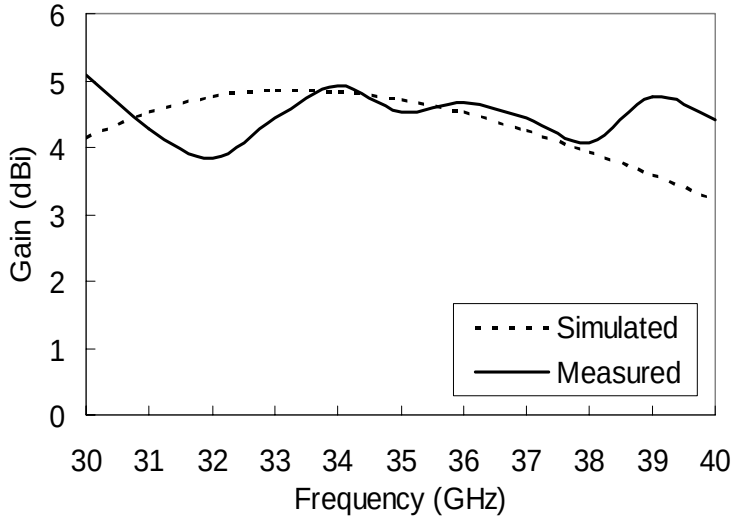

Fig. 37. Measured and simulated gains of the tested dual-ring antenna.

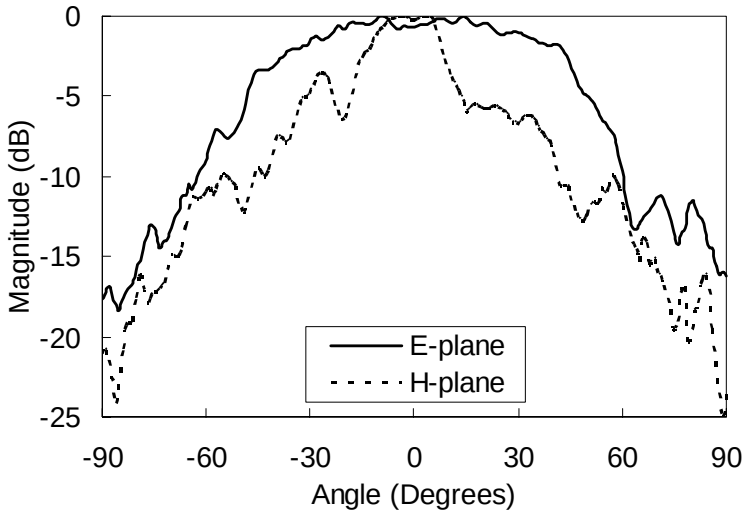

Fig. 38. Radiation patterns of the dual-ring antenna at 35 GHz.

3. Rectenna array design

A. Single element design

The rectenna element, as shown in Figure 39, consists of two broadband antenna elements, one rectifying diode (MA4E1317), and a load resistance (R_L) of 50 Ω. Using

two antenna elements enhances the rectenna gain. The distance (d) between the antenna elements and the elements feed-lines (l_1-l_2) are designed to be approximately $\lambda_0/2$ at 35 GHz to avoid the grating lobes. In this design, no lowpass filter or bandpass filter is needed because of the inherent second order harmonic-rejection of the dual-ring antenna. This saves significant space in the rectenna circuit.

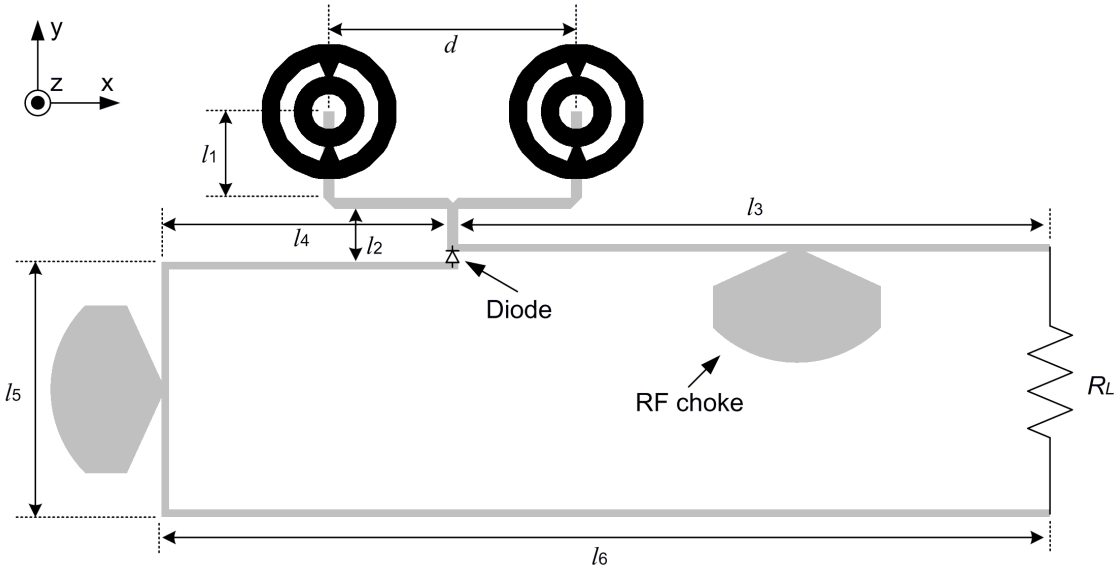

Fig. 39. Geometry of the rectenna element, where the gray-lines are the transmission line networks: d = 4.18 mm, l_1 = 1.46 mm, l_2 = 0.9 mm, l_3 = 10 mm, l_4 = 4.83 mm, l_5 = 4.18 mm, and l_6 = 15.01 mm.

The thin transmission lines (l_3-l_6) serve as the DC loop for the detector and the load. Two RF chokes are used to reject RF signals generated by the diodes and to avoid RF signals from leaking to other rectenna pairs in an array, which is optimized with the DC paths. For a single rectenna element, the RF chokes are not necessary. However, the RF chokes are included in the single element design to prepare it for the array

environment.

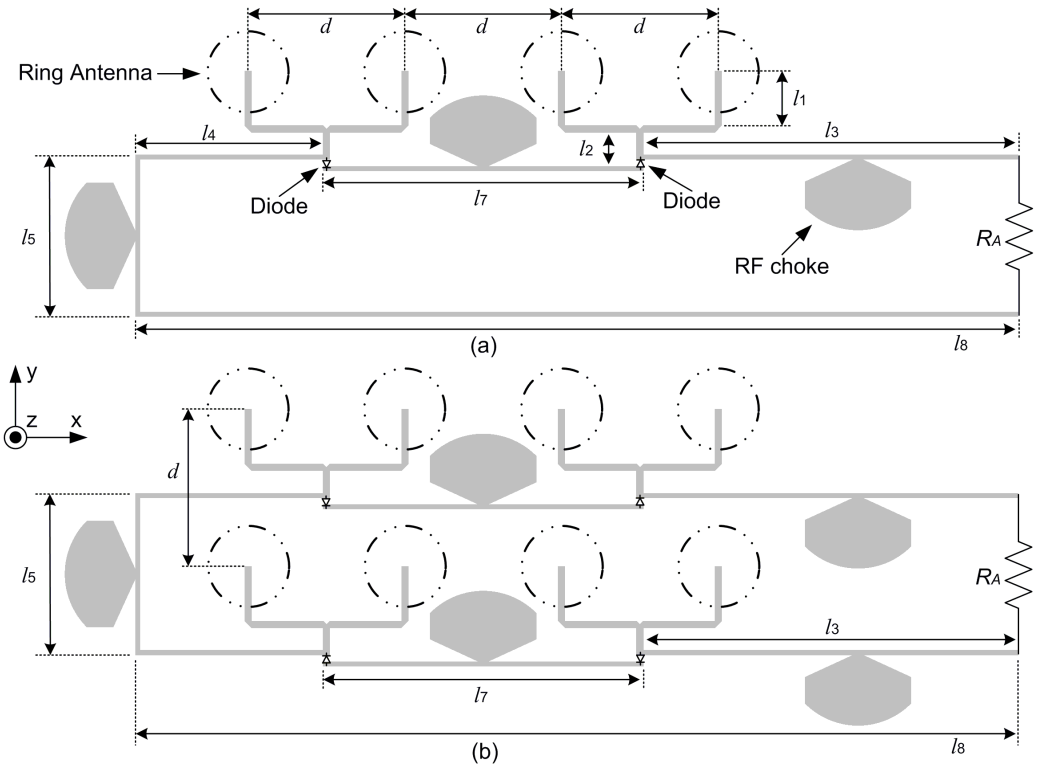

Fig. 40. Transmission line networks of the rectenna arrays: (a) 1x2 array and (b) 2x2 array, with l_7 = 8.54 mm, and l_8 = 23.55 mm.

B. Array design

Two single element rectennas are used to build a 1x2 rectenna array as shown in Figure 40(a). The array can be viewed as two cascaded rectenna elements. Since the rectenna elements are cascaded to form the rectenna array, the load resistance of the rectenna array can be calculated by

$$R_A = N_x N_y R_L \tag{74}$$

where N_x and N_y represent the element numbers in the x-axis and the y-axis, respectively.

For the 1x2 array, $N_x = 2$ and $N_y = 1$ so its load resistance R_A is equal to 100 Ω.

The 2x2 rectenna array is shown in Figure 40(b), which is built using the same method of constructing the 1x2 array. For the 2x2 array, $N_x = 2$ and $N_y = 2$, and therefore its load resistance is 200 Ω. To build a larger array, more rectenna elements can be cascaded in both the x- and the y-directions. This simple connection structure gives a predictable DC output voltage and power, and does not require a complex array design.

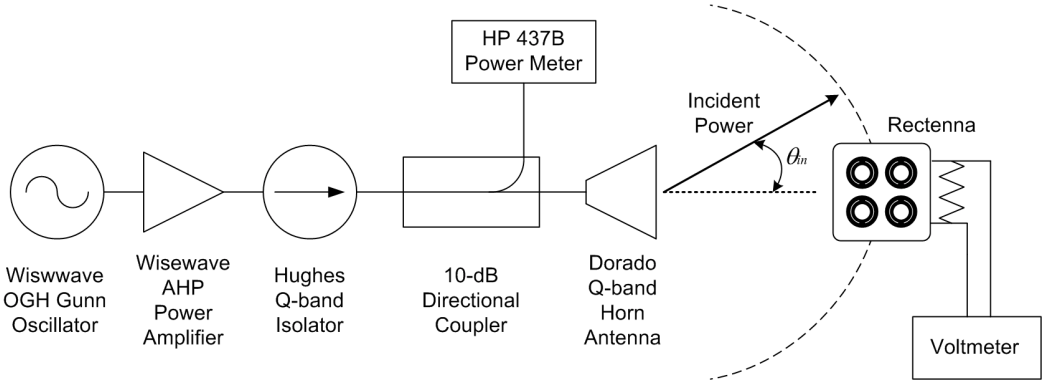

Fig. 41. 35 GHz rectenna measurement setup diagram.

C. Measurements and discussions

Free space rectenna measurements were carried out. The measurement setup at 35 GHz is shown in Figure 41. The RF-to-DC conversion efficiency for the array is defined as

$$\eta = \frac{P_{DC}}{P_r} = \frac{V_{DC}^2}{R_A}\frac{1}{P_r} = \frac{V_{DC}^2}{R_A}\frac{1}{P_d A_e} \tag{75}$$

where P_{DC} is the DC output power, P_r is the received RF power, V_{DC} is the DC voltage detected at the load resistance, P_d is the power density, and A_e is the effective area. For a

single element, $R_A = R_L$.

The DC output voltages and the RF-to-DC conversion efficiencies are shown in Figure 42 as a function of the received RF power levels at 35 GHz. The calculated outputs agree with the experiments for both the single rectenna element and the rectenna arrays though there are more losses in the arrays. One possible reason is that the received power is more uniform in the single element than over the array. Therefore, not all of the rectenna elements in the arrays receive the same amount of the power resulting in lower output voltages for the arrays. The second reason may be that there is not enough power to drive all diodes into the high efficiency region. Due to these reasons, the rectenna array output decreases slightly and hence its conversion efficiency drops. Table 4 concludes the measured results with the minimum and the maximum received power levels.

TABLE 4. Summary of the dual-ring rectenna performance.

	P_r = 4.6 mW			P_r = 34.4 mW		
Rectenna parameters	V_{DC} (V)	η (%)	V_R	V_{DC} (V)	η (%)	V_R
1 element	0.15	9.75	1	1.05	64.03	1
1x2 array	0.31	10.41	2.07	1.97	56.35	1.88
2x2 array	0.56	8.49	3.73	3.42	42.46	3.26

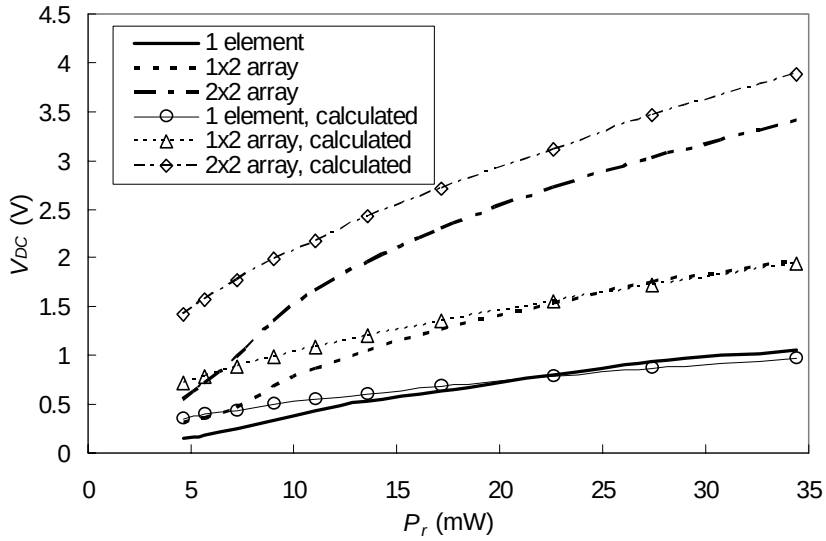

(a)

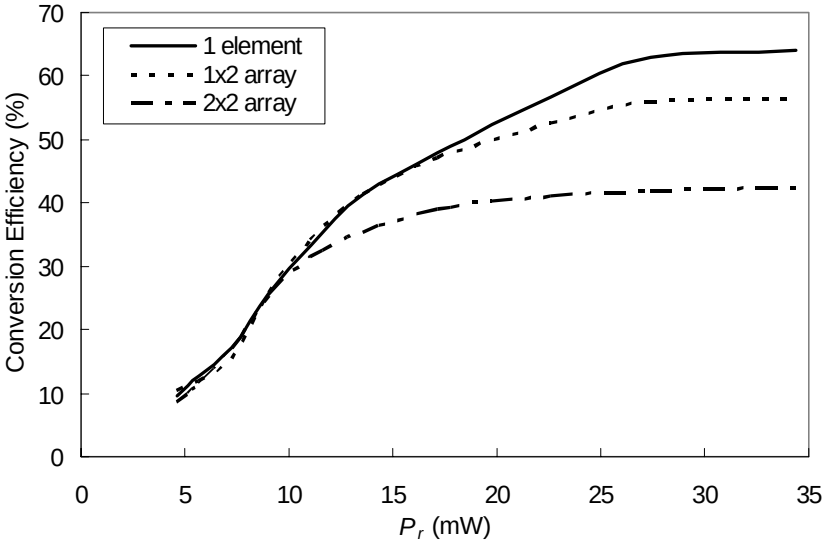

(b)

Fig. 42. Measured and calculated (a) DC output voltages and (b) conversion efficiencies at 35 GHz.

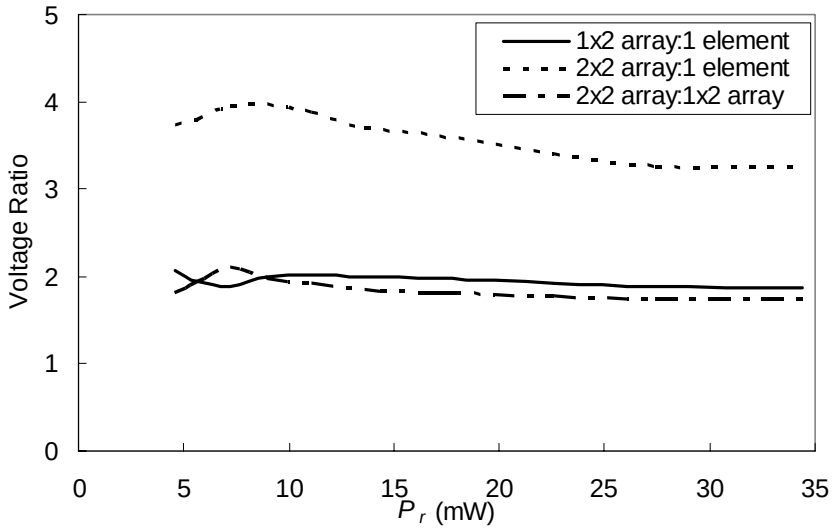

Fig. 43. Voltage ratios of 1x2 array versus single element, 2x2 array versus single element, and 2x2 array versus 1x2 array.

Since the rectenna array is cascaded, its linearity can be evaluated by the voltage ratio (V_R), which is given by

$$V_R = \frac{V_{DC}}{N_x N_y V_{DC,reference}} \tag{76}$$

The measured results demonstrate that the linearity of the rectenna is good, as shown in Figure 43. The voltage ratio of 1x2 array versus single element and that of 2x2 array versus 1x2 array are very close to 2. The performance of the rectenna element and rectenna arrays is summarized in Table 4 with the minimum and the maximum received power levels. When the number of the rectenna elements in the array increases, the linearity of the array deteriorates gradually. So, to build a large array and obtain an accurate predicted output, it is suggested to build and test sub-arrays with various numbers of elements.

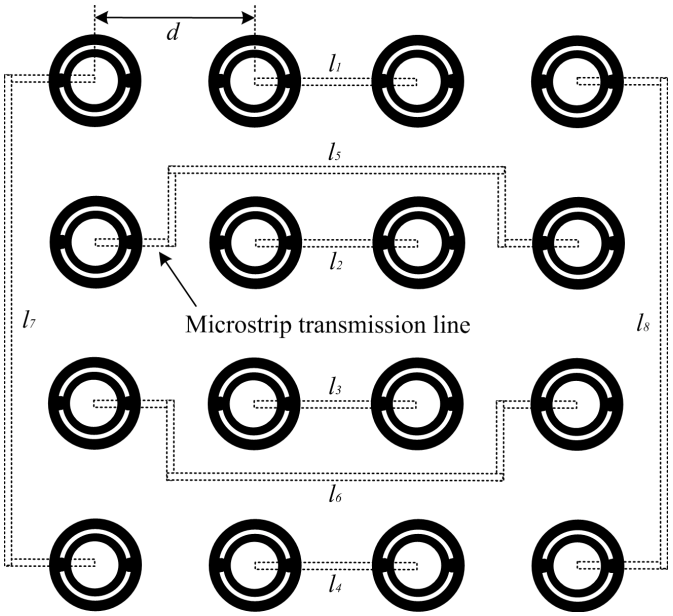

Fig. 44. Geometry of the 4x4 retrodirective sub-array where the dash-lines are the microstrip transmission line networks.

4. Retrodirective array design

A. 4x4 sub-array and 8x16 array designs

The 8x16 retrodirective array is built by designing a 4x4 sub-array at first, as shown in Figure 44. The retrodirective array is a planar Van Atta array. The transmission lines connecting each pair of array elements have the same length or have a length difference equal to a multiple of the guided-wavelength ($\lambda_g = \lambda_0 / \varepsilon_{r,eff}^{1/2}$), i.e., $\Delta l = n\lambda_g$, where n = 0, 1, 2, 3…. The element spacing is set as $d = 0.46\lambda_0$ to avoid the grating lobes. The lengths of the microstrip transmission lines are given: $l_1 = l_2 = l_3 = l_4 = 0.46\lambda_0 = 0.65\lambda_g$ and $l_5 = l_6 = l_7 = l_8 = 2.65\lambda_g$. Here, the center frequency is chosen at 35 GHz so λ_0 = 8.57 mm and λ_g = 6.17mm.

The 4x4 sub-array can be used to build a large array with a specified size. Here, eight 4x4 arrays are assembled to form an 8x16 array, as shown in Figure 45. This 8x16

retrodirective array has a dimension of 66x30 mm^2. To enhance the re-radiated power and reduce loss, the substrate thickness is designed to be a quarter wavelength [62]. The re-transmitted field can be described by [19]

$$E = e^{j(\varpi t+\phi)} \sum_{n=-\frac{N}{2}}^{\frac{N}{2}} A_n \exp\left(j(\frac{2\pi x_n}{\lambda_0})(\sin\theta_r - \sin\theta_t) \right) \tag{77}$$

where ω is the angular frequency, ϕ is a constant phase difference between elements, N is the total element number, A_n is the amplitude of the n-th signal, x_n is the distance of the n-th element from the array center, θ_t is the signal incident angle, and θ_r is the signal re-transmitted angle. The scattered field has been neglected in this equation.

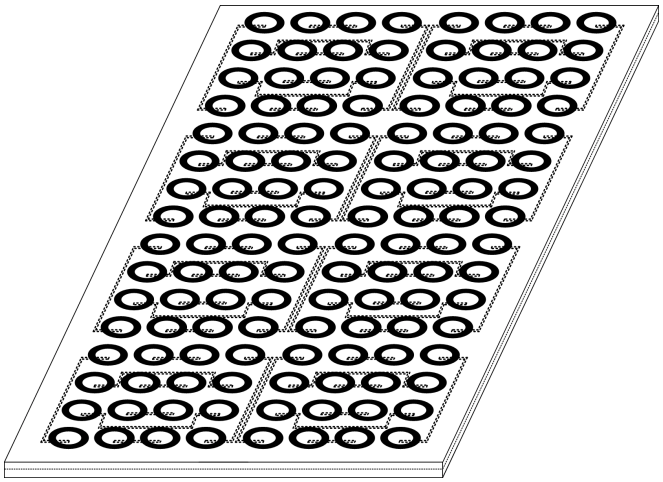

Fig. 45. Geometry of the 8x16 retrodirective array that consists of eight 4x4 sub-arrays.

B. Measurements and discussions

Measured and calculated patterns of the 8x16 retrodirective array at 35 GHz are shown in Figure 46, where the incoming waves come from 0^o and 40^o. The measured patterns

match those calculated closely. These results demonstrate that the 8x16 array can perform the automatic beam steering and tracking very well. To enhance the gain of the re-transmitted signals, a power amplifier can be integrated with the passive array to form an active array.

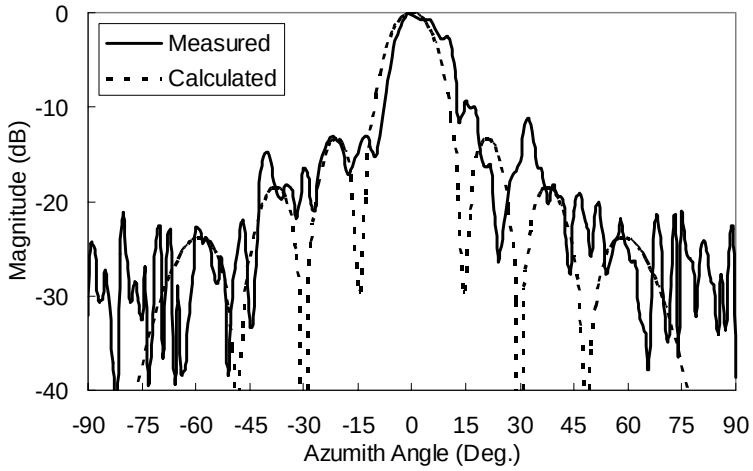

(a)

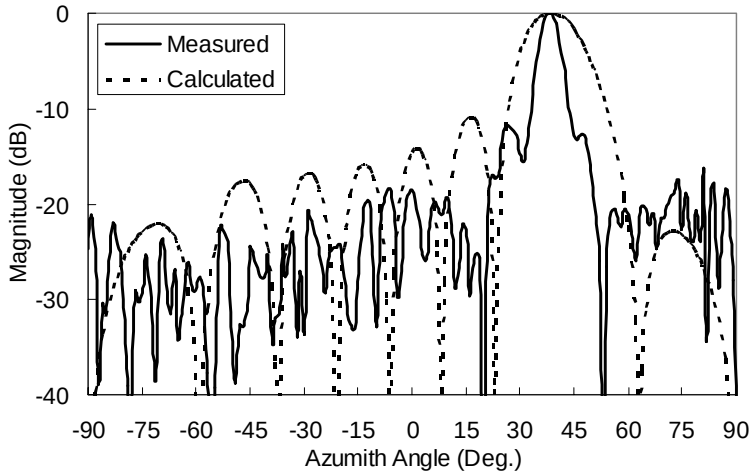

(b)

Fig. 46. Measured bistatic patterns of the 8x16 retrodirective array at (a) 0^o and (b) 40^o.

To demonstrate the broadband characteristic of the array, the 8x16 array is tested

by transmitting the signals with different frequencies. The array patterns measured at 32, 38, and 40 GHz are shown in Figure 47 as compared to patterns at 35 GHz. The measured results demonstrate the array patterns from 31 GHz to 43 GHz are very similar so the retrodirective array can be used for broadband millimeter-wave applications.

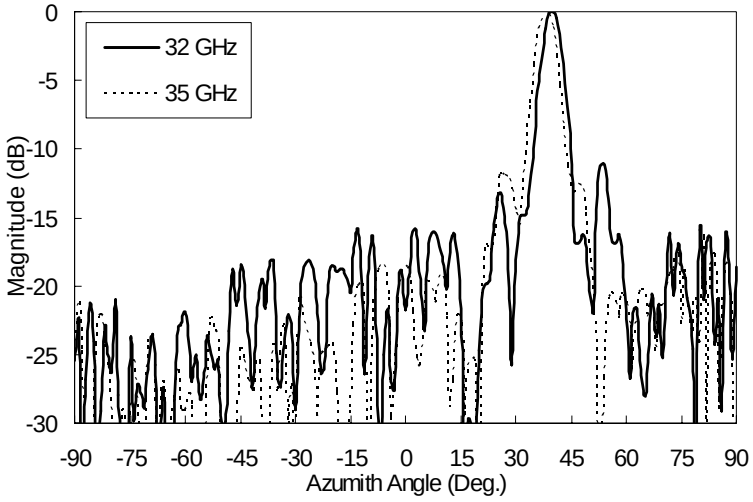

(a)

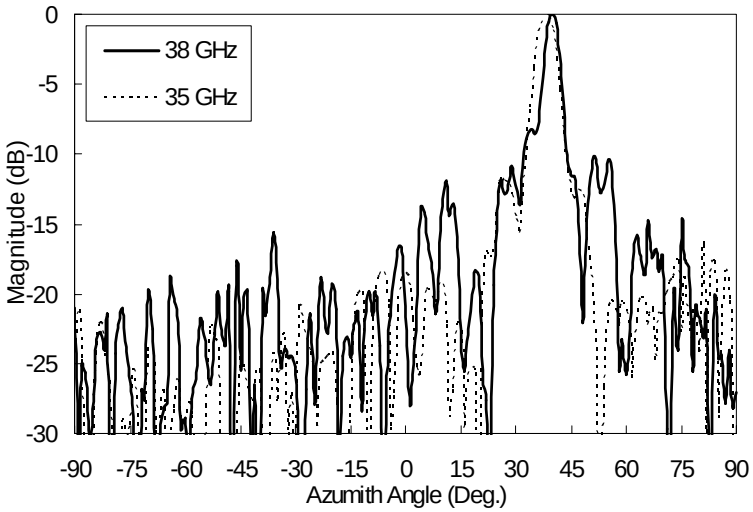

(b)

Fig. 47. Measured bistatic patterns of the 8x16 retrodirective array at (a) 32 GHz, (b) 38 GHz, and (c) 40 GHz.

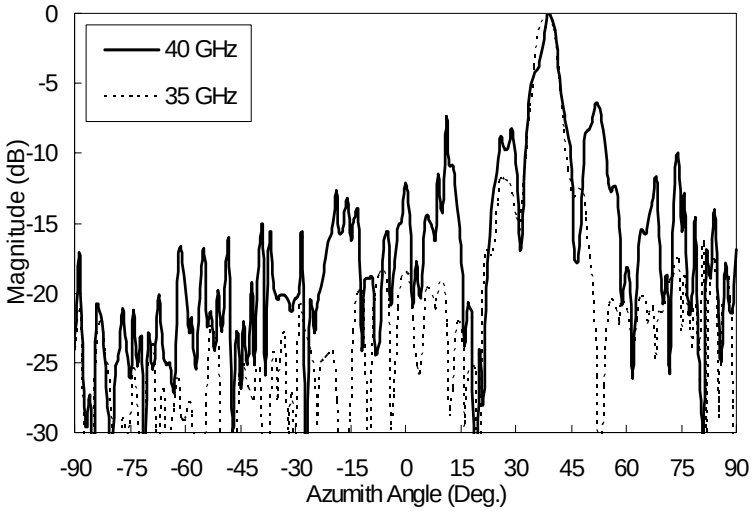

(c)

Fig. 47. Continued.

5. Conclusions

In this chapter, a ultra-wideband dual-ring antenna, a new millimeter-wave rectenna and its arrays are developed. The antenna is designed by combining the TM_{110} modes of two ring resonators on a thick two-layer substrate. The antenna element has a bandwidth of 33.2% (31-42.8 GHz) and an average gain of 4.49 dBi with stable radiation patterns. Using the ultra-wideband antennas, a millimeter-wave rectenna element, a 1x2 rectenna array, and a 2x2 rectenna array are built with conversion efficiencies of 64, 56, and 42%, respectively. These correspond to output voltages of 1.05, 1.97, and 3.42 V. The rectenna arrays are easy to build by cascading rectenna elements and their performances are predictable.

A broadband 8x16 retrodirective array is also presented, which can cover millimeter-wave frequencies from 31 GHz to 43 GHz. The dual-ring antenna is used to design a 4x4 Van Atta array as a sub-array. Placing the array elements and the

transmission line networks on two layers, a large array can be easily built by combining many sub-arrays. It has demonstrated that the 8x16 retrodirective array has a very good beam steering ability. It is believed that these newly developed rectenna array and retrodirective array will be useful in the future millimeter-wave communications and other applications due to its broadband characteristics.

CHAPTER V

COMPACT DUAL-FREQUENCY RECTENNA USING MEANDERED SLOTLINE WITH HIGH-ORDER HARMONIC REJECTION

1. Introduction

With the usage of multiple frequency bands in wireless communication systems, some dual-frequency rectennas have been developed for the ISM band [9][13]. In these designs, the antenna elements usually have a dimension of one wavelength length or even more. To be integrated with other wireless communication or sensor components, a miniature rectenna is preferred, while the receiving antenna of the rectenna can be shared with other components and the rectenna can simultaneously provide DC voltage to neighbored electronic devices or to recharge batteries. On the other hand, the harmonic signal is an important concern in wireless communications. In the rectenna design, it is also intend to suppress harmonics to avoid the efficiency reduction.

In this chapter, a novel dual-frequency rectenna is presented, which is designed at 2.45 GHz and 5.8 GHz so the rectenna can operate at either frequency dependent upon power availability. Two reduced sized slot ring antennas are used with one is located inside the other. To reject the harmonic signals generated by the diode, a compact hairpin lowpass filter is combined. The rectifying circuit of the rectenna adopts a half-wave rectifier. An EM-simulator IE3D is used to optimize the antennas, the feed-line,

and the lowpass filter.

2. Compact rectenna design

A. Meandered slot antenna

The geometry of the proposed rectenna is shown in Figure 48. The rectenna is printed on RT/Duroid 5880 substrate with ε_r = 2.2 and a thickness (h) of 0.508 mm (= 20 mil). It consists of a slot annual ring antenna, a slot rectangular ring antenna, a lowpass filter, and a rectifying circuit. Detailed design parameters are given in Table 5. The slot annual ring antenna operates at lower frequency (2.45 GHz) and the slot rectangular ring antenna is used to excite the higher frequency (5.8 GHz). For the slot structure, the slot wavelength λ_s is given by [63]

$$\lambda_s = \lambda_0 \{1.045 - 0.365 \ln \varepsilon_r + \frac{6.3W\varepsilon_r^{0.945}}{238.64h + 100W} - [0.148 - \frac{8.81(\varepsilon_r + 0.95)}{100\varepsilon_r}] \cdot \ln(\frac{h}{\lambda_0})\} \quad (78)$$

where λ_0 is the free-space wavelength and W is the slot width. Here, one slot wavelength of 2.45 GHz is 109.85 mm. The slot annual ring antenna is a compact design by using the notched meander line and the circumference (= $\pi(R_{out}+R_{in})$) of the ring antenna is $0.72\lambda_s$. The antenna only has a 24% antenna area of the previous design that has a circumference of $1.4\lambda_s$ [9]. The slot rectangular ring is inset within the meandered slot annual ring. The circumference of the slot rectangular ring is 45.38 mm, which is equal to $0.96\lambda_s$ of 5.8 GHz. A simple microstrip feed-line is used to excite both antennas.

The return loss looking into the feed-line is shown in Figure 49. There are five resonant frequencies including 2.45 and 5.8 GHz. The harmonics of the second and the

third orders of 2.45 GHz, i.e. 4.9 GHz and 7.35 GHz, are rejected. The lowpass filter will be used to block other undesired harmonic frequencies. Rectenna return loss, radiation patterns, and gain are measured after combining the antennas with the lowpass filter to represent the overall harmonic rejection performance.

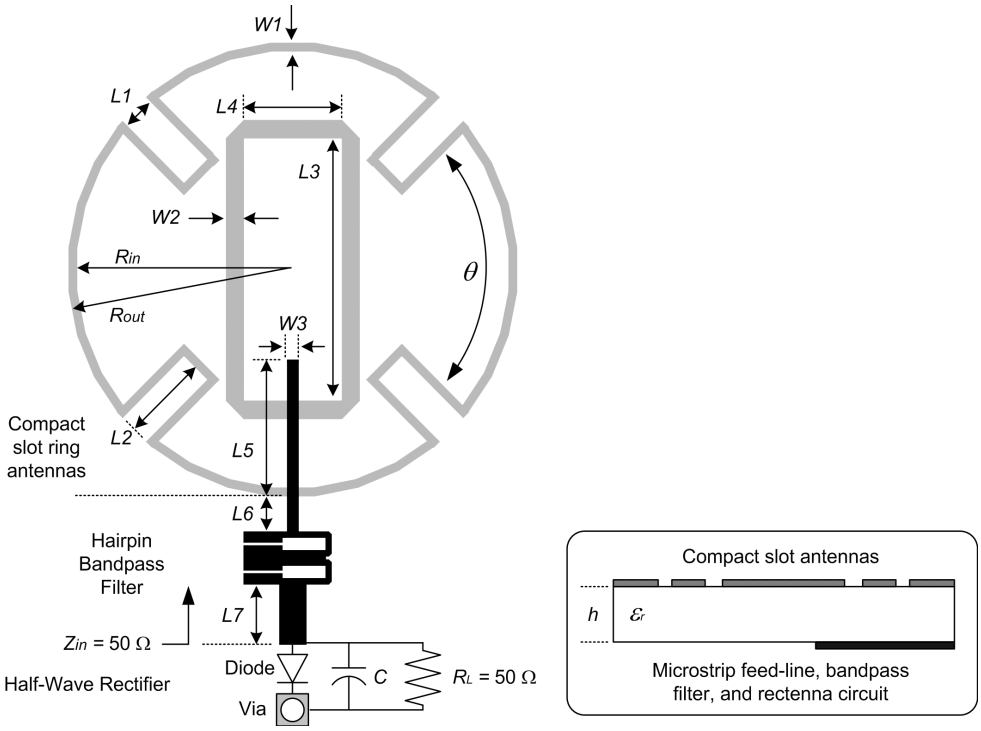

Fig. 48. The configuration of the compact dual-frequency rectenna. The gray line represents the slot ring antenna and the slot rectangular antenna. The black line represents the microstrip feed-line, band-pass filter, and rectenna circuit.

TABLE 5. Summary of the dual-frequency rectenna dimensions.

Item	(mm)	Item	(mm)	Item	(mm)
R_{out}	12.77	L_5	7.68	W_3	0.64
R_{in}	12.29	L_6	2.0	W_4	1.53
L_1	1.9	L_7	3.4	W_5	0.33
L_2	4.94	L_8	5.0	W_6	0.61
L_3	14.79	W_1	0.475	W_7	0.17
L_4	5.6	W_2	1.02	θ	76.72°

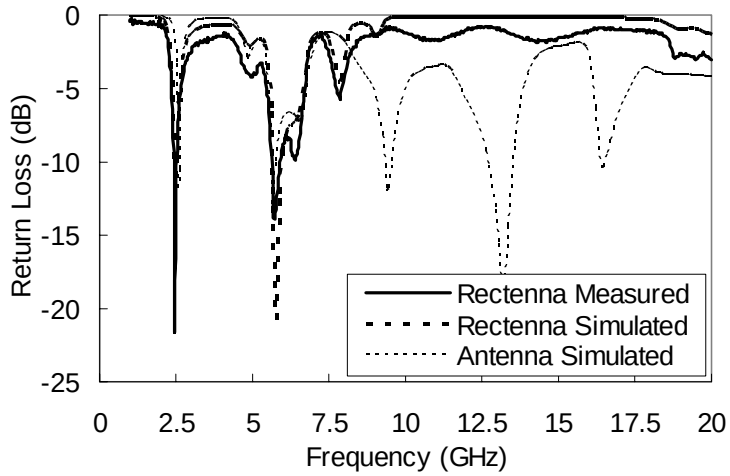

Fig. 49. Frequency responses of the antenna element and the rectenna (the ring antennas with the filter).

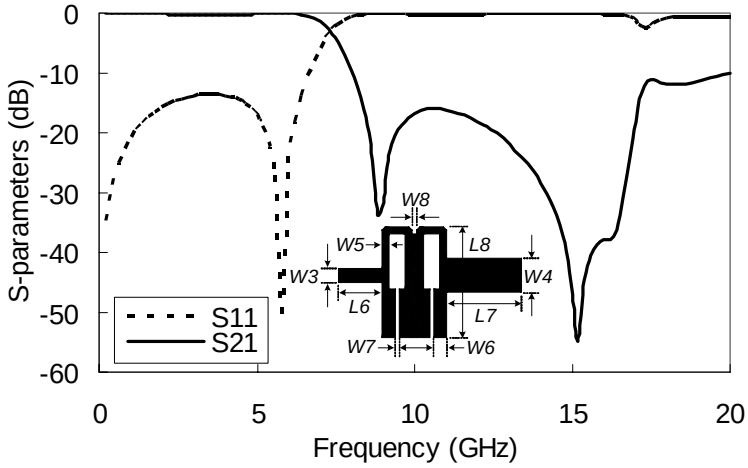

Fig. 50. Geometry and S-parameters of the hairpin lowpass filter.

B. Lowpass filter

The lowpass filter shown in Figures 48 and 50 is designed based on the elliptic-function filter using hair resonators reported in [64]. Two hairpin resonator components are cascaded to obtain a sharper cutoff frequency response. The filter dimension parameters are given in Table 5. The filter is designed to reject harmonic signals above 8

GHz. Its measured return loss and the insertion loss are shown in Figure 50. The filter has a 3-dB passband from DC to 7.3 GHz where its insertion loss is less than 0.22 dB. It is observed that the filter can reject higher order harmonics of both 2.45 GHz and 5.8 GHz.

C. Rectifier

The rectifying circuit used here is a half-wave rectifier. This kind of rectifiers has been analyzed in [52] and [65]. It has been known that the maximum output voltage can be obtained when the value of $R_L C >> 1/f_0$ where f_0 is the operating frequency. At this time, the ripple voltage is very small and can be neglected. Here, the GaAs Schottky diode MA4E1317 is used as the rectifying device. The load resistance (R_L) and C were chosen as 51.3 Ω and 470 μf, respectively.

TABLE 6. Return loss of the dual-frequency rectenna.

Freq. (GHz)	Order	RL (dB)	Freq. (GHz)	Order	RL (dB)
2.45	1st	17	5.8	1st	13
4.9	2nd	4.07	11.6	2nd	1.38
7.35	3rd	1.74	17.4	3rd	1.01
9.8	4th	1.13			
12.25	5th	0.84			
14.7	6th	1.63			

3. Experiment results

The measured and simulated return loss of the rectenna (antennas combined with the filter) is shown in Figure 49. The measured results agree very well with the

simulations. The rectenna can effectively reject the harmonics signals generated by the rectifying diode and prevent them from reradiating by the antenna. The return losses at fundamental and harmonic frequencies are summarized in Table 6. The rectenna have maximum gains of 2.2 dBi and 3.6 dBi at 2.45 GHz and 5.8 GHz, respectively.

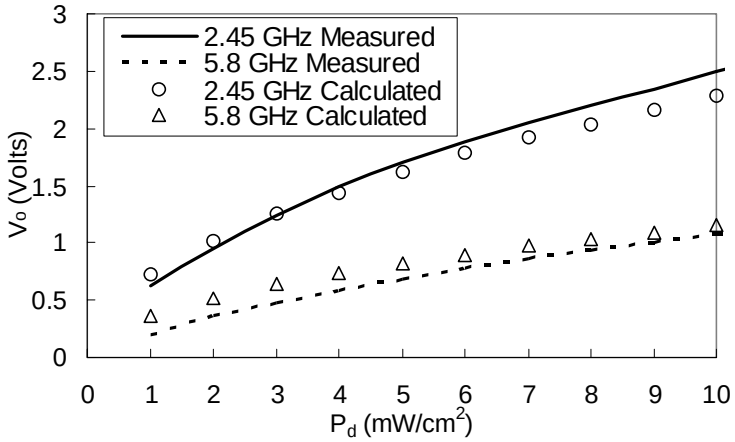

(a)

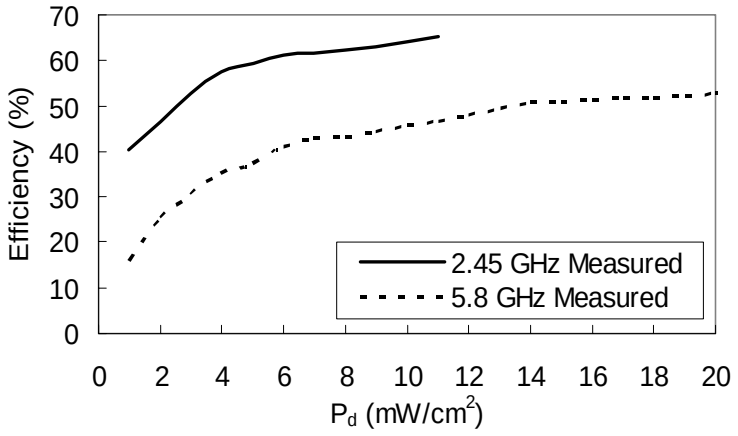

(b)

Fig. 51. Dual-frequency rectenna performance as a function of the incident power density: (a) output voltage and (b) conversion efficiency.

The rectenna is tested by using a waveguide simulator [12]. The output voltage and

the rectenna conversion efficiency are shown in Figure 51, as a function of the power density. The measured results match the calculated results closely. At the same power density, the output of 2.45 GHz is higher than that of 5.8 GHz due to a larger effective area. To achieve the same output voltage, operating at 5.8 GHz needs a power density about 4 times that at 2.45 GHz.

The output voltage versus the received power is shown in Figure 52. While receiving the same power, the rectenna operating at either 2.45 or 5.8 GHz has almost the same performance. When P_r = 200 mW, the rectenna at 2.45 GHz has a DC output of 2.6 V and a conversion efficiency of 65%. The output voltage and efficiency increase with the received power.

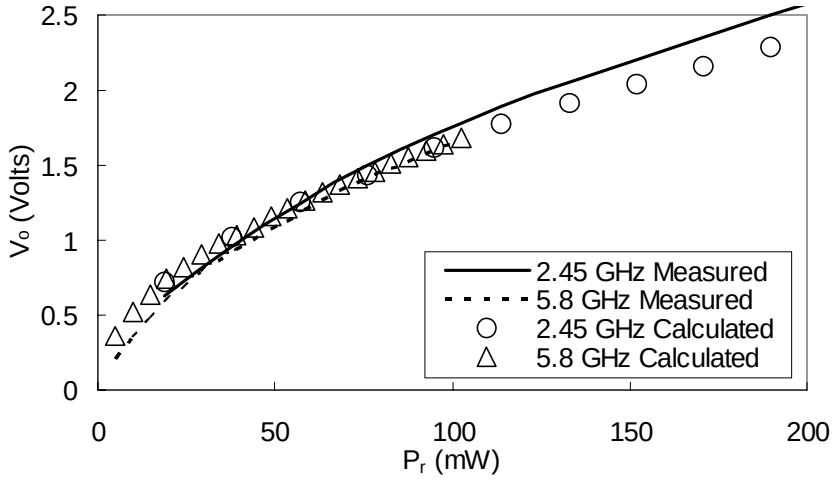

Fig. 52. Dual-frequency rectenna DC output voltage versus the received RF power.

4. Conclusions

In this chapter, a new dual-frequency rectenna has been developed, which can simultaneously operate at two ISM-bands, i.e., 2.45 and 5.8 GHz. Two compact slot ring

antennas are designed and then integrated with a hairpin lowpass filter to reject unwanted harmonic signals up to the sixth order. The rectenna has gains of 2.19 and 3.6 dBi at 2.45 and 5.8 GHz, respectively. The rectenna has been tested and it can provide a DC voltage of 2.6 V with a conversion efficiency of 65% as the power density is 10 mW/cm^2. The dual-frequency rectenna can be used in the applications of microwave power transmission, RFID tag, embedded sensor, or combined with other wireless communication components.

CHAPTER VI

NEWLY DEVELOPED ULTRA-WIDEBAND PLANAR MICROSTRIP ANTENNAS*

1. Introduction

The UWB radio systems have become one of the most important communication systems since the demanding of the high data rate between the base station/mobile station and the mobile station. Many UWB antennas fed by microstrip and coplanar waveguide have been reported in the literatures [66-71]. These antennas use the monopole configuration such as square, triangle, circular, and hexagonal antennas; the dipole configuration like bow-tie antennas. Some of reported UWB antennas do not have a planar structure due to their ground planes perpendicular to the radiators. The use of a printed planar structure has many advantages such as ease of fabrication, low cost, and lightweight. Furthermore, due to the planar structure, the antennas can be easily integrated with other circuit components on the printed circuit board to form a complete system. The ring antennas and the patch antennas, which have the planar configuration, are hence good candidates in UWB applications.

In this chapter, four ultra-wideband antennas fed by a microstrip line or a CPW are presented. Traditional ring antennas have a quite narrow bandwidth. However, this

drawback has been overcome in the new design. The new annual ring antenna adopts a proximity-coupled configuration. The parameters affecting the antenna wideband characteristic are discussed. Then an elliptical ring antenna fed by a CPW with a truncated ground plane is demonstrated. The antenna can not only cover microwave frequencies but also can be tuned to cover the UHF band. Finally a UHF house-shaped patch antenna is reported. The return loss, antenna gain, and antenna pattern of these ultra-wideband antennas will be presented.

2. Annual ring antenna

A. Antenna design

The geometry of the proposed UWB ring antenna is shown in Figure 53. The antenna has a dimension of 44 x 44 mm^2 and is printed on RT/Duroid 5880 substrate of 1.42 mm (= 56 mil) thickness, where h_1 = 1.29 mm and h_2 = 0.13 mm. The substrate has a relative dielectric constant of 2.2 ($\varepsilon_1 = \varepsilon_2$). The UWB antenna consists of a proximity-coupled ring antenna, a feed-line, and two finite metal planes. The feed-line, realized by a microstrip line, is sandwiched between the annual ring and the two metal planes as the ground plane. The inner radius (r) and the outer radius (R) of the ring are 3.5 mm and 11 mm, respectively. The feed-line has a length of L_f = 33 mm and width of W_f = 2.97 mm. The ground plane has a length of L_g = 44 and width of W_g = 11 mm.

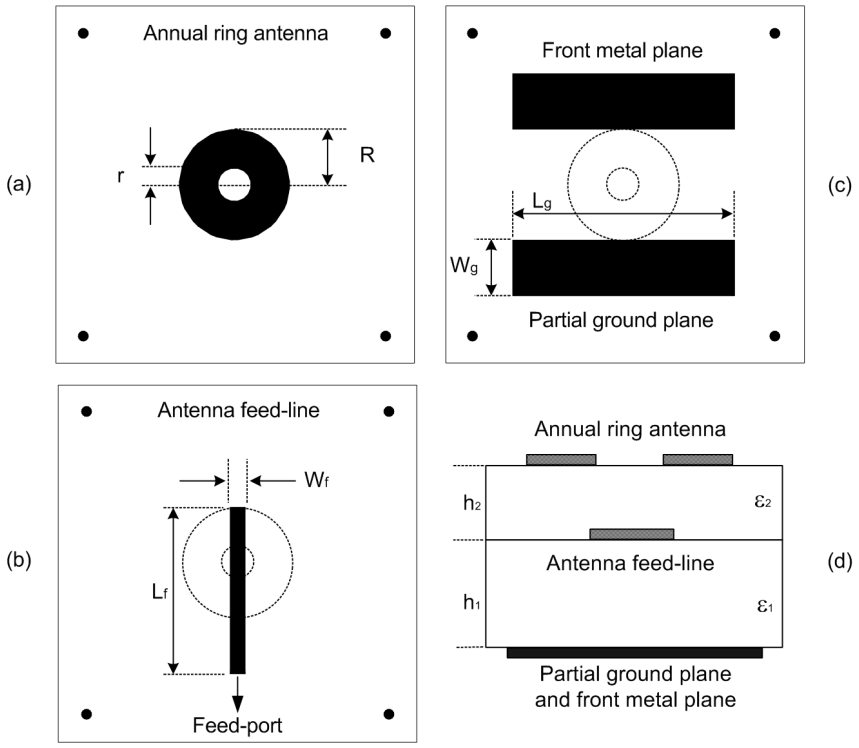

Fig. 53. Geometry of the UWB annual ring antenna: (a) Annual ring antenna layer, (b) microstrip feed-line layer, (c) bottom ground plane layer, and (d) cross-section view.

The IE3D was used to simulate the ultra-wideband antenna. It has been found that the feed-line length affects the operation bandwidth of the UWB antenna while the feed-line width is set constant, as shown in Figure 54. It is observed that the antenna with L_f = 33 mm has the best return loss while the other feed-line lengths result in wider stop-band (return loss < 10 dB) bandwidths. So the feed-line of 33 mm is chosen in the final work. The dimension of two metal planes has been tuned for better matching bandwidth. Without the front metal plane, there will be a stop-band between 5-7 GHz, which results in a reduced effective bandwidth. The metal plane behaves as a parasitic resonator to increase the bandwidth. Another parameter affecting the bandwidth is the inner radius of the ring when the outer radius is fixed for simplifying the design. As the inner radius

increased, the return loss becomes smaller and hence the bandwidth decreases gradually. Here, the best inner radius of 3.5 mm has been used.

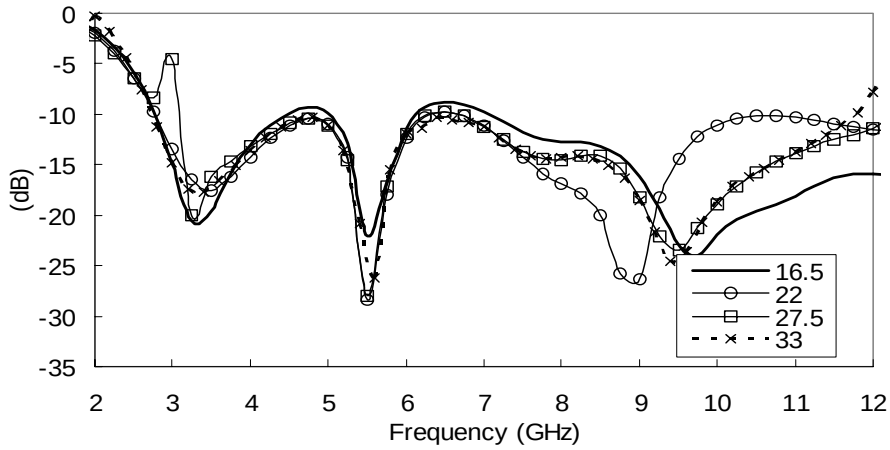

Fig. 54. Simulated return loss for different feed-line lengths (L_f = 16.5, 22, 27.5, and 33 mm).

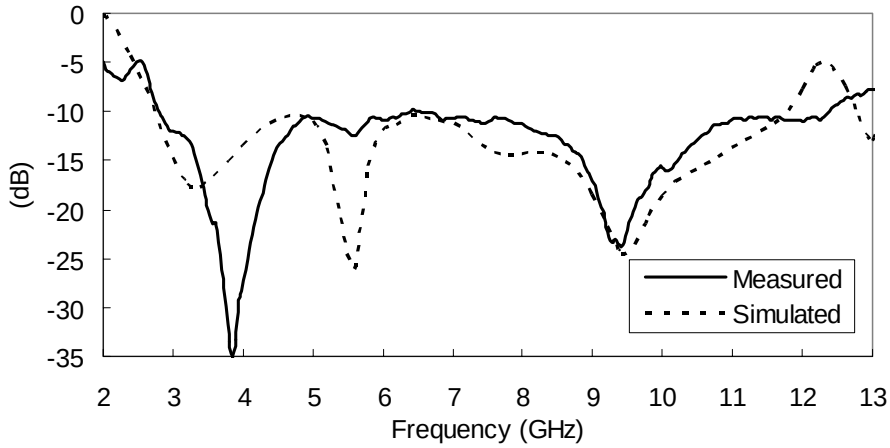

Fig. 55. Measured and simulated return losses with L_f = 33 mm.

B. Measurement results

Measured and simulated return losses of the UWB ring antenna are shown in

Figure 56. The measured operating bandwidth is very close to the simulated results (2.7-11.8 GHz). The band of the return loss less than 10 dB is from 2.8 GHz to 12.3 GHz, corresponding to a bandwidth of 8.5 GHz. This performance satisfies the requirement of the UWB antenna of 3.1-10.6 GHz. It is noted that without the front metal plane, the bandwidth will reduce to 6.9 GHz. The measured peak antenna gains versus the frequency are shown in Figure 55. The maximum gain is 5 dBi at 7 GHz and the average gain is 2.93 dBi.

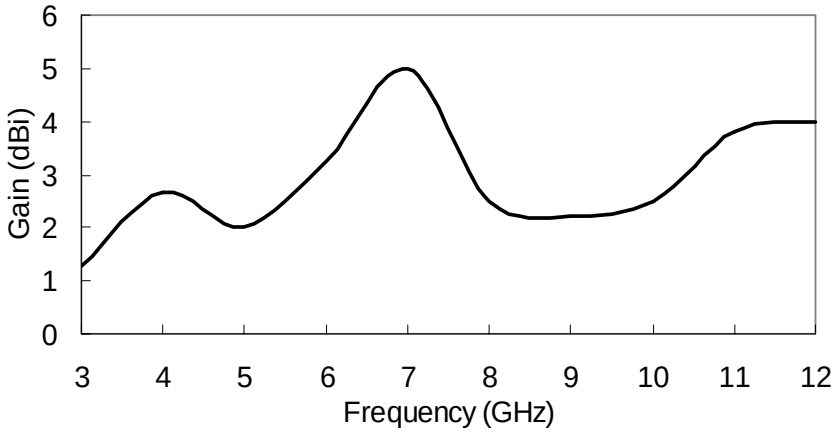

Fig. 56. Measured maximum gain of the UWB annual ring antenna.

The antenna radiation patterns on E-plane and H-plane for 3 GHz, 6 GHz, and 9 GHz are shown in Figure 57. It is observed that the patterns do not change much at these frequencies. E-plane patterns are similar to the omni-directional pattern and H-plane patterns have four main lobes looking like a butterfly, which are almost perpendicular to each other. The radiation patterns also display symmetry to the broadside. These results represent the radiation patterns are quite stable within the operating bandwidth. It is

noted that at 9 GHz the pattern gains in 90^{o} and 270^{o} become lower, which may be due to the parasitic effects of the metal plane.

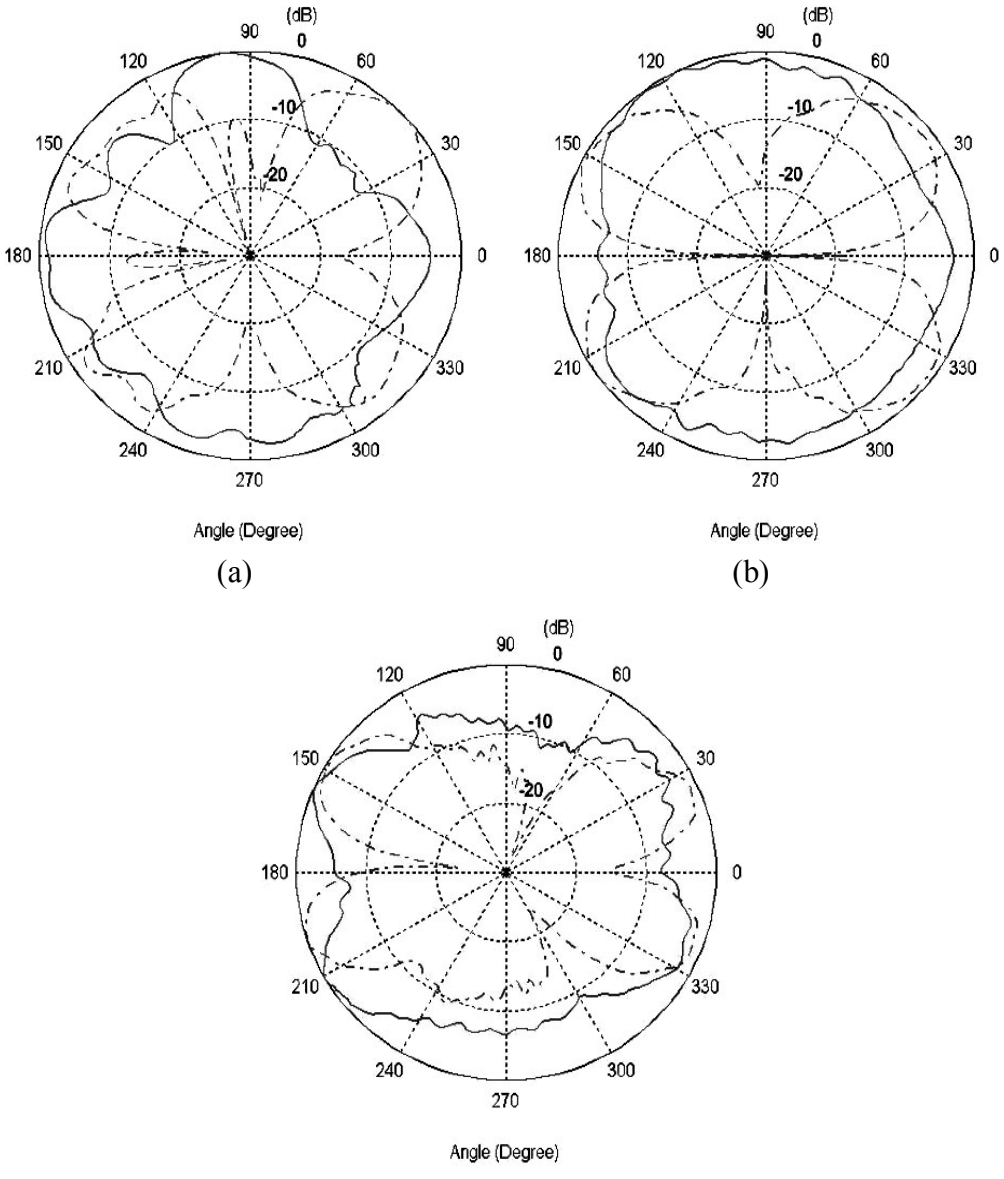

Fig. 57. Measured antenna radiation patterns on E-plane (solid lines) and H-plane (dash lines) at (a) 3 GHz, (b) 6 GHz, and (c) 9 GHz.

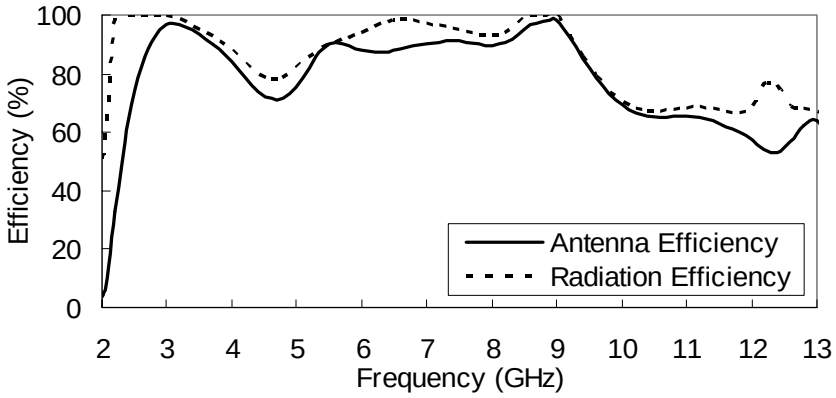

Fig. 58. Simulated efficiency of the UWB annual ring antenna.

The antenna efficiency of the ring antenna, which is equal to the radiation efficiency minus the return loss, is shown in Figure 58. The antenna efficiency has a maximum value of 98% and a minimum value of 53% within the frequency range from 2.8 GHz to 12.3 GHz. The average antenna efficiency is 81%.

3. Elliptical ring antenna

A. Antenna design

The geometry of the proposed UWB elliptic ring antenna is shown in Figure 59. The antenna has a dimension of 29 x 26 mm^2 and is printed on RT/Duroid 5880 substrate of 2.36 mm (= 93 mil) thickness (h), with a relative dielectric constant (ε_r) of 2.2. This antenna consists of an elliptical ring on the front side and a CPW feed-line on the backside. The CPW-fed stripline has to be extended across the elliptical ring to achieve the wideband operation. The optimal parameters are given as: r = 1.78 mm, R = 8.09 mm, L_e = 12.87 mm, L_f = 25.52 mm, W_f = 2.6 mm, G_f = 0.4 mm, W_g = 9.8 mm, and L_g = 6.48 mm.

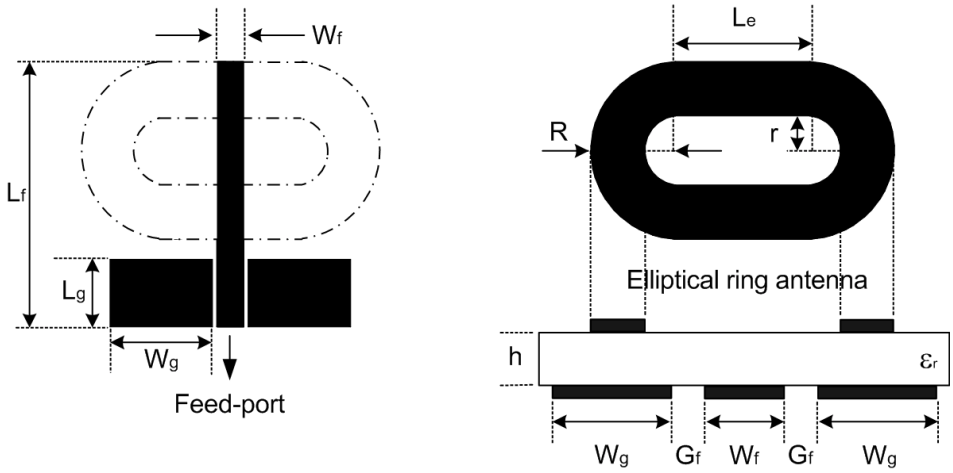

Fig. 59. Geometry of the UWB elliptical ring antenna.

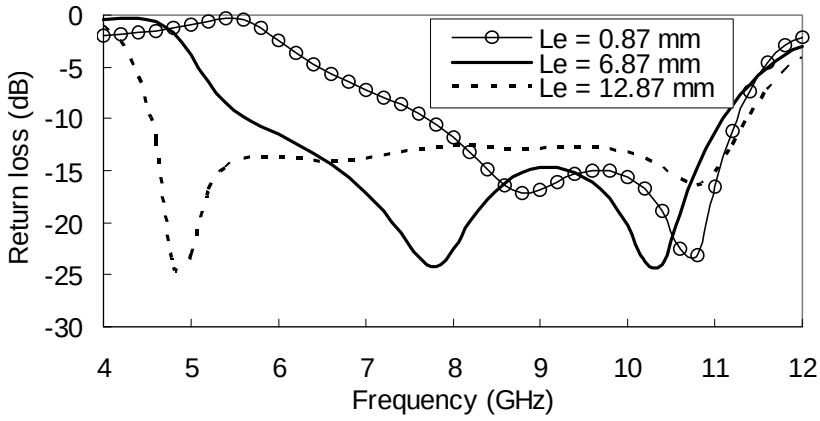

Fig. 60. Simulated return loss for different major axis lengths.

The elliptical ring antenna is designed based on a well-matched wideband annual ring antenna. The annual ring antenna is formed by setting L_e equal to 0.87 mm. When the length of the major axis increases, the annual ring becomes an elliptic ring and its bandwidth is increased gradually, as shown in Figure 60. This length of L_e controls the effective area of the elliptical ring and hence is the primary parameter to determine the

coupling between the antenna element and the ground plane. The thickness of the substrate also affects the bandwidth. If it is increased, the return loss will become worse. Another parameter affecting the bandwidth is the gap width of the CPW (G_f). When the gap becomes smaller, a stop-band (return loss < 10 dB) forms centered at 8 GHz. When the gap width is increased, the return loss will become worse and hence the bandwidth decreases gradually.

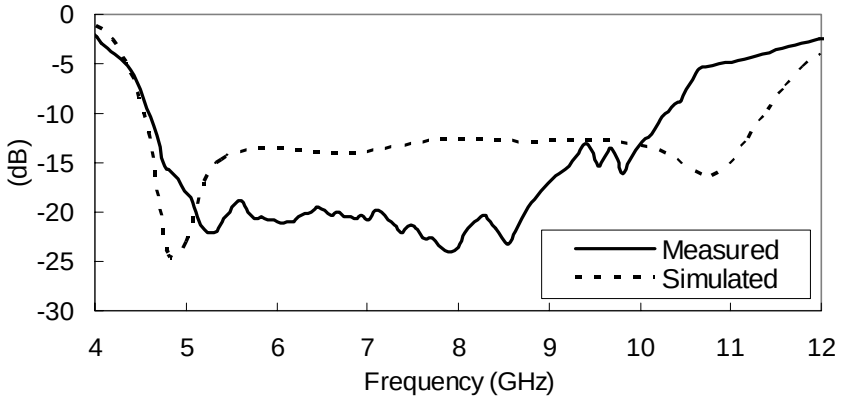

Fig. 61. Measured and simulated return losses with L_e = 12.87 mm.

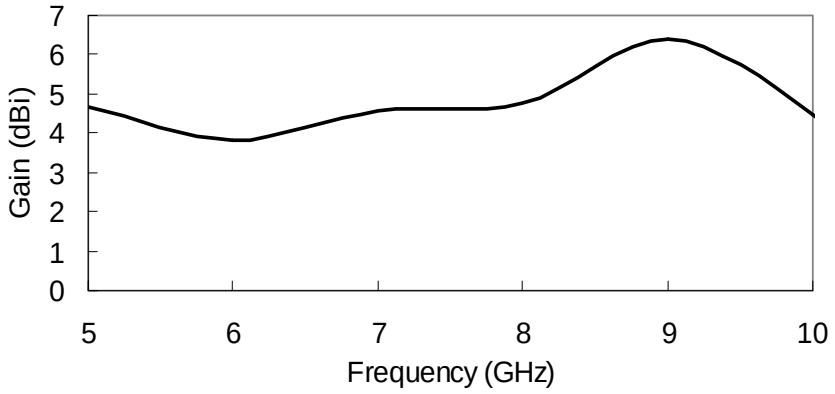

Fig. 62. Measured maximum gain of the UWB elliptical ring antenna.

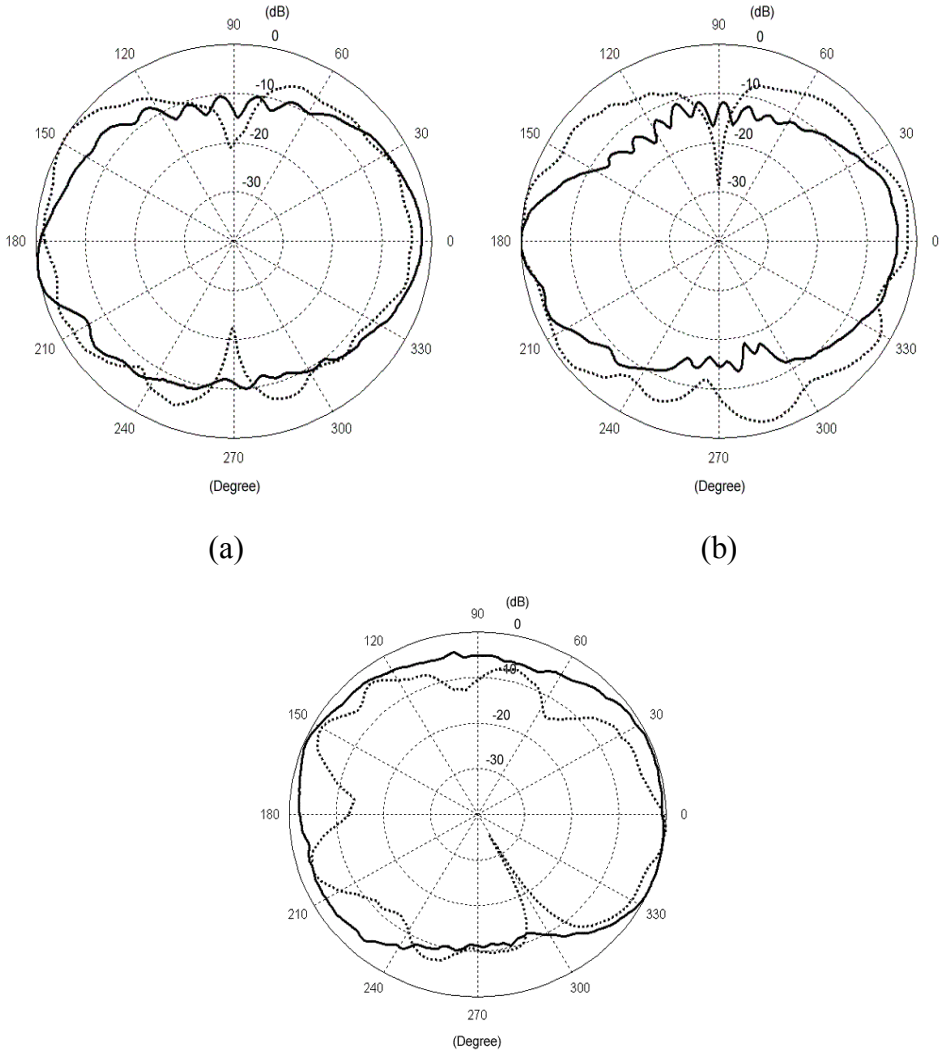

Fig. 63. Measured elliptical ring antenna radiation patterns on E-plane and H-plane at (a) 5 GHz, (b) 7 GHz, and (c) 9 GHz.

B. Experiment results

Simulated and measured return losses of the UWB elliptical ring antenna are shown in Figure 61. The measured operating bandwidth is from 4.6 GHz to 10.3 GHz, which is very close to the simulated results (4.5-11.3 GHz). The measured maximum

antenna gain versus the frequency is shown in Figure 62. The average gain is 4.48 dBi and the maximum gain is 6.38 dBi at 9 GHz. The radiation patterns on E-plane and H-plane for 5 GHz, 7 GHz, and 9 GHz are shown in Figure 63. It is observed that the patterns do not change much at these frequencies. E-plane patterns are similar to H-plane patterns. The radiation patterns also display symmetry to the broadside. The cross-polarization patterns are not shown here. They are about 20 dB less than the co-polarization patterns at broadside direction. These results display the radiation patterns are quite stable over all the UWB bandwidth.

4. L-band antenna

A. Elliptical ring antenna design

The purpose of designing this antenna is to use it as the antenna element of the short-distance data transmission for the L-band (1-2 GHz). The geometry of the L-band elliptical ring antenna is the same as the one shown in Figure 58 except its different dimensions. The antenna is printed on RT/Duroid 6010.2 substrate with a thickness (h) of 3.81 mm (= 150 mil) and a relative dielectric constant (ε_r) of 10.2. The input impedance of the antenna is 50 Ω. The antenna parameters are given: r = 8.03 mm, R = 22.64 mm, L_e = 33.6 mm, L_f = 82 mm, W_f = 8 mm, G_f = 2 mm, W_g = 29.2 mm, and L_g = 34.29 mm. The antenna has a dimension of 79x82 mm^2.

One main parameter to control the bandwidth is the thickness (h) of the substrate. If the thickness is reduced, the bandwidth will decrease. However, at this time, the coupling between the ring patch element and the feed-line becomes stronger so the

antenna gain increases. The second parameter is the length of the major axis (L_e), which determines the coupling area between the ring and the ground plane. Therefore, the width of the ground plane (W_g) is proportional to the major axis length. Both of them have been optimized here.

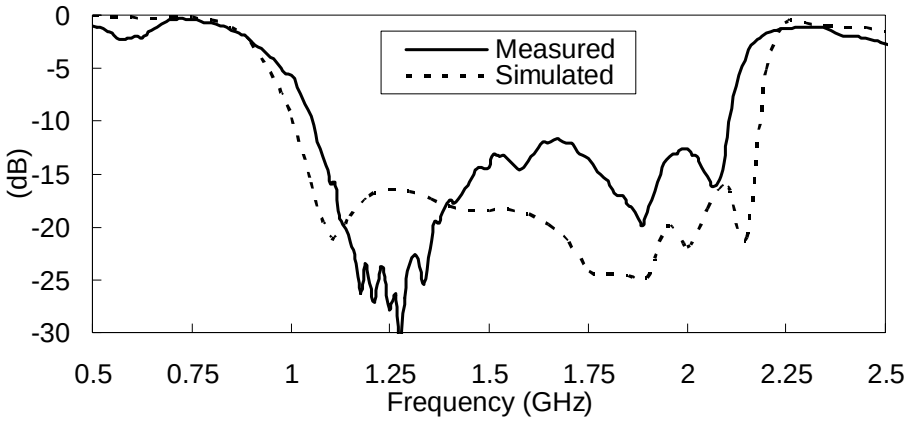

Fig. 64. Measured and simulated return losses of the L-band antenna.

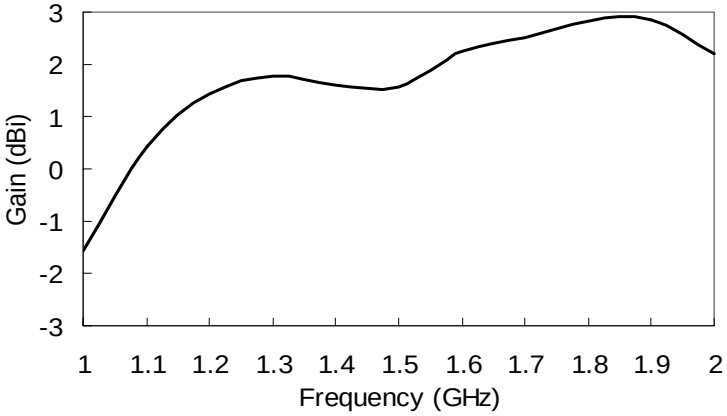

Fig. 65. Maximum gains of the L-band antenna.

B. Measurement results and discussions

Simulated and measured return losses of the L-band elliptical ring antenna are

shown in Figure 64. The measured operating band is from 1.05 GHz to 2.1 GHz while the simulated operating band is from 1 GHz to 2.18 GHz. This frequency band provides an effective bandwidth for the L-band applications. The measured results shift a little toward to the lower frequency. However, the measured results have a similar trend to the simulated results. The antenna has a bandwidth of 71% (center at 1.48 GHz) while the simulated one is 80%.

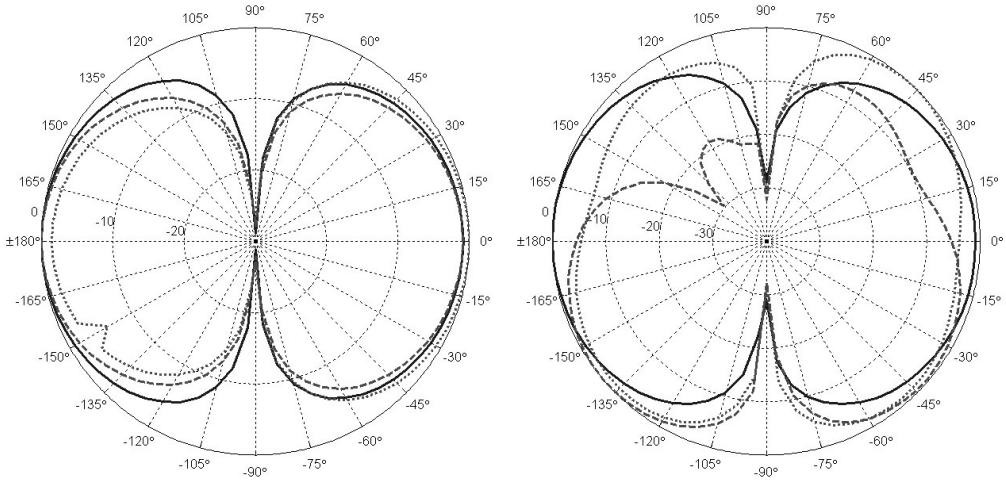

(a) (b)

Fig. 66. Radiation patterns of the L-band antenna at (a) $\phi = 0^o$ and (b) $\phi = 90^o$. Solid lines: 1.0 GHz; dash lines: 1.5 GHz; dot line: 2.0 GHz.

The simulated maximum antenna gains are shown in Figure 65. The average gain is 1.62 dBi. Lower gain is obtained due to the thick substrate. The simulated E_ϕ-plane patterns of 1, 1.5, and 2 GHz are shown in Figure 66 The radiation patterns display nearly symmetry to the broadside and are similar to the patterns of a dipole antenna. The measured results are not shown here due to the frequency limit of our antenna testing

system.

5. UHF antenna

A. House-shaped patch antenna

The geometry of the proposed ultra-wideband UHF antenna is shown in Figure 67. The antenna is printed on RT/Duroid 5880 substrate with a thickness (h) of 1.91 mm (= 75 mil) and a relative dielectric constant (ε_r) of 2.2. This antenna consists of a house-shaped microstrip patch antenna on the front side and a partial notched ground plane on the backside. The characteristic impedance of the antenna feed-line is 50 Ω. The antenna parameters are designed as: L_0 = 44.3 mm, L_1 = 67.8 mm, L_2 = 46.2 mm, L_3 = 46.7 mm, W_0 = 6.6 mm, W_1 = 143 mm, W_2 = 39.8 mm, W_3 = 11.2 mm, W_4 = 54.9 mm, and W_5 = 16.6 mm. The antenna has a dimension of 143x137 mm^2. The HFSS was used to optimize the ultra-wideband antenna design.

One main parameter to control the bandwidth is the thickness of the substrate h. If the thickness is reduced, the bandwidth will decrease. However, at this time, the coupling between the patch element and the ground plane becomes stronger so the antenna gain will increase. Other important parameters are L_3 and W_4 in the roof part of the house-shaped patch, which affect the poles of the frequency response. All these parameters have been optimized for the broadband operation.

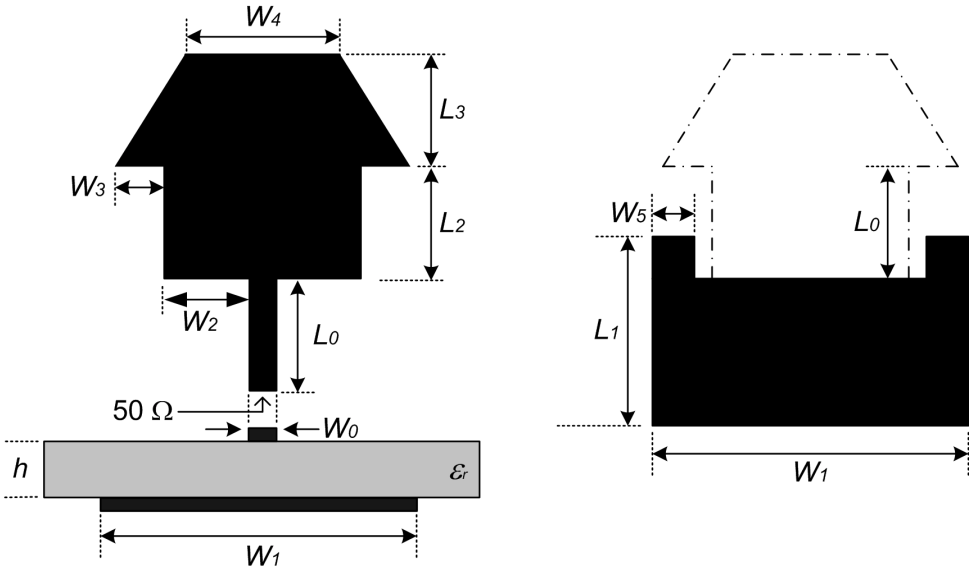

Fig. 67. Geometry of the ultra-wideband house-shaped patch antenna: (a) front side and cross-section view and (b) backside.

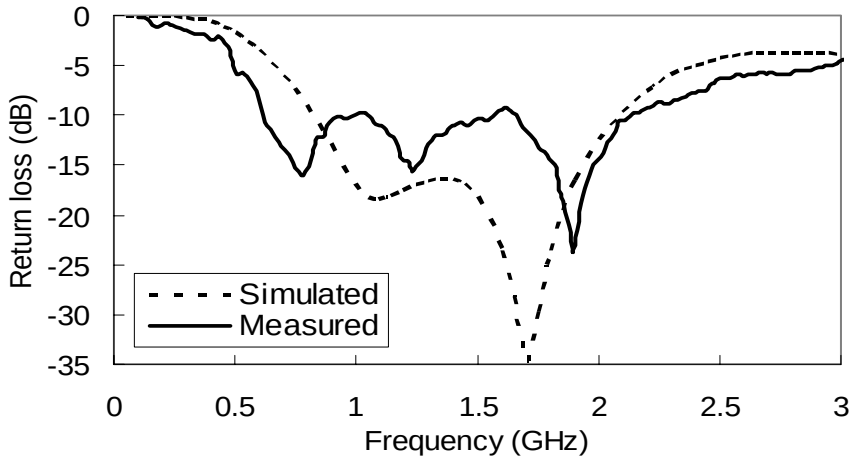

Fig. 68. Simulated and measured return losses of the UHF house-shaped antenna.

B. Measurement results and discussions

Simulated and measured return losses of the UHF antenna are shown in Figure 68. The measured 10-dB operation bandwidth is approximately from 0.62 GHz to 2.13 GHz,

while the simulated bandwidth is from 0.83 to 2.09 GHz. The measured results have a similar trend as the simulated results. The antenna has a 10-dB bandwidth of 104% (center at 1.32 GHz), while the simulated one is 95%.

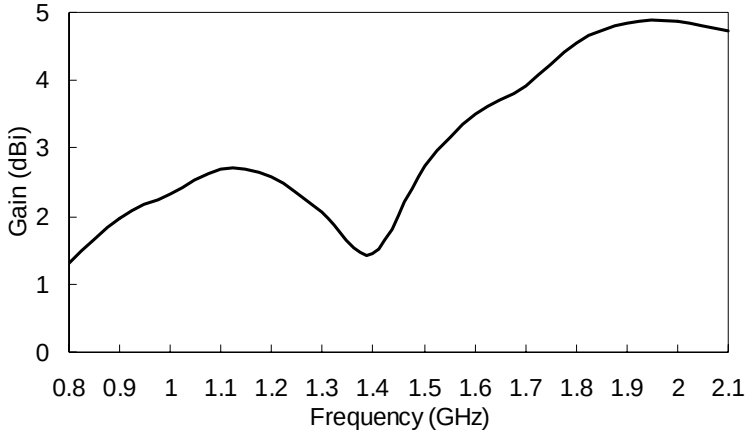

Fig. 69. Maximum gains of the ultra-wideband UHF antenna.

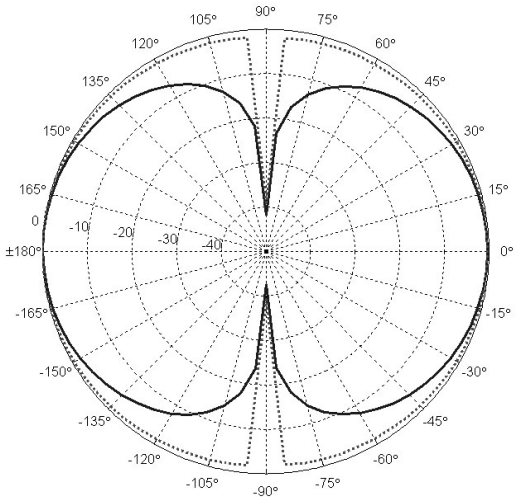

Fig. 70. Radiation patterns of the UHF antenna at 1.0 GHz. Solid lines: $\phi = 0^{o}$; dot lines: $\phi = 90^{o}$.

The simulated maximum antenna gains from 0.8 GHz to 2.1 GHz are shown in Figure 69, with an average value of 3.11 dBi. The radiation patterns of the antenna are similar to those of a dipole antenna. The simulated radiation patterns on the E_{ϕ}-plane at 1 GHz are shown in Figure 70.

6. Conclusions

In this chapter, four ultra-wideband antennas are explored and studied, including design parameters affecting the antenna wideband characteristics and measured performances. The first one is an annual ring antenna. Its feed-line affects the return loss much and a finite metal plane is added to improve the bandwidth. Measured return loss, antenna gain, and radiation patterns demonstrate that the antenna can be used for the ultra-wideband applications from 2.8 GHz to 12.3 GHz with an average gain of 2.93 dBi. Its radiation patterns are very stable within its operating bandwidth. The average antenna efficiency is 81 %.

The second one is a CPW-fed ultra-wideband elliptical ring antenna. Parameters are discussed. The antenna has a 2:1 VSWR from 4.6 GHz to 10.3 GHz with an average gain of 4.48 dBi. The radiation patterns are very stable over the operating bandwidth. The elliptical antenna is then redesigned for the UHF usages with a bandwidth of 71%. Despite the lower gain due to the thick substrate, the return loss is good and the antenna patterns are stable, so it is believed that the antenna can be a good candidate for L-band applications.

Finally, an ultra-wideband microstrip house-shaped patch antenna covering the

UHF band is reported. It has an operation bandwidth from 0.62 GHz to 2.13 GHz, corresponding to a bandwidth of 104% with an average gain is 3.11 dBi. The antenna radiation patterns display a similar appearance as the dipole antenna. Due to the planar structure, the new UHF antenna can be easily integrated with other microstrip circuit components. All of these antennas will be very useful for future ultra-wideband communication, radar, and remote sensing systems.

CHAPTER VII

A NEW CLASS OF HARMONIC COMPONENTS FOR MILLIMETER-WAVE APPLICATIONS

1. Introduction

In the traditional microwave component design, harmonic signals are avoided. These harmonics are due to the resonant modes (m, n) of the component. With suitable signal filtering and rejection, the second-order, or other high-order harmonic modes, can be rejected. However, in millimeter-wave or sub-millimeter-wave bands, fundamental frequency (the lowest mode) components are very small. This results in a problem that a microstrip line is used to feed a planar resonator, because a 50Ω-line width is comparable to the resonator width. Therefore, it would be advantageous to design the high-order mode components to have larger sizes by operating at harmonic frequencies, which reduce the difficulty of the fabrication, feeding, and power handling [72]. The resonant frequency of the high-order mode can be calculated using the transmission line model or the cavity model [73-74].

The objective of this paper is to develop a new class of millimeter-wave harmonic components with comparable performance to those of fundamental frequency components that have been commonly used. Several commonly used components are presented, including a rectangular patch antenna, a bandpass filter, and a 2x4 array. The center frequency is set at 35 GHz. All of these harmonic components are printed on

RT/Duroid 5880 substrate with a thickness of 0.254 mm (= 10 mil) and a relative dielectric constant (ε_r) of 2.2, coated with 1 oz copper whose thickness is 0.036 mm. The HFSS is used to design the harmonic components.

2. Harmonic component analysis

The harmonic component is designed by exciting the high-order resonant mode of the component to operate at the desired harmonic frequency. For the rectangular patch antenna with dimensions W and L (in cm), the resonant frequency f_{mn} (in GHz) for the (m, n) mode is given by [75]

$$f_{mn} = \frac{15}{\sqrt{\varepsilon_r}} \sqrt{\left(\frac{m}{W}\right)^2 + \left(\frac{n}{L}\right)^2} \tag{79}$$

where ε_r is the substrate dielectric constant. Usually the operating mode is the first resonant mode (0, 1). By using a higher-order mode, a higher resonant frequency can be excited without changing the patch dimensions, as shown in Figure 71(a) where it is assumed patch length is equal to patch width, $L = W$, for a square patch element. Only the first three modes with the maximum pattern magnitude in the broadside direction are shown. The patterns of the both modes (0, 2) and (0, 4) have nulls in the broadside direction and hence are not shown. From Figure 71(a), it is observed that a 35 GHz antenna can be built using different patch lengths by utilizing high-order modes. The unwanted resonant frequencies can be suppressed by using a bandpass filter.

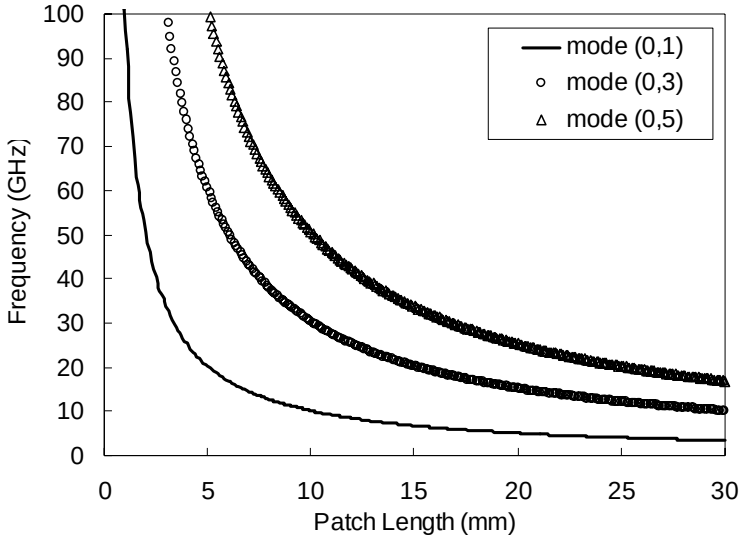

(a)

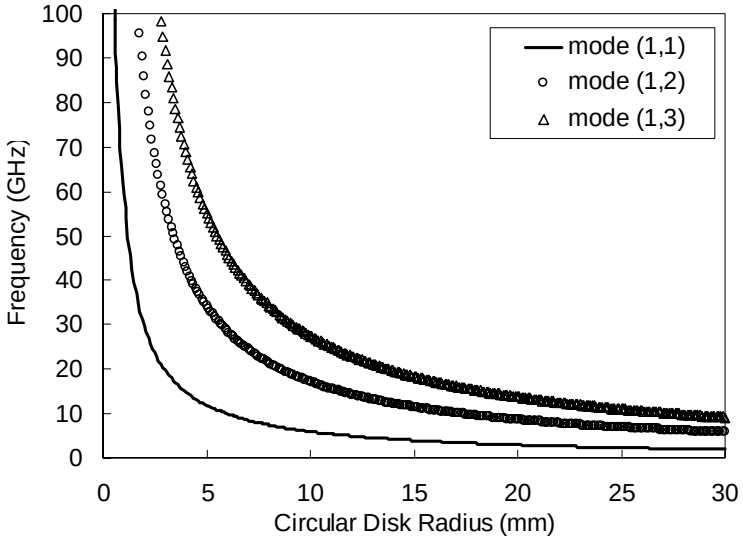

(b)

Fig. 71. Mode charts of (a) rectangular patch antenna and (b) circular disk antenna.

Similar to the rectangular patch, the resonant frequency (in GHz) of the circular disk is given by [75]

$$f_{mn} = \frac{15}{\pi\sqrt{\varepsilon_r}} \frac{\chi_{mn}}{a} \tag{80}$$

where the eigenvalue χ_{mn} decides the resonant mode/frequency and a (in cm) is the radius of the disk. The mode chart of the circular disk is shown in Figure 71(b). The mode (2, m) has a null pattern in the broadside direction and it is not shown. In this research, we will focus on the design of rectangular patch antennas.

To design the band-pass filter, a square ring resonator is used, whose circumference l_r is given by [76]

$$l_r = p\lambda_g \tag{81}$$

where p is the mode number and λ_g is the guided wavelength. For high frequency component design, by using high-order mode (i.e. large p) one can keep the resonator size the same as that of low frequency. Note that the equations mentioned above do not consider the fringing field effects, which may result in a small difference between the physical size and the calculated size of the patch element or the filter.

3. Third-order harmonic antenna

Two rectangular patch antennas, one designed at the fundamental frequency mode (0, 1) of 35 GHz and the other at the harmonic frequency, mode (0, 3) of 11.67 GHz, are shown in Figure 72. Calculated patch lengths are 2.9 mm at 35 GHz and 8.7 mm at 11.67 GHz, respectively. The actual lengths are slightly different after they are optimized by the electromagnetic simulator. The truncated position controls the axial ratio for circular polarization. The dimensions of the harmonic antenna (HA) are about three times of those in the traditional antenna (TA). Obviously the large size of the harmonic antenna makes it much easier to fabricate with good fabrication accuracy. This

is especially true for even higher frequency operation such as the W-band.

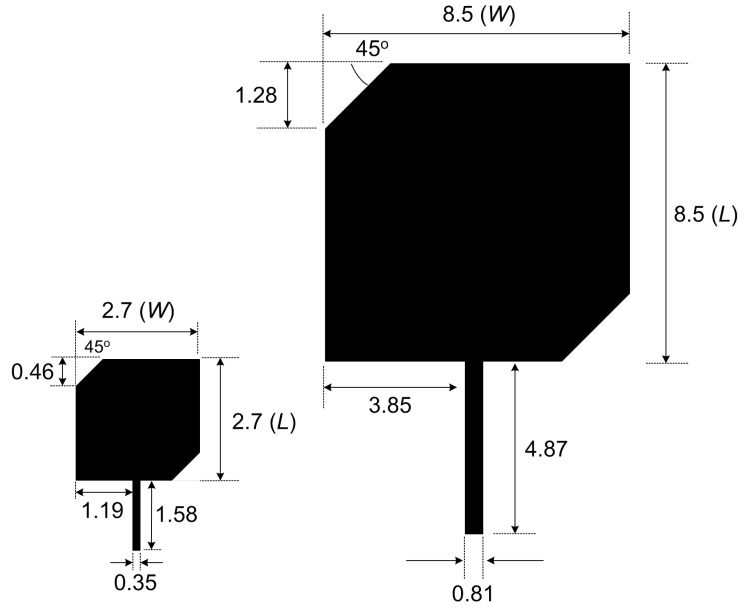

Fig. 72. 35 GHz patch antennas: the left one is the traditional antenna operating at the fundamental mode and the right one is the harmonic antenna operating at third mode. All dimensions are in millimeter.

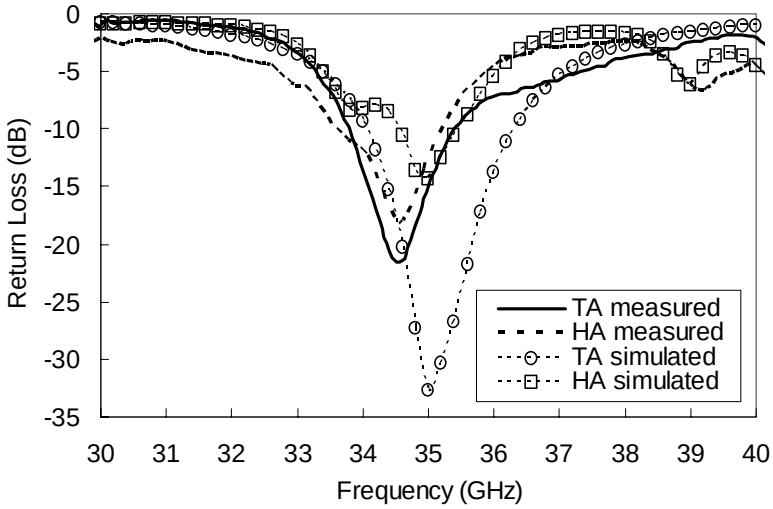

(a)

Fig. 73. Measured results of the traditional and harmonic patch antennas: (a) return losses, (b) antenna gains, and (c) axial ratios.

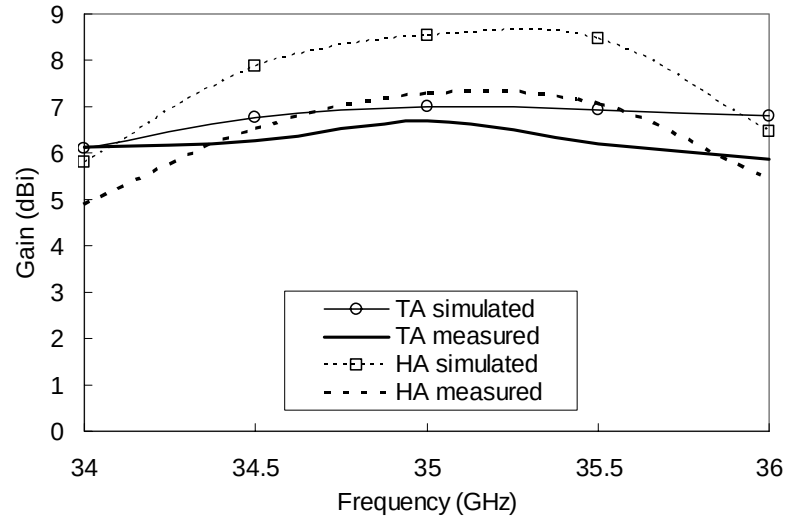

(b)

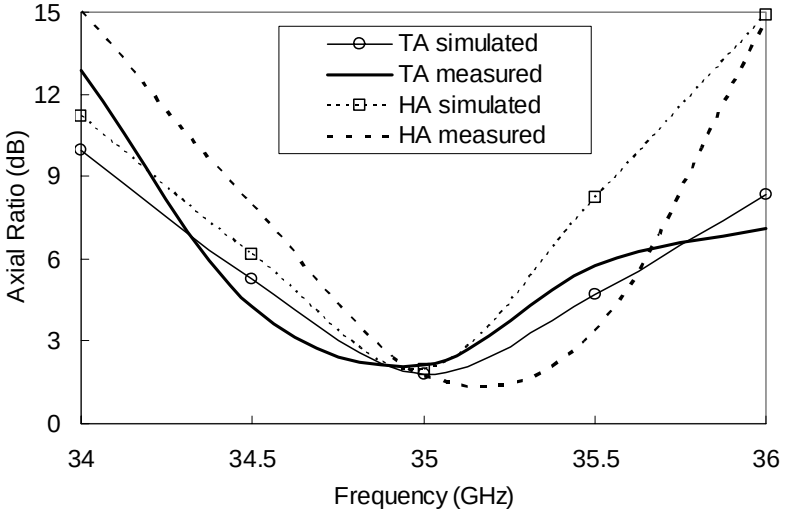

(c)

Fig. 73. Continued.

The return losses of the 35 GHz CP harmonic antenna and traditional antenna are shown in Figure 73(a) for comparison. The antenna gains and the axial ratios are shown in Figures 73(b) and 73(c). The harmonic antenna patterns are shown in Figure 74. From the measurements, the harmonic antenna has similar performance to the traditional

antenna. The measured results match the simulated results, except that the measured HA gains are 1.5 dB lower than the simulated HA gains. At 35 GHz, the harmonic antenna has a measured return loss of 18 dB, a gain of 7.3 dBi, and an axial ratio of 1.74 dB while the traditional antenna has a measured return loss of 20 dB, a gain of 6.7 dBi, and an axial ratio of 2.11 dB.

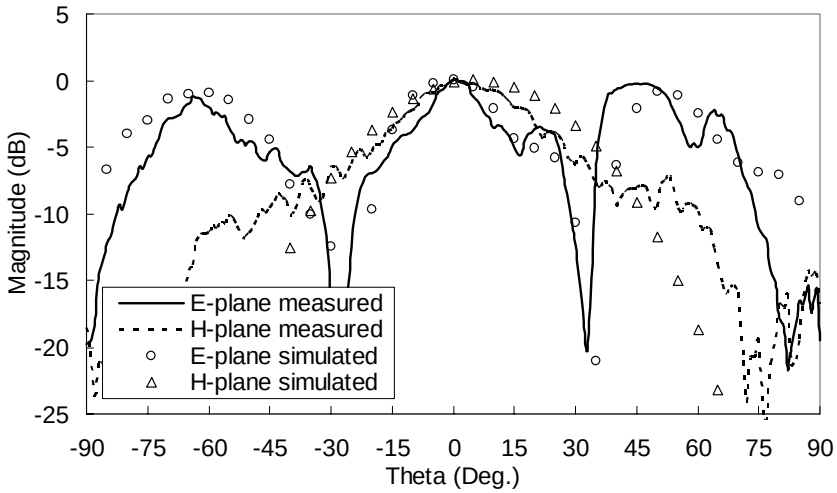

Fig. 74. Measured patterns of the harmonic patch antenna.

4. Second-order harmonic filter

The harmonic microstrip square ring bandpass filters are designed based on the filter reported in [77], whose layout is shown in Figure 75. In the previous design, only the first passband is used to pass the signal, and other high-order harmonics are suppressed to reject unwanted signals. Here the bandpass filter is designed to adopt the second passband, (i.e. the second harmonic) of 17.5 GHz. Two stubs are added on the outside of the resonator for better high-order mode rejection performance. By varying the dimensions of these stubs, the third and higher-order harmonic signals can be

blocked. The dimensions of the harmonic bandpass filter are about twice that of the traditional bandpass filter.

The measured and simulated insertion loss and return loss of the harmonic bandpass filter are shown in Figure 76. It is observed that measured S-parameters are very close to those simulated. At 35 GHz, the return loss and the insertion loss are 25.54 dB and 3.08 dB, respectively. The insertion loss includes two coaxial to microstrip connectors and feed lines for the bandpass filter.

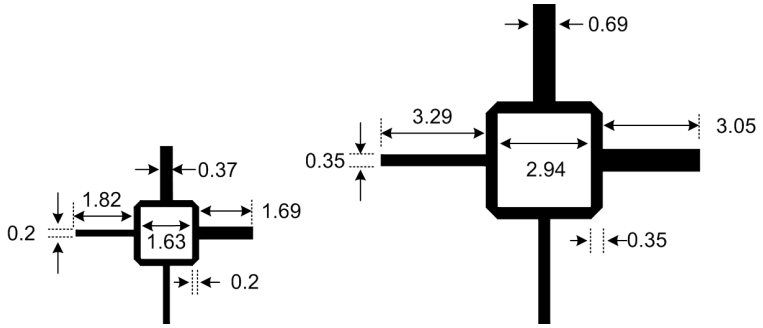

Fig. 75. 35 GHz square ring bandpass filters: the left one is the traditional filter and the right one is the harmonic filter. All dimensions are in millimeter.

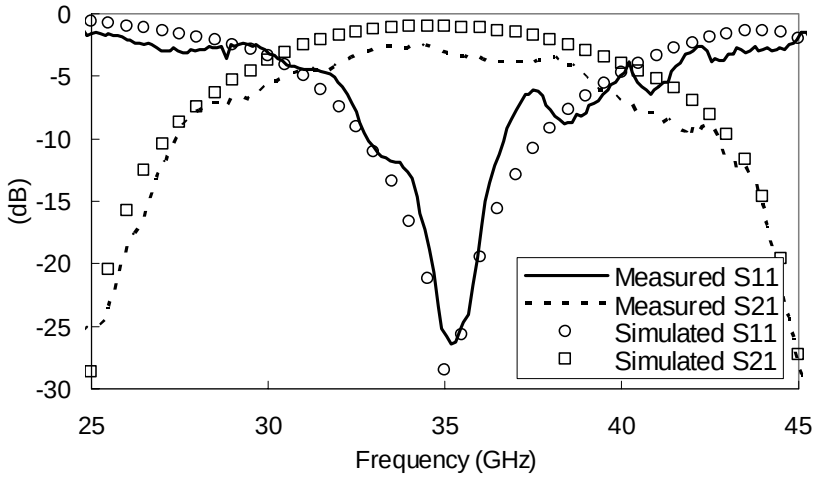

Fig. 76. The insertion loss (S_{21}) and return loss (S_{11}) of the harmonic bandpass filter.

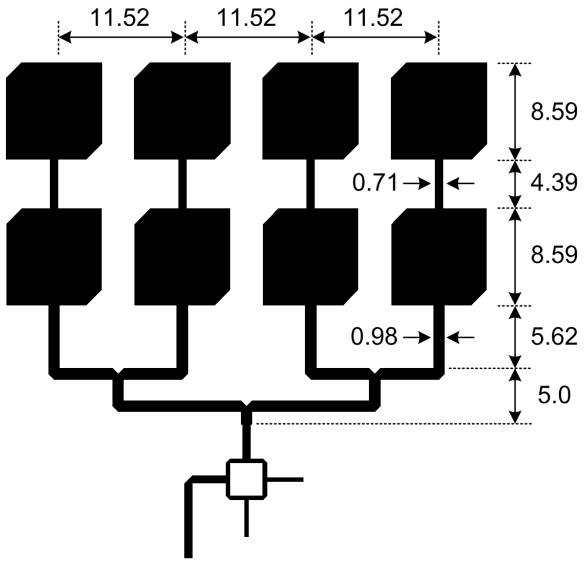

Fig. 77. The 2x4 harmonic antenna array operating at 35 GHz. All dimensions are in millimeter.

5. Harmonic antenna array

The harmonic antenna and filter described earlier are integrated to build a 35 GHz 2x4 harmonic array, as shown in Figure 78. The antenna feed-line has been tuned to match the array impedance. A power divider is used to connect the antenna elements and the filter. A section of transmission line is connected to the band-pass filter port for measurement. The filter is used to pass a 35 GHz signal. The element distance is equal to $1.88\lambda_g$ (= 11.52 mm). The return losses and the pattern of the array are shown in Figure 77. At 35 GHz, this array has a measured return loss of 13.5 dB, a gain of 13.9 dBi, and an axial ratio of 0.42 dB. The 2x4 harmonic array has a simulated gain of 15.5 dBi that is 1.6 dB higher than the measured gain. The difference is probably due to the power divider with relatively long transmission lines connecting the elements.

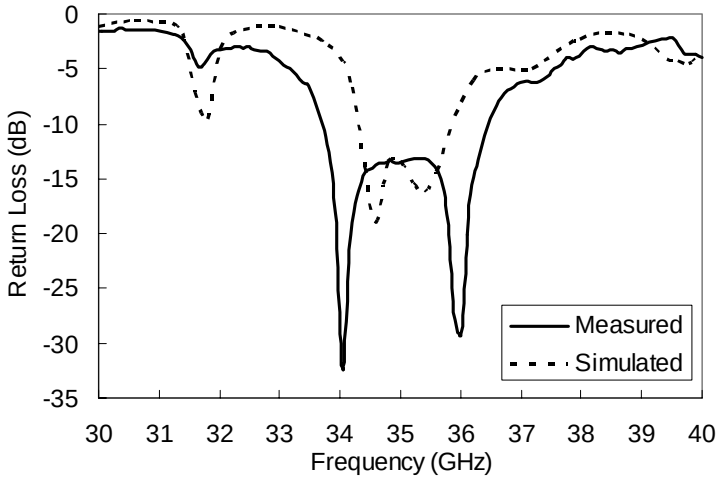

(a)

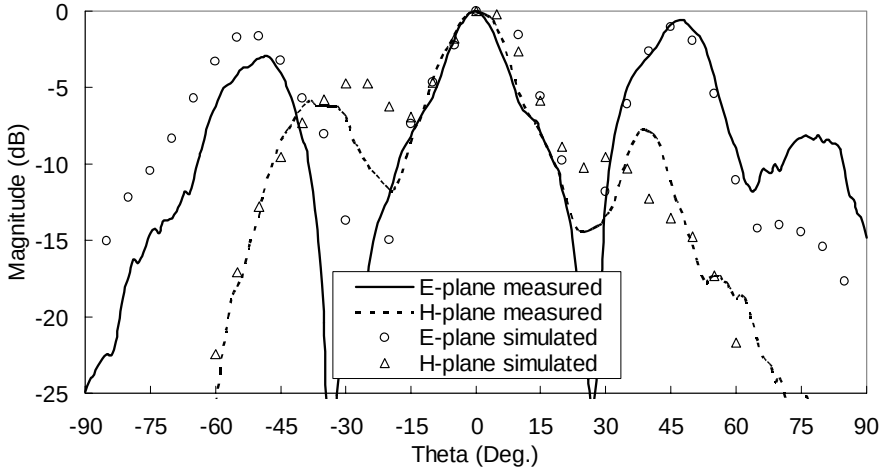

(b)

Fig. 78. The performances of the harmonic 2x4 antenna array: (a) return loss and (b) measured patterns.

6. Harmonic rectenna

The harmonic rectenna is built by inserting a rectifying circuit in the transmission line connecting the center two elements of the array, as shown in Figure 79(a). At broadside, each paired array can generate DC output. The rectifying circuit behaves like a voltage source and hence can be series-connected to obtain higher output voltage. The rectifying circuit consists of a RF-to-DC detector diode (MA4E1317) and a load

resistance (R_L) of 100 Ω. Usually using a diode with a smaller junction capacitance results in better conversion efficiency, especially in a high frequency such as 35 GHz.

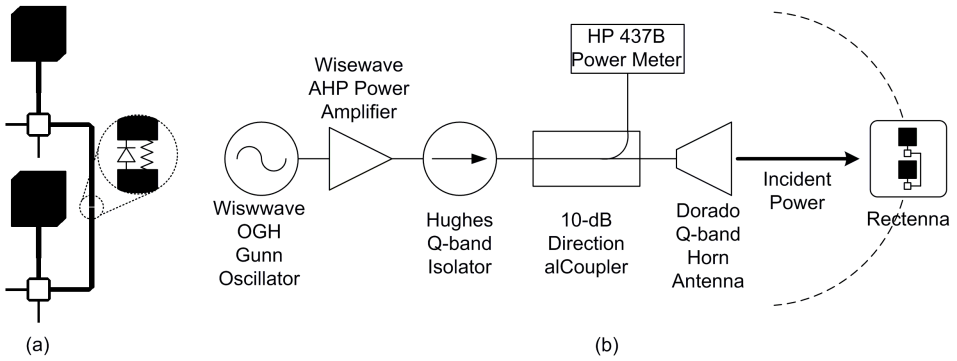

Fig. 79. (a) The inserted rectifying circuit and (b) the measurement system of the 35 GHz rectenna.

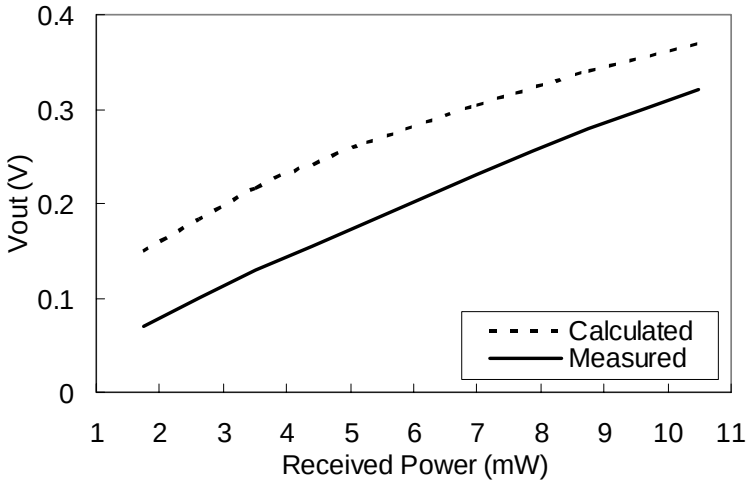

Fig. 80. Measured harmonic rectenna output voltages.

The measurement setup is shown in Figure 79(b). Figures 80 shows the DC output voltage with different received power (P_r) levels at broadside. When the RF input power is 10.5 mW, the rectenna has a measured DC output of 0.32 V and a conversion

efficiency of 10%, while the computed results are 0.37 V and 13%, respectively. These results are close to those reported in [50]. Higher conversion efficiency and DC output can be achieved by using a higher power source.

7. Conclusions

In this chapter, 35 GHz harmonic components are presented, including a CP patch antenna, a bandpass filter, a 2x4 antenna array, and a rectenna. From measurement results, these harmonic components demonstrate similar performance to traditional millimeter-wave components. The harmonic components have the advantages of larger sizes that will relax fabrication tolerance at high millimeter-wave frequencies. It is believed that the harmonic components would be useful for millimeter-wave applications in future wireless communication and power transmission systems.

CHAPTER VIII

CONCLUSIONS

1. Summary

In this dissertation, various rectennas and rectenna arrays for microwave and millimeter-wave frequencies have been developed for wireless power transmission applications. A novel dual-diode rectenna has been developed to provide higher DC output voltage using the same layout dimensions as the single-diode rectenna. New rectenna arrays with different array interconnections are also demonstrated. Connecting more antenna elements, the receiving antenna of the rectenna can form a traveling-wave antenna array with higher gain. To solve the alignment problem of the wireless power transmission system, the non-uniform array and the retrodirective array have been applied in the rectenna design. It has been shown that using the retrodirective array is the preferred method, and both Van Atta array and phase-conjugated array could be used. Millimeter-wave rectennas and rectenna arrays have also been developed using the ultra-wideband dual-ring antennas. The sub-rectenna array can be used as the building-block to assemble a very large rectenna array with a predicable output performance. The dual-ring antennas are also used to build a broadband planar retrodirective array by assembling many sub-arrays. For ultra-wideband communication allocations, four ultra-wideband antennas are demonstrated for UHF and microwave frequencies. Their design parameters and measured performances are presented and discussed. Finally, harmonic

components using high-order modes are designed, including a commonly used antenna, bandpass filter, array, and rectenna. They have similar performance to the traditional components using the fundamental mode. The research topics and accomplishments covered in this dissertation are summarized chapter by chapter in the followings.

In Chapter II, a new circularly polarized rectenna is developed whose rectifying circuit includes two diodes. The rectenna consists of a coplanar stripline truncated patch antenna and a coplanar stripline bandpass filter, which can block harmonic signals up to the third order reradiating from the rectifying circuit. The new dual-diode rectenna can provide at least twice the DC output voltage than the traditional rectenna with only a single diode, which has the same layout dimension as the single diode rectenna. The dual-diode rectenna achieves a RF-to-DC conversion efficiency of 76% at 5.8 GHz. The proposed rectennas can be interconnected to form the rectenna arrays by series, parallel, and cascaded connections. It is found that a cascade connected rectenna array can provide the highest output voltage. The antenna element can be easily extended to become a traveling wave antenna or array suitable for high output voltage or current in wireless power transmission applications. A simple linear rectenna model has been used to analyze the rectenna element and the rectenna arrays.

In Chapter III, a non-uniform rectenna array with a flatten pattern is proposed to prevent the output variation due to the improper mainbeam alignment. Although the non-uniform rectenna indeed makes the mainbeam broadened, numerous antenna elements with various sizes are needed that reduces the array gain compared to the uniform rectenna. The process is complicated and hence difficult to implement on a very

large array. Therefore, circularly polarized retrodirective rectenna arrays are introduced, including a 2x2 array and a 4x4 array. A proximity-coupled microstrip ring antenna is used as the retrodirective rectenna array element, which can automatically block harmonic signals up to the third order from reradiating by the rectifying circuit. The new retrodirective rectenna array can track the incoming power source signals automatically and is less sensitive to the power incident angle variations, i.e., mainbeam alignment deviation. It can provide a nearly constant DC output voltage within $\pm 10^{o}$ and 90% DC output voltage within $\pm 45^{o}$. The conversion efficiencies of the two arrays are 73.3% and 55%, respectively, when the power density is 10 mW/cm^2. An active phase-conjugated retrodirective rectenna array is also proposed for the long-distance low-power density applications for microwave wireless power transmissions.

In Chapter IV, millimeter-wave rectifying antenna arrays and retrodirective arrays are presented. A new ultra-wideband dual-ring antenna is designed as the array element whose bandwidth is 33.2%, covering from 31 to 42.8 GHz. The rectenna arrays are built by cascading rectenna elements, and can easily form a large array for high DC output. The single element, the 1x2 array, and the 2x2 array achieve RF-to-DC conversion efficiencies of 64, 56, and 42% at 35 GHz, which correspond to DC output voltages of 1.05, 1.97, and 3.42 V, respectively. These small arrays can be used as the building blocks to assemble a very large array. Then the antenna is used to build a 4x4 planar retrodirective array as a sub-array. The sub-arrays are assembled to form an 8x16 array. The design method of the arrays and the measurement performances from 32 GHz to 40 GHz are presented.

In Chapter V, a novel dual-frequency rectifying antenna operating at 2.45 GHz and 5.8 GHz is developed. The rectifying antenna consists of two compact ring slot antennas, a hairpin lowpass filter, and a rectifying circuit. The annual slot ring antenna uses a meander line structure to reduce its size to 52% of the regular ring slot antenna. The hairpin lowpass filter helps the rectenna suppress the harmonics up to the sixth order. The dual-frequency rectenna achieves RF-to-DC conversion efficiencies of 65% and 46% at 2.45 GHz and 5.8 GHz, respectively, while the power density is 10 mW/cm^2. The rectenna is the smallest dual-frequency rectenna ever reported.

In Chapter VI, four ultra-wideband antennas are demonstrated. The first one is an annual ring antenna. The annual ring antenna has a return loss better than 10-dB from 2.8 to 12.3 GHz. It has an average gain of 2.93 dBi and has a maximum gain of 5 dBi at 7 GHz. The antenna radiation patterns are stable within its operation band. The second one is an elliptical ring antenna fed by a CPW, whose wideband performance is achieved by extending the length of the elliptical ring major axis. The elliptical ring antenna has an effective bandwidth from 4.6 to 10.3 GHz with an average gain of 4.48 dBi. The antenna radiation patterns also show a stable variation within its operation frequencies. The elliptical ring antenna is then redesigned to cover the L-band from 1.05 GHz to 2.1 GHz, corresponding to 71% bandwidth. Its radiation patterns display nearly symmetry to the broadside and are similar to the patterns of a dipole antenna. The antenna average gain is 1.62 dBi, whose lower gain is obtained due to its thick substrate. Finally, an ultra-wideband microstrip house-shaped patch antenna for UHF applications is demonstrated. The antenna has a 10-dB bandwidth of 104%, from 0.62 to 2.13 GHz, and its average

gain is 3.11 dBi. For all of these antennas, the parameters determining their wideband characteristics and the measured performances are presented and discussed.

In Chapter VII, new harmonic components for millimeter-wave applications are presented, including a commonly used patch antenna, a bandpass filter, an antenna array, and a rectenna. They are designed at 35 GHz using the high-order mode of 11.6 or 17.5 GHz. These harmonic components have the advantages of larger size and easier fabrication compared with the traditional components operating at the fundamental mode. Good performances are also obtained from these millimeter-wave components in comparison with the traditional components.

2. Recommendations for future research

Many rectennas and rectenna arrays for microwave and millimeter-wave power transmission have been developed so far. Although several diode models for the rectenna design can be found in the open literatures, they have not been compared with the measurement results. A more accurate rectenna model is needed for building the rectenna element and array. Furthermore, to speed up the rectenna design, the computer-aided design should be applied because it has been done in many microwave circuits using commercially available software, which is able to give an efficient and correct design.

It is important to explore commercial or military applications for rectennas and rectenna arrays by combining with other components and subsystems such as communications, RFID, embedded sensors, recharging, switches, vehicles, and aircrafts,

et al. For example, the rectenna should be able to charge the battery of the mobile devices such as the cellular phone and the laptop. Besides the basic rectenna elements, a recharging control circuit using a fixed voltage regulator is needed to provide a stable and constant voltage or current flowing into the battery. If the recharging time is too long, a thermal self-protection device has to be activated to protect the circuits, as shown in Figure 81.

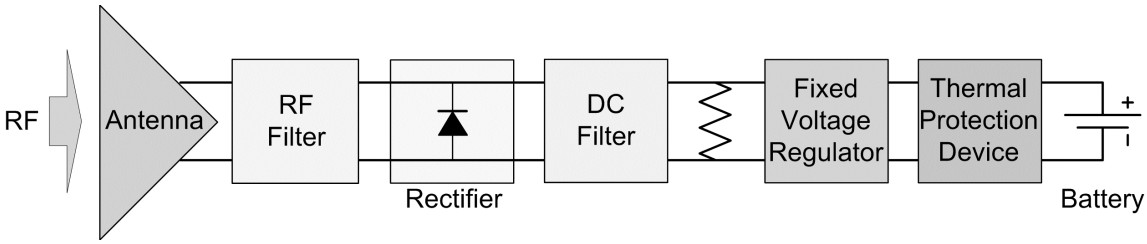

Fig. 81. Rectenna charger block diagram

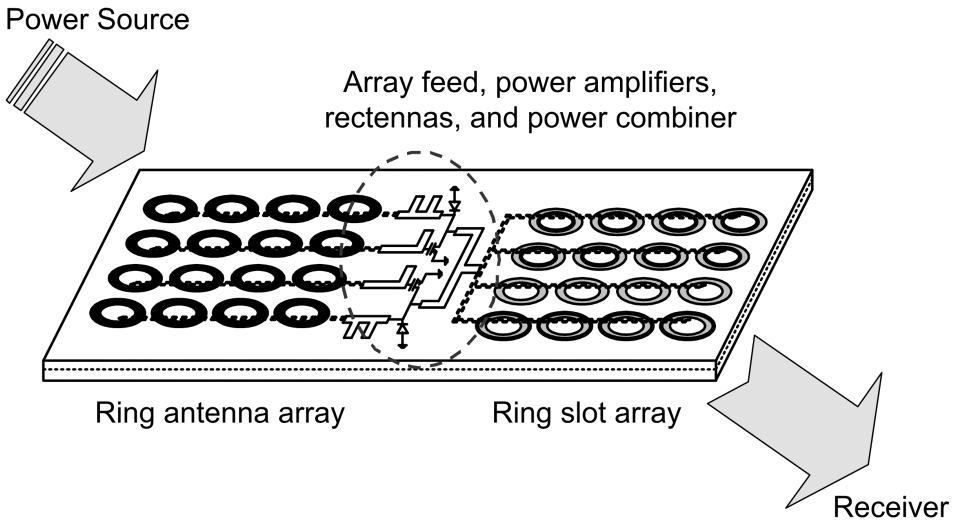

Fig. 82. A power combining system using rectennas as the voltage source of the power amplifiers.

Due to the ability to provide the DC voltages, the rectenna can behave as a voltage

source for other electronic devices or systems. For example, it can supply the operation DC power for power amplifiers in the power combining system, as shown in Figure 82. The rectennas and the power amplifiers are sandwiched between the receiving and the transmitting antenna arrays. This system does not need additional power supplies to drive the power amplifiers.

Not only used in wireless power transmission, communication, and radar systems, the retrodirective array can also be applied to vehicle/aircraft collision avoidance system and the intelligent transportation systems (ITS). The retrodirective array provides automatic tracking ability without complicated signal processing and any prior known information.

Broadband communications has become a trend in future communication systems. With an ultra-wideband antenna, data communications and power transmission can be processed at the same time, which means the base station can supply power or charge the battery for the mobile stations. This would be especially useful for the wireless communication systems in micro-cell and pico-cell environments because of short distance and low power requirements.

REFERENCES

[1] W. C. Brown, "The technology and application of free-space power transmission by microwave beam," *Proceedings of the IEEE*, vol. 62, no. 1, pp. 11-25, Jan. 1974.

[2] W. C. Brown, "The history of power transmission by radio waves," *IEEE Trans. Microwave Theory and Techniques*, vol. MTT-32, no. 9, pp.1230-1242, Sep. 1984.

[3] J. O. McSpadden and J. C. Mankins, "Space solar power programs and microwave wireless power transmission technology," *IEEE Microwave Magazine*, vol. 3, no. 4, pp.46-57, Dec. 2002.

[4] B. H. Strassner and K. Chang, "Microwave power transmission," in *Encyclopedia of RF and Microwave Engineering*, Hoboken, NJ: John Wiley & Sons, Inc., vol. 4, pp.2906-2919, 2005.

[5] J. Heikkinen and M. Kivikoski, "Low-profile circularly polarized rectifying antenna for wireless power transmission at 5.8 GHz," *IEEE Microwave and Wireless Components Letters*, vol. 14, no. 4, pp.162-164, 2004.

[6] J. -Y. Park, S. -M. Han, and T. Itoh, "A rectenna design with harmonic-rejecting circular-sector antenna," *IEEE Antennas and Wireless Propagation Letters*, vol. 3, pp.52-54, 2004.

[7] C. -H. Chin, Q. Xue, and C. H. Chan, "Design of a 5.8-GHz rectenna incorporating a new patch antenna," *IEEE Antennas and Wireless Propagation Letters*, vol. 4, pp.175-178, 2004.

[8] M. Ali, G. Yang, and R. Dougal, "A new circularly polarized rectenna for wireless power transmission and data communication," *IEEE Antennas and Wireless Propagation Letters*, vol. 4, pp.205-208, 2005.

[9] J. Heikkinen and M. Kivikoski, "A novel dual-frequency circularly polarized rectenna," *IEEE Antennas and Wireless Propagation Letters*, vol. 2, pp.330-333, 2003.

[10] J. A. Hagerty and Z. Popovic, "An experimental and theoretical characterization of a broadband arbitrarily-polarized rectenna array," *IEEE MTT-S International Microwave Symposium Digest*, vol. 3, pp.1855-1858, May 2001.

[11] B. Strassner and K. Chang, "Highly efficient C-band circularly polarized rectifying antenna array for wireless microwave power transmission," *IEEE Trans. Antennas and Propagation*, vol. 51, no. 6, pp.1347-1356, Jun. 2003.

[12] J. O. McSpadden, L. Fan, and K. Chang, "Design and experiments of a high-conversion-efficiency 5.8-GHz rectenna," *IEEE Trans. Microwave Theory and Techniques*, vol. 46, no. 12, pp.2053-2059, Dec. 1998.

[13] Y. -H. Suh and K. Chang, "A high-efficiency dual-frequency rectenna for 2.45- and 5.8-GHz wireless power transmission," *IEEE Trans. Microwave Theory and Techniques*, vol. 50, no. 7, pp.1784-1789, Jul. 2002.

[14] B. Strassner and K. Chang, "5.8-GHz circularly polarized dual-rhombic-loop traveling-wave rectifying antenna for low power-density wireless power transmission applications," *IEEE Trans. Microwave Theory and Techniques*, vol. 51, no. 5, pp.1548-1553, May 2003.

[15] Y. Murao and T. Takano, "An investigation on the design of a transmission antenna and a rectenna with arrayed apertures for microwave power transmission," *Electronics and Communications in Japan*, Part 1, vol. 83, no. 2, pp.1-9, 2002.

[16] L. -H. Hsieh, B. H. Strassner, S. J. Kokel, C. T. Rodenbeck, M. Y. Li, K. Chang, F. E. Little, G. D. Arndt, and P. H. Ngo, "Development of a retrodirective wireless microwave power transmission system," *IEEE AP-S Antennas and Propagation International Symposium Digest*, vol. 2, pp.393-396, Jun. 2003.

[17] K. Hashimoto and H. Matsumoto, "Microwave beam control system for solar power satellite," *IEEE Proceedings, Asia-Pacific Radio Science Conference*, pp.616-617, Aug. 2004.

[18] C. Rodenbeck, M. Li, and K. Chang, "A phased-array architecture for retrodirective microwave power transmission from the space solar power satellite," *IEEE MTT-S International Microwave Symposium Digest*, vol. 3, pp.1679-1682, Jun. 2004.

[19] V. F. Fusco and S. L. Karode, "Self-phasing antenna array techniques for mobile communications applications," *IEE Electronics & Communication Engineering Journal*, vol.11, no. 6, pp.279-286, Dec. 1999.

[20] R. Y. Miyamoto and T. Itoh, "Retrodirective arrays for wireless communications," *IEEE Microwave Magazine*, vol. 3, no 1, pp.71-79, Mar. 2002.

[21] K. M. K. H. Leong, R. Y. Miyamoto, and T. Itoh, "Moving forward in retrodirective antenna arrays," *IEEE Potentials*, vol. 22, no. 3, pp.16-21, Aug.-Sep. 2003.

[22] W. A. Shiroma, R. Y. Miyamoto, G. S. Shiroma, A. T. Ohta, M. A. Tamamoto, and B. T. Turakumi, "Retrodirective systems," in *Encyclopedia of RF and Microwave Engineering*, Hoboken, NJ: John Wiley & Sons, Inc., vol. 5, pp.4493-

4507, 2005.

[23] J. Tuovinen, G. S. Shiroma, W. E. Forsyth, and W. A. Shiroma, "Multipath communications using a phase-conjugate array," *IEEE MTT-S International Microwave Symposium Digest*, vol. 3, pp.1681-1684, Jun. 2003.

[24] B. Subbarao and F. Fusco, "Radial cavity-fed spatial power combiner with retrodirective array behavior," *IEEE Trans. Antennas and Propagation*, vol. 52, no. 5, pp.1281-1285, May 2004.

[25] S. -J. Chung, S. -M. Chen, and Y. -C. Lee, "A novel bi-directional amplifier with applications in active Van Atta retrodirective arrays," *IEEE Trans. Microwave Theory and Techniques*, vol. 51, no. 2, pp.542-547, Feb. 2003.

[26] L .W. Epp, A. R. Khan, H. K. Smith, and R. P. Smith, "A compact dual-polarized 8.51-GHz rectenna for high-voltage (50 V) actuator applications," *IEEE Trans. Microwave Theory and Techniques*, vol. 48, no. 1, pp.111-119, Jan. 2000.

[27] N. Shinohara and H. Matsumoto, "Experimental study of large rectenna array for microwave energy transmission," *IEEE Trans. Microwave Theory and Techniques*, vol. 46, no. 3, pp.261-268, Mar. 1998.

[28] N. Shinohara and H. Matsumoto, "Dependence of DC output of a rectenna array on the method of interconnection of its array elements," *Scripta Technica Electrical Engineering in Japan*, vol. 125, no. 1, pp.9-17, 1998.

[29] Z. L. Wang, K. Hashimoto, N. Shinohara, and H. Matsumoto, "Frequency-selective surface for microwave power transmission," *IEEE Trans. Microwave Theory and Techniques*, vol. 47, no. 10, pp.2039-2042, Oct. 1999.

[30] J. O. McSpadden, T. Yoo, and K. Chang, "Theoretical and experimental investigation of a rectenna element for microwave power transmission," *IEEE Trans. Microwave Theory and Techniques*, vol. 40, no. 12, pp.2359-2366, Dec. 1992.

[31] R. Thomas and J. Huang, "Ultra-wideband UHF microstrip array for GeoSAR application," *IEEE AP-S Antennas and Propagation International Symposium Digest*, vol. 4, pp.21-26, Jun. 1998.

[32] A. Deshmukh and G. Kumar, "Compact broadband C-shaped stacked microstrip antennas," *IEEE AP-S Antennas and Propagation International Symposium Digest*, vol. 2, pp.16-21, Jun. 2002.

[33] K. Chan, B. Peng, and H. Oh, "Measured performance of a ultra broadband wide scan dual polarized VHF-UHF array," *IEEE Twelfth International Conference on*

Antennas and Propagation, vol. 2, pp.501-504, Mar. 31 – Apr. 3, 2003.

[34] H. Kawakami, T. Haga, S. Kon, M. Arishiro, and T. Yamashita, "Characteristics of wideband ring loop antenna for digital terrestrial broadcasting," *IEEE AP-S Antennas and Propagation International Symposium Digest*, vol. 2B, pp.544-547, Jul. 2005.

[35] S. Zhong, X. Liang, and F. Yao, "Compact broadband slot antenna for UHF-band application," *IEEE AP-S Antennas and Propagation International Symposium Digest*, pp.2567-2570, Jul. 2006.

[36] W. C. Chew, "A broad-band annular-ring microstrip antenna," *IEEE Trans. Antennas and Propagation*, vol. AP-30, no. 5, pp.918-922, Sep. 1982.

[37] N. Behdad and K. Sarabandi, "Wideband double-element ring slot antenna," *IEE Electronics Letters*, vol. 40, no. 7, pp.408-409, Apr. 2004.

[38] J. Row, C. Sim and K. Lin, "Broadband printed ring-slot array with circular polarisation," *IEE Electronics Letters*, vol. 41, no. 3, 3rd Feb. 2005.

[39] Q. Garcia, "Broadband stacked annular ring," *IEE Ninth International Conference on Antennas and Propagation*, vol. 1, pp.508-512, Apr. 1995.

[40] J. Baligar, U. Revankar, and K. Acharya, "Broadband stacked annular ring coupled shorted circular microstrip antenna," *IEE Electronics Letters*, vol. 36, no. 21, pp.1756-1757, Oct. 2000.

[41] Y. Guo, Y. Ruan, and X. Shi, "Wide-band stacked double annular-ring dielectric resonator antenna at the end-fire mode operation," *IEEE Trans. Antennas and Propagation*, vol. 53, no. 10, pp.3394-3397, Oct. 2005.

[42] H. Shin and N. Kim, "Wideband annular ring slot microstrip antenna with low impedance feed line," *IEEE AP-S Antennas and Propagation International Symposium Digest*, vol. 2, pp.288-291, Jun. 2002.

[43] Y. Guo and K. Luk, "L-probe proximity-fed annular ring microstrip antennas," *IEEE Trans. Antennas and Propagation*, vol. 49, no. 1, pp.19-21, Jan. 2001.

[44] D. Chang and H. Lien, "The study of wideband single fed CP ring antenna," *IEEE 4th International Conference on Microwave and Millimeter Wave Technology Proceedings*, pp.50-53, Aug. 2004.

[45] H. G. Schantz, "Planar elliptical element ultra-wideband dipole antennas," *IEEE AP-S Antennas and Propagation International Symposium Digest*, vol. 3, pp.16-21, Jun. 2002.

[46] H. G. Schantz, "Bottom fed planar elliptical element UWB antennas," *IEEE Conference on Ultra Wideband Systems and Technologies*, pp.219-223, Nov. 2003.

[47] K. C. L. Chan, Y. Huang, and X Zhu, "A planar elliptical monopole antenna for UWB applications," *IEEE Conference on Wireless Communications and Applied Computational Electromagnetics*, pp.182-185, Apr. 2005.

[48] C. -Y. Huang and W. -C. Hsia, "Planar elliptical antenna for ultra-wideband communications," *IEE Electronics Letters*, vol. 41, no. 6, pp.296-297, 17 Mar. 2005.

[49] X. -L. Liang, S. -S. Zhong, and W. Wang, "Elliptical planar monopole antenna with extremely wide bandwidth," *IEE Electronics Letters*, vol. 42, no. 8, pp.441-442, 13 Apr. 2006.

[50] T. -W. Yoo and K. Chang, "Theoretical and experimental development of 10 and 35 GHz rectennas," *IEEE Trans. Microwave Theory and Techniques*, vol. 40, no. 6, pp.1259-1266, Jun. 1992.

[51] J. Joe and M. Y. W. Chia, "Voltage, efficiency calculation and measurement of low power rectenna rectifying circuit," *IEEE AP-S Antennas and Propagation International Symposium Digest*, vol. 4, pp.1854-1857, Jun. 1998.

[52] J. A. G. Akkermans, M. C. van Beurden, G. J. N. Doodeman, and H. J. Visser, "Analytical models for low-power rectenna design," *IEEE Antennas and Wireless Propagation Letters*, vol. 4, pp.187-190, 2005.

[53] A. Sedra and K. Smith, *Microelectronic circuits*, Fourth Edition, New York, NY: Oxford University Press, Inc., 1998.

[54] *IE3D version 10.2*, Fremont, CA: Zeland Software, Inc., 2004.

[55] R. R. Ramirez, F. D. Flaviis, and N. G. Alexopoulos, "Single-feed circularly polarized microstrip ring antenna and arrays," *IEEE Trans. Antennas and Propagation*, vol. 48, no. 7, pp.1040-1047, Jul. 2000.

[56] R. H. Rasshofer and M. O. Thieme, and E. M. Biebl, "Circularly polarized millimeter-wave rectenna in silicon substrate," *IEEE Trans. Microwave Theory and Techniques*, vol. 46, no. 5, pp.715-718, May 1998.

[57] H. L. Deng and L. Kong, "A novel high-efficiency rectenna for 35 GHz wireless power transmission," *IEEE 4th International Conference Microwave and Millimeter Wave Technology Proceedings*, pp.114-117, Aug. 2004.

[58] J. A. Hagerty, F. B. Helmbrecht, W. H. McCalpin, R. Zane, and Z. B. Popovic,

"Recycling ambient microwave energy with broad-band rectenna arrays," *IEEE Trans. Microwave Theory and Techniques*, vol. 52, no. 3, pp.1014-1024, Mar. 2004.

[59] *HFSS version 10*, Pittsburgh, PA: Ansoft Software, Inc., 2006.

[60] R. Garg, P. Bhartia, I. Bahl, and A. Ittipiboon, *Microwave Antenna Design Handbook*, Norwood, MA: Artech House, Inc., 2001.

[61] I. Bahl, S. Stuchly, and M. Stuchly, "A new microstrip radiator for medical applications," *IEEE Trans. Microwave Theory and Techniques*, vol. MTT-28, no. 12, pp.1646-1468, Dec. 1998.

[62] E. Nielsen, "Square Van Atta reflector with conducting mounting plane," *IEEE Trans. Antennas and Propagation*, vol. AP-18, no. 1, pp.48-54, Jan. 1970.

[63] R. Janaswamy and D. H. Schaubert, "Characteristic impedance of a wide slotline on low-permittivity substrates," *IEEE Trans. Microwave Theory and Techniques*, vol. MTT-34, no. 8, pp.900-902, Aug. 1986.

[64] L. H. Hsieh and K. Chang, "Compact elliptic-function low-pass filter using microstrip stepped-impedance hairpin resonators," *IEEE Trans. Microwave Theory and Techniques*, vol. 51, no. 1, pp.193-199, Jan. 2003.

[65] J. Zbitou, M. Latrach, and S. Toutain, "Hybrid rectenna and monolithic integrated zero-bias microwave rectifier," *IEEE Trans. Microwave Theory and Techniques*, vol. 54, no. 1, pp.147-152, Jan. 2006.

[66] D. -H. Kwon and Y. Kim, "CPW-fed planar ultra-wideband antenna with hexagonal radiating elements," *IEEE AP-S Antennas and Propagation Int. Symp. Dig.*, vol. 3, pp.2947-2950, Jun. 2004.

[67] J. Liang, C. C. Chiau, X. Chen, and C. G. Parini, "Printed circular disc monopole antenna for ultra-wideband applications," *IEE Electronics Letters*, vol. 30, no. 20, Sep. 2004.

[68] K. Kiminami, A. Hirata, and T. Shiozawa, "Double-sided printed bow-tie antenna for UWB communications," *IEEE Antennas and Wireless Propagation Letters*, vol. 3, no. 1, pp.152-153, 2004.

[69] S. -Y. Suh, W. L. Stutzman, W. A. Davis, A. E. Waltho. K. W. Skeba, and J. L. Schiffer, "A UWB antenna with a stop-band notch in the 5-GHz WLAN band," *IEEE International Conference Wireless Communications and Applied Computational Electromagnetics*, pp.203-207, Apr. 2005.

[70] C. -C. Lin, Y. -C. Kan, L. -C. Kuo, and H. -R. Chuang, "A planar triangular monopole antenna for UWB communication," *IEEE Microwave and Wireless Components Letters*, vol. 15, no. 10, pp.624-626, Oct. 2005.

[71] J. Jung, W. Choi, and J. Choi, "A small wideband microstrip-fed monopole antenna," *IEEE Microwave and Wireless Components Letters*, vol. 15, no. 10, pp.703-705, Oct. 2005.

[72] E. Okon and C. Turner, "High order mode planar resonators for mm-wave applications," *IEEE 1999 Symposium on High Performance Electron Devices for Microwave and Optoelectronic Applications*, London, U.K., pp.307-311, Nov. 1999.

[73] F. Demuynck and A. Van de Capelle, "Higher order modes in microstrip antenna design via the transmission line model," *IEE Electronics Letters*, vol. 28, no. 18, pp.1732-1734, Aug. 1992.

[74] Rajanish and T. Vedavathy, "Resonant frequency of higher order modes for circular microstrip antennas," *IEEE 1999 Asia-Pacific Microwave Conference*, vol. 3, pp.936-939, Nov. 30 – Dec. 3, 1999.

[75] K. Chang, Editor, *Handbook of RF/Microwave components and engineering*, Hoboken, NJ: John Wiley & Sons, Inc., 2003.

[76] K. Chang and L. Hsieh, *Microwave ring circuits and related structure*, Hoboken, NJ: John Wiley & Sons, Inc., 2004.

[77] L. Hsieh and K. Chang, "Compact, low insertion-loss, sharp-rejection, and wide-band microstrip bandpass filters," *IEEE Trans. Microwave Theory and Techniques*, vol. 51, no. 4, pp.1241-1246, Apr. 2003.

VITA

Yu-Jiun Ren received B.S. in electrical engineering from National Chung-Hsing University, Taiwan, and M.S. degree in communication engineering from National Chiao-Tung University, Taiwan, in 2000 and 2002, respectively. In 1999, he joined the Electromagnetic Laboratory of National Chung-Hsing University and analyzed the structures of stripline, slot, and coplanar waveguide using the numerical methods. From 2000 to 2003, he was a research assistant with the Radio Wave Propagation and Scattering Laboratory of National Chiao-Tung University and involved in wireless communications, radio channel modeling and sounding, and cell planning. From 2003, he started working towards his Ph.D. degree in electrical engineering at Texas A&M University, College Station, TX, and was directed by Prof. Kai Chang in the Electromagnetics and Microwave Laboratory. His research interests include microwave solid-state circuits and devices, advanced antennas and phased arrays, wireless power transmission and combining, and mobile radio propagations. He can be reached through Professor Kai Chang, Department of Electrical and Computer Engineering, Texas A&M University, College Station, TX 77843-3128.